Chapter 8

New Methods for Mechanism Kinematics

Results that describe new methods for kniematic synthesis and analysis presented at various conferences and in archival journals are reprinted in slightly modified form in the following sections. The material presented in the first paper was disseminated in the *Proceedings of the International Federation of Machines and Mechanisms (IFToMM) Tenth World Congress on the Theory of Machines and Mechanisms*, in Oulu, Finland in a paper entitled "The Effect of Data-set Cardinality on the Design and Structural Errors of Four-bar Function-generators" [1]. This paper presents the initial observation that as the input-output (IO) data-set cardinality increases the Euclidean norms of the design and structural errors converge for planar 4R mechanisms. The important implication is that the minimisation of the Euclidean norm of the structural error can be accomplished indirectly via the minimisation of the corresponding norm of the design error provided that a suitably large number of input-output pairs is prescribed.

The second paper, entitled "Continuous Approximate Synthesis of Planar Function-generators Minimising the Design Error" [2], first appeared in the archival journal *Mechanism and Machine Theory* in June 2016. In this paper the Freudenstein synthesis equations are integrated in the range between minimum and maximum input values, thereby reposing the discrete approximate synthesis problem as a continuous one. Moreover, it is proved that a lower bound of the Euclidean norm, and indeed of any p-norm, of the design error for planar 4R function-generating linkages exists and is attained with continuous approximate

synthesis. However, the synthesis equations in this work are intimidatingly complicated due to the reliance on trigonometric functions.

The third paper, "Planar and Spherical Four-bar Linkage v_i-v_j Algebraic Input-output Equations" [3], addresses the unnecessary representation-induced complications imposed by trigonometry by deriving input-output equations using only algebraic means. The algebraic polynomial IO equations relating any two of the relative joint displacement parameters, called v_i and v_j, between any of the six distinct pairs of rigid links in arbitrary planar and spherical four-bar mechanisms are derived. First, the forward kinematics transformation matrices of the corresponding serial kinematic chains are computed in terms of their Denavit-Hartenberg parameters, but with all angles converted to tangent half-angle parameters. These matrices are mapped to their corresponding Study soma coordinates. The serial kinematic chain is closed by equating the soma coordinates to the identity array. Algebraic polynomial elimination methods are then used to obtain a single polynomial in terms of only the design and the selected IO joint displacement parameters. This yields six independent algebraic IO Equations for each of the planar and spherical 4R linkages; the same techniques are applied to derive six additional algebraic IO equations for each of the RRRP and PRRP planar linkages providing a catalogue of 24.

The extension of the planar and spherical algebraic IO equations leads to the RSSR mechanism. The fourth paper, "Kinematic Geometry of Spatial RSSR Mechanisms" [4] describes two different novel methods to derive the IO equation of arbitrary RSSR linkages are described. Both methods share some common elements, i.e., they use the standard Denavit-Hartenberg notation to first describe the linkage as an open kinematic chain, and Study's kinematic mapping to describe the displacement of the coordinate frame attached to the end-effector of the chain with respect to the relatively non-moving base frame. The kinematic closure equation is obtained in the seven-dimensional projective kinematic mapping image space by equating the eight Study soma coordinates to the identity array. Then two methods are successfully applied to eliminate the intermediate joint angle parameters leading to the degree four biquadratic implicit algebraic IO equation: a) the linear implicitisation algorithm [5, 6], which can be applied after rearranging the closure equation such that the linkage can be viewed as two serial RS chains, and b) numerical elimination theory using pseudowitness sets [7]. Both approaches lead to the same IO equation.

The fifth paper, entitled "Multi-modal Continuous Approximate Synthesis of Planar Four-bar Function Generator" [8], introduces a novel multi-modal continuous approximate synthesis algorithm for planar four-bar function gen-

erators. Multi-modal in this sense means concurrently synthesising multiple functions between different joint variable parameter pairs in a four-bar linkage over the desired continuous IO ranges between different pairs of variables. These are not competing functions, rather perturbed functions. The continuous multi-modal synthesis equation is the sum of the squared input-output equations integrated over the different prescribed input variable parameter ranges. Every planar four-bar mechanism explicitly generates six distinct functions each uniquely determined by one set of link parameter constants. We will examine the simultaneous continuous approximate synthesis of two related perturbed functions between different pairs of joint variables that, in general, require different link constants to generate. The optimisation involves identifying the best compromise link constants to approximately generate the two prescribed functions. Planar 4R and RRRP examples are presented where two different functions, one primary and the other perturbed secondary, are generated over continuous ranges between the specified input variable parameter and the associated output variable parameter. We evaluate the continuous multi-modal synthesis results by comparing the areas between the generated degree 4 planar algebraic curves in the parameter planes of the input and output joint variables to those of the prescribed IO functions over their continuous ranges, thereby simultaneously evaluating a measure of the Euclidean norm of both the design and structural errors.

The sixth paper, "Solving the Burmester Problem Using Kinematic Mapping" [9], initially appeared in the *Proceedings of the American Society of Mechanical Engineers (ASME) Design Engineering Technical Conferences: Mechanisms Conference*, and was presented in Montréal, QC, Canada in September 2002. In this paper a method to solve the five-pose Burmester problem for rigid body guidance using the planar kinematic mapping of Grünwald [10] and Blashke [11] introduced simultaneously, but independently in 1911, is presented. This procedure was generalised to all possible planar four-bar mechanisms in [12].

The seventh paper presents work intended to integrate type and dimensional synthesis solving the five-position Burmester problem and is entitled "Towards Integrated Type and Dimensional Synthesis of Mechanisms for Rigid Body Guidance" [13]. In this paper kinematic mapping is used to take the first steps towards development of a general algorithm combining both type and dimensional synthesis of planar mechanisms for rigid body guidance. In this work an algorithm is presented that can size link lengths, locate joint axes, and, using heuristics, decide between RR- and PR-dyads that, when combined, can guide

a rigid body exactly through five specified positions and orientations, i.e., the five-position Burmester problem. The paper was presented at the 2004 *Canadian Society for Mechanical Engineering Forum* in London, ON, in June 2004, and appears in the associated Proceedings.

The eighth paper in this chapter, entitled "Integrated Type And Dimensional Synthesis of Planar Four-Bar Mechanisms" [14], appears in a book containing the proceedings of the eleventh in the series of *Advances in Robot Kinematics Conference*, and was presented in June 2012 in Innsbruck, Austria. In the paper a novel approach to integrated type and approximate dimensional synthesis of general planar four-bar mechanisms (i.e. linkages comprised of any two of RR, PR, RP, and PP dyads) for rigid-body guidance is proposed. The essence is to correlate coordinates of the coupler attachment points in two different coordinate frames, thereby reducing the number of independent variables defining a suitable dyad for the desired rigid-body motion from five to two. After applying these geometric constraints, numerical methods are used to size link lengths, locate joint axes, and decide between RR, PR, RP and PP dyads that, when combined, guide a rigid body through the best approximation, in a least-squares sense, of n specified positions and orientations, where $n > 5$. No initial guesses of type or dimension are required.

Finally, a new approach for approximate synthesis of planar four-bar mechanisms that solve the rigid body guidance problem is presented in the ninth paper, entitled "Quadric Surface Fitting Applications to Approximate Dimensional Synthesis" [15]. This paper appeared in the *Proceedings of the International Federation of Machines and Mechanisms (IFToMM) Thirteenth World Congress on the Theory of Machines and Mechanisms*, and was presented in Guanajuato, Mexico in June 2011. In this paper an approximate synthesis method is presented that takes a given set of n desired poses of the coupler of a four-bar planar mechanism and finds the "best" mechanism that can achieve them. This is accomplished by solving an equivalent unconstrained non-linear minimisation problem. The hyperboloids of one sheet or hyperbolic paraboloids that minimise the distance between the given n poses in the kinematic mapping image space of Grünwald and Blashke and n corresponding points that belong to the quadric surfaces, represent the "best" mechanism that can achieve the desired poses.

Bibliography

[1] M.J.D. Hayes, K. Parsa, and J. Angeles. "The Effect of Data-Set Cardinality on the Design and Structural Errors of Four-Bar Function-Generators". *Proceedings of the Tenth World Congress on the Theory of Machines and Mechanisms,* Oulu, Finland, pages 437–442, 1999.

[2] A. Guigue and M.J.D. Hayes. "Continuous Approximate Synthesis of Planar Function-generators Minimising the Design Error". *Mechanism and Machine Theory*, vol. 101: pages 158–167, DOI: 10.1016/j.mechmachtheory.2016.03.012, 2016.

[3] M.J.D. Hayes, M. Rotzoll, Q. Bucciol, and Z.A. Copeland. Planar and Spherical Four-bar Linkage v_i-v_j Algebraic Input-output Equations. *Mechanism and Machine Theory*, 182, 2023.

[4] M. Rotzoll, M.H. Regan, M.L. Husty, and M.J.D. Hayes. Kinematic Geometry of Spatial RSSR Mechanisms. *Mechanism and Machine Theory*, 185, 2023.

[5] Dominic R. Walter and Manfred L. Husty. On implicitization of kinematic constraint equations. *Machine Design & Research (CCMMS 2010)*, 26:218–226, 2010.

[6] Manfred L. Husty and Dominic R. Walter. *Mechanism Constraints and Singularities - The Algebraic Formulation*, pages 101–180. CISM International Centre for Mechanical Sciences 589. Springer International Publishing, Cham, Switzerland, 2019.

[7] J.D. Hauenstein and A.J. Sommese. Witness sets of projections. *Applied Mathematics and Computation*, 217(7):3349–3354, 2010.

[8] Z.A. Copeland and M.J.D. Hayes. Multi-modal Continuous Approximate Synthesis of Planar Four-bar Function Generators. *International Journal of Mechanisms and Robotic Systems*, vol. 5, no. 3: pages 246–269, 2023.

[9] M.J.D. Hayes and P.J. Zsombor-Murray. "Solving the Burmester Problem Using Kinematic Mapping". *Proc. of the ASME Design Engineering Technical Conferences: Mechanisms Conference,* Montréal, QC, Canada, on CD, Sept. 2002.

[10] J. Grünwald. "Ein Abbildungsprinzip, welches die ebene Geometrie und Kinematik mit der räumlichen Geometrie verknüpft". *Sitzber. Ak. Wiss. Wien*, vol. 120: pages 677–741, 1911.

[11] W. Blaschke. "Euklidische Kinematik und Nichteuklidische Geometrie". *Zeitschr. Math. Phys.*, vol. 60: pages 61–91 and 203–204, 1911.

[12] K. Brunnthaler, M. Pfurner, and M.L. Husty. "Synthesis of Planar Four-bar Mechanisms". *Transactions of the Canadian Society for Mechanical Engineering*, vol. 30, no. 2: pages 297–313, 2006.

[13] M.J.D. Hayes and P.J. Zsombor-Murray. "Towards Integrated Type and Dimensional Synthesis of Mechanisms for Rigid Body Guidance". *Proceedings of the CSME Forum 2004,* University of Western Ontario, London, ON., Canada, June 1-4, 2004.

[14] T.J. Luu and M.J.D. Hayes. "Integrated Type and Approximate Dimensional Synthesis of Four-Bar Planar Mechanisms for Rigid Body Guidance". *Latest Advances in Robot Kinematics,* eds. J. Lenarčič and M.L Husty, Springer, New York, 2012.

[15] M.J.D. Hayes and S. Radacina Rusu. "Quadric Surface Fitting Applications to Approximate Dimensional Synthesis". *Proceedings of the Thirteenth World Congress on the Theory of Machines and Mechanisms,* Guanajuato, Mexico, June 19-23, 2011.

TENTH WORLD CONGRESS ON THE THEORY OF
MACHINES AND MECHANISMS
Oulu, Finland, June 20–24, 1999

THE EFFECT OF DATA-SET CARDINALITY ON THE DESIGN AND STRUCTURAL ERRORS OF FOUR-BAR FUNCTION-GENERATORS

M.J.D. Hayes, K. Parsa, J. Angeles
McGill University, Department of Mechanical Engineering and Centre for Intelligent Machines,
817 Sherbrooke W., Montreal, Quebec, H3A 2K6 Canada.
email: *johnh@cim.mcgill.ca, kourosh@cim.mcgill.ca, angeles@cim.mcgill.ca*

Keywords: approximate kinematic synthesis, design, structural error, function-generators.

1 Introduction

Design and structural errors are important performance indicators in the assessment and optimisation of function-generating linkages arising by means of approximate synthesis. The design error indicates the error residual incurred by a specific linkage regarding the verification of the synthesis equations. The structural error, in turn, is the difference between the prescribed linkage output and the actual generated output for a given input value [Tinubu and Gupta 1984]. From a design point of view it may be successfully argued that the structural error is the one that really matters, for it is directly related to the performance of the linkage.

The main goal of this paper is to demonstrate that, as the data-set cardinality increases, the Euclidean norms of the design and structural errors converge. The important implication is that the minimisation of the Euclidean norm of the structural error can be accomplished indirectly via the minimisation of the corresponding norm of the design error, provided that a suitably large number of input-output (I/O) pairs is prescribed. Note that the minimisation of the Euclidean norm of the design error leads to a linear least-square problem whose solution can be obtained directly [Wilde 1982], while the minimisation of the same norm of the structural error leads to a nonlinear least-squares problem, and hence, calls for an iterative solution [Tinubu and Gupta 1984].

2 Procedure

The synthesis problem of four-bar function-generators consists of determining all relevant design parameters such that the mechanism can produce a prescribed set of m input-output (I/O) pairs, $\{\psi_i, \phi_i\}_1^m$, where ψ_i and ϕ_i represent the i^{th} input and output variables, respectively, and m is the cardinality of the data-set.

Let n be the number of independent design parameters required to characterise the mechanism. For planar $RRRR$ linkages, $n = 3$ [Freudenstein 1955], while for spherical $RRRR$ linkages $n = 4$ [Hartenberg and Denavit 1964]. For spatial $RCCC$ function-generators, the issue is not as straightforward. The output of this type of linkage consists of both angular and translational displacements, although they are coupled. If we only consider the angular output, which is necessary if comparisons are to be made with the other two for generating identical functions, then $n = 4$ [Liu 1993].

Approximate synthesis problems involve sets of I/O equations such that $m > n$. If $m = n$, the problem is termed *exact synthesis* and may be considered a special case of the former [Liu and Angles 1992]. The optimisation problem of four-bar function-generators usually involves the approximate solution of an overdetermined linear system of equations with the minimum error. The I/O equations can be written in the form

$$\mathbf{Sk} = \mathbf{b}, \tag{1}$$

where $\mathbf{S}$ is the $m \times n$ *synthesis matrix*, $\mathbf{b}$ is an m-dimensional vector, whereas $\mathbf{k}$ is the n-dimensional vector of design variables, usually called the *Freudenstein parameters* as they were first introduced in [Freudenstein 1955] for the synthesis of planar four-bar linkages. Moreover, the i^{th} row of $\mathbf{S}$, $\mathbf{s}_i^T$, and the i^{th} component of $\mathbf{b}$, b_i, are functions of ψ_i and ϕ_i only. For the planar $RRRR$ mechanism:

$$\mathbf{s}_i^T = [\ 1 \quad \cos\phi_i \quad -\cos\psi_i\ ], \quad i = 1, ..., m, \tag{2}$$

$$b_i = [\ \cos(\psi_i - \phi_i)\ ], \quad i = 1, ..., m, \tag{3}$$

$$\mathbf{k} = [\ k_1 \quad k_2 \quad k_3\ ]^T. \tag{4}$$

For the spherical $RRRR$ mechanism:

$$\mathbf{s}_i^T = [\ 1 \quad -\cos\phi_i \quad \cos\psi_i \quad \cos\phi_i\cos\psi_i\ ], \quad i = 1, ..., m, \tag{5}$$

$$b_i = [\ -\sin\psi_i \sin\phi_i\ ], \quad i = 1, ..., m, \tag{6}$$

$$\mathbf{k} = [\ k_1 \quad k_2 \quad k_3 \quad k_4\ ]^T. \tag{7}$$

For the spatial $RCCC$ mechanism:

$$\mathbf{s}_i^T = [\ 1 \quad \sin\phi_i \quad \sin\psi_i \quad \sin\phi_i\sin\psi_i\ ], \quad i = 1, ..., m, \tag{8}$$

$$b_i = [\ \cos\psi_i\cos\phi_i\ ], \quad i = 1, ..., m, \tag{9}$$

$$\mathbf{k} = [\ k_1 \quad k_2 \quad k_3 \quad k_4\ ]^T. \tag{10}$$

These synthesis equations are linear in the components of $\mathbf{k}$. This matrix form has obvious representational advantages, but more importantly, it allows us to determine values of the I/O dial zeros, α and β, that will best condition the synthesis matrix, $\mathbf{S}$ [Liu and Angeles 1993]. Here, we regard the I/O pairs as a set of incremental angular changes, $\{\Delta\psi_i\ \Delta\phi_i\}_1^m$. The I/O data set is then

$$\psi_i = \alpha + \Delta\psi_i, \quad \phi_i = \beta + \Delta\phi_i \quad i = 1, \ldots, m. \tag{11}$$

The Nelder-Mead *downhill simplex algorithm in multi-dimensions* [Liu and Angeles 1993] is employed to estimate the optimal values for α and β. It should be mentioned that, while changing the dial zeros of the I/O angles improves the condition number, κ, of planar $RRRR$, spherical $RRRR$ and spatial $RCCC$ linkages, this method does not always work for spatial $RSSR$ linkages [Liu and Angeles 1993].

When $m > n$ there is, in general, no $\mathbf{k}$ which will exactly satisfy all the equations. There are two well established indicators to assess the approximation error, namely the design and structural errors. We define the design error vector $\mathbf{d}$ as

$$\mathbf{d} \equiv \mathbf{Sk} - \mathbf{b}. \tag{12}$$

The Freudenstein parameters, $\mathbf{k}$, may be optimised by minimising the Euclidean norm of $\mathbf{d}$. The scalar objective function is

$$z \equiv \frac{1}{2}(\mathbf{d}^T\mathbf{W}\mathbf{d}), \tag{13}$$

which must be minimised over $\mathbf{k}$. The scalar quantity $\mathbf{d}^T\mathbf{W}\mathbf{d}$ is the weighted Euclidean norm of $\mathbf{d}$. The matrix $\mathbf{W}$ is a diagonal matrix of positive weighting factors, which can be used to make some of the data points affect the minimisation more, or less, than others, depending on their relative importance to the design. For the sake of simplicity $\mathbf{W}$ will be set equal to the identity matrix in this article, $\mathbf{d}^T\mathbf{W}\mathbf{d}$ being indicated by $\|\mathbf{d}\|_2$.

The quantity $\|\mathbf{d}\|_2$ can be minimised, in a least squares sense, very efficiently by transforming $\mathbf{S}$ using Householder reflections [Golub and Van Loan 1989], the Moore-Penrose generalised inverse thus not being explicitly computed. Design error minimisation is therefore a linear problem; a desirable trait, indeed. Unfortunately, as a performance indicator, the design error is not directly related to the I/O performance of the function-generator.

Alternatively we may approach the optimisation problem by minimising the same norm of the structural error. Since this error is defined as the difference between the generated and prescribed outputs for a given input, it is directly related to function-generator performance. Let the structural error vector $\mathbf{s}$ be defined as

$$\mathbf{s} \equiv \begin{bmatrix} \varphi_1 - \phi_1 \\ \vdots \\ \varphi_m - \phi_m \end{bmatrix}, \tag{14}$$

where φ_i is the generated value of the output ϕ attained at $\psi = \psi_i$, and ϕ_i is, as defined earlier, the prescribed value of the output angle at $\psi = \psi_i$. It can be shown that the structural and design errors are related by

$$\mathbf{d} = \mathbf{d}(\mathbf{s}) \equiv \mathbf{S}\mathbf{k} - \mathbf{b}, \tag{15}$$

where $\mathbf{d}$ is a nonlinear function of $\mathbf{s}$ [Tinubu and Gupta 1984]. Hence, it is evident that minimising $\|\mathbf{d}\|_2$ is not equivalent to minimising the Euclidean norm of the structural error, $\|\mathbf{s}\|_2$.

To minimise the Euclidean norm of this error, the iterative Gauss-Newton procedure is employed. The conditions under which the procedure converges in the neighbourhood of a minimum are discussed in [Dahlquist and Björck 1969]. In this case, the scalar objective function to be minimised over $\mathbf{k}$ is

$$\zeta \equiv \frac{1}{2}(\mathbf{s}^T\mathbf{W}\mathbf{s}). \tag{16}$$

Here, again, $\mathbf{W}$ is set equal to the identity matrix, the weighted Euclidean norm being indicated by $\|\mathbf{s}\|_2$.

We start with an initial guess for the Freudenstein parameters that minimise the Euclidean norm of the design error, and modify the guess until the normality condition,

$$\frac{\partial \zeta}{\partial \mathbf{k}} = \mathbf{0}, \tag{17}$$

is satisfied to a specified tolerance, ϵ, such that

$$\frac{\partial \zeta}{\partial \mathbf{k}} < \epsilon, \quad \text{for } \epsilon > 0. \tag{18}$$

We do not actually evaluate the normal equations, since they are typically ill-conditioned. Rather, we proceed in the following way: the i^{th} I/O equation is a function of ψ_i, ϕ_i and the Freudenstein parameters, $\mathbf{k}$, and may be written as

$$f_i(\psi_i, \phi_i; \mathbf{k}) = 0. \tag{19}$$

The Jacobian of $\mathbf{f}$ with respect to the vector of output values, $\boldsymbol{\phi}$, is the following diagonal matrix:

$$\frac{\partial \mathbf{f}}{\partial \boldsymbol{\phi}} \;=\; \mathrm{diag}\left(\frac{\partial f_1}{\partial \phi_1}, \ldots, \frac{\partial f_m}{\partial \phi_m}\right) \;\equiv\; \mathbf{D}. \tag{20}$$

If we regard Eq. (19) as a function of only ϕ_i we can write

$$\boldsymbol{\phi}(\mathbf{k}) \;=\; \boldsymbol{\phi}. \tag{21}$$

However, we want

$$\boldsymbol{\phi}(\mathbf{k}) \;=\; \boldsymbol{\varphi}. \tag{22}$$

Assume we have an approximation to $\mathbf{k}_{\mathrm{opt}}$, which we call $\mathbf{k}^{\nu}$, obtained from the ν^{th} iteration. We now require a correction vector, $\Delta\mathbf{k}$, so that

$$\boldsymbol{\phi}(\mathbf{k}^{\nu} + \Delta\mathbf{k}) \;=\; \boldsymbol{\varphi}. \tag{23}$$

It can be shown [Dahlquist and Björck 1969], after expanding the left-hand side of Eq. (23) in series, and ignoring higher order terms, that

$$\boldsymbol{\phi}(\mathbf{k}^{\nu}) - \boldsymbol{\varphi} \;=\; \mathbf{D}^{-1}\mathbf{S}\Delta\mathbf{k}, \tag{24}$$

the left-hand side of Eq. (24) being $-\mathbf{s}^{\nu}$. Now we find $\Delta\mathbf{k}$ as the least-square approximation of Eq. (24). It can be proven that $\Delta\mathbf{k} \approx \mathbf{0}$ implies $\partial\zeta/\partial\mathbf{k} \approx \mathbf{0}$, which means that we can satisfy the normality condition without evaluating it explicitly.

We show with one example below that, as the cardinality m of the data points increases, the design and structural errors converge.

3 Example

We synthesise here a planar $RRRR$, a spherical $RRRR$ and a spatial $RCCC$ four-bar mechanism to generate a quadratic function for an input range of $0^{\circ} \leq \Delta\psi \leq 60^{\circ}$, namely,

$$\Delta\phi_i \;=\; \frac{9\Delta\psi_i^2}{8\pi}. \tag{25}$$

For each mechanism the I/O dial zeros (α, β) are selected to minimise the condition number κ of $\mathbf{S}$ for each data-set [Liu and Angeles 1993]. Then both the design and structural errors are determined for the linkages that minimise the respective Euclidean norms for data-sets with cardinalities of $m = \{10, 40, 70, \text{ and } 100\}$. These results are listed in Tables 1–4. Finally the structural errors, corresponding to $m = 40$, of the linkages that minimise the Euclidean norms of the design and structural errors are graphically displayed in Fig. 1.

Table 1: Results for $m = 10$.

	Planar $RRRR$	Spherical $RRRR$	Spatial $RCCC$
α_{opt} (deg.)	123.8668	43.3182	-46.6817
β_{opt} (deg.)	91.7157	89.5221	-0.4781
κ_{opt}	33.2974	200.5262	200.5262
$\|\mathbf{d}\|_2$	7.273×10^{-3}	7.60×10^{-4}	7.60×10^{-4}
$\|\mathbf{s}\|_2$	5.965×10^{-3}	4.17×10^{-4}	4.17×10^{-4}

Table 2: Results for $m = 40$.

	Planar $RRRR$	Spherical $RRRR$	Spatial $RCCC$
α_{opt} (deg.)	117.4593	42.7696	-47.2301
β_{opt} (deg.)	89.4020	88.8964	-1.1037
κ_{opt}	32.5549	203.0317	203.0317
$\|\mathbf{d}\|_2$	1.571×10^{-2}	1.887×10^{-3}	1.887×10^{-3}
$\|\mathbf{s}\|_2$	1.502×10^{-2}	1.057×10^{-3}	1.057×10^{-3}

Table 3: Results for $m = 70$.

	Planar $RRRR$	Spherical $RRRR$	Spatial $RCCC$
α_{opt} (deg.)	116.4699	42.7014	-47.2987
β_{opt} (deg.)	89.0488	88.8045	-1.1956
κ_{opt}	32.5242	204.7696	204.7696
$\|\mathbf{d}\|_2$	2.088×10^{-2}	2.536×10^{-3}	2.536×10^{-3}
$\|\mathbf{s}\|_2$	2.040×10^{-2}	1.423×10^{-3}	1.423×10^{-3}

Table 4: Results for $m = 100$.

	Planar $RRRR$	Spherical $RRRR$	Spatial $RCCC$
α_{opt} (deg.)	116.0679	42.6740	-47.3261
β_{opt} (deg.)	88.9057	88.7674	-1.2326
κ_{opt}	32.5170	205.5603	205.5603
$\|\mathbf{d}\|_2$	2.499×10^{-2}	3.047×10^{-3}	3.047×10^{-3}
$\|\mathbf{s}\|_2$	2.464×10^{-2}	1.712×10^{-3}	1.712×10^{-3}

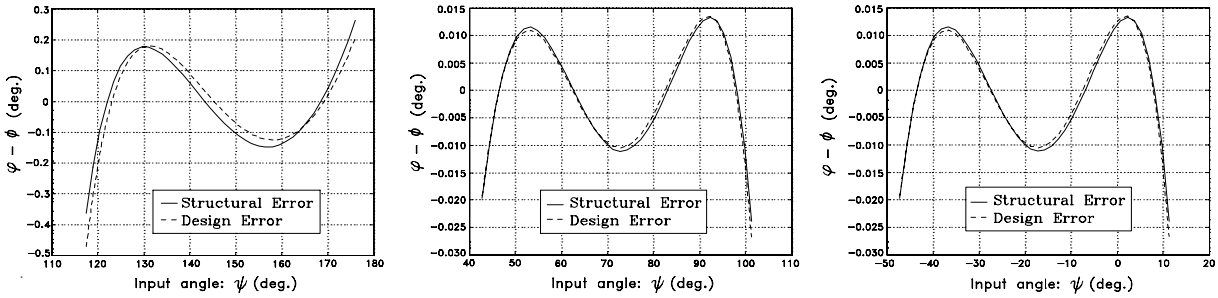

Figure 1. Structural error comparison for *(i)* planar, *(ii)* spherical $RRRR$ and *(iii)* spatial $RCCC$ mechanisms minimising $\|\mathbf{s}\|_2$ & $\|\mathbf{d}\|_2$.

4 Discussion and Conclusions

Examining Tables 1–4, it can be seen that $\|\mathbf{d}\|_2$ and $\|\mathbf{s}\|_2$ increase with m for each mechanism. The trend for the planar $RRRR$ is towards convergence. It is interesting to note that the error results are identical for the spherical $RRRR$ and the spatial $RCCC$ linkages, except that α_{opt} and β_{opt} are different. In a sense, this is not surprising because of the symmetrical nature of the function in the $\psi - \phi$ plane. Moreover, the synthesis equations for these two linkages are, with the exception of sign, trigonometric complements in the form considered in this article. However, compared to the planar $RRRR$, we see

the errors converge near $m = 40$, but then diverge again for higher values of m. Fig. 1 shows the close agreement of the respective structural error curves for $m = 40$. In all cases treated, a number of prescribed I/O values of at least $m = 10$ is sufficient for the minimisation of the Euclidean norm of the design error to lead to the same norm of the structural error within a reasonable difference.

These results support our hypothesis that for a suitably large data-set cardinality linkage optimisation using design and structural error based objective functions result in virtually identical function-generating mechanisms. The obvious weakness is that the cardinality of the data-set for which convergence is obtained is not known *a priori*. Nonetheless, further pursuit of this result is worthwhile because of its computational simplicity.

5 Acknowledgements

The support of Canada's Natural Sciences and Engineering Research Council through a research grant to the third author and a graduate fellowship to the first author is highly acknowledged.

References:

Tinubu, S.O. and Gupta, K.C., Optimal Synthesis of Function Generators Without the Branch Defect, ASME, J. of Mech., Trans., and Autom. in Design, Vol. 106, Sept. 1984, pp. 348–354.

Wilde, D.J., Error Linearization in the Least-Squares Design of Function Generating Mechanisms, ASME, J. of Mech., Des., Vol. 104, Oct. 1982, pp. 881–884.

Freudenstein, F., Approximate Synthesis of Four-Bar Linkages, Trans. ASME, Vol. 77, Aug. 1955, pp. 853-861.

Hartenberg, R.S. and Denavit, J., Kinematic Synthesis of Linkages, McGraw-Hill Book Co., New York, N.Y., U.S.A., 1964.

Liu, Z., Kinematic Optimization of Linkages, Ph.D. Thesis, Dept. of Mech. Eng., McGill University, Montreal, Canada, 1993.

Liu, Z. and Angeles, J., Least-Square Optimization of Planar and Spherical Four-Bar Function Generator Under Mobility Constraints, ASME, J. of Mech. Des., Vol. 114, Dec. 1992, pp. 569–573.

Liu, Z. and Angeles, J., Data Conditioning in the Optimization of Function-Generating Linkages, ASME, Adv. in Design Auto., DE-Vol 65-1, Vol. 1, 1993, pp. 419–425.

Golub, G.H. and Van Loan, C.F., Matrix Computations, The Johns Hopkins University Press, Baltimore, U.S.A., 1989.

Dahlquist, G. and Björck, Å., Numerical Methods, translated by Anderson, N., Prentice-Hall, Inc., 1969, pp. 248–251, 442–446.

Mechanism and Machine Theory 101 (2016) 158–167

Contents lists available at ScienceDirect

Mechanism and Machine Theory

journal homepage: www.elsevier.com/locate/mechmt

Continuous approximate synthesis of planar function-generators minimising the design error

Alexis Guigue[a], M. John D. Hayes[b,*]

[a] Softree Technical Systems Inc., Vancouver, British Columbia, Canada
[b] Mechanical and Aerospace Engineering, Carleton University, Ottawa, Ontario, Canada

ARTICLE INFO

Article history:
Received 3 December 2015
Received in revised form 17 March 2016
Accepted 18 March 2016
Available online 6 April 2016

Keywords:
Approximate and continuous
kinematic synthesis
Design error
Structural error
Function-generating linkage

ABSTRACT

It has been observed in the literature that as the cardinality of the prescribed discrete input–output data set increases, the corresponding four-bar linkages that minimise the Euclidean norm of the design and structural errors tend to converge to the same linkage. The important implication is that minimising the Euclidean norm, or any p-norm, of the structural error, which leads to a nonlinear least-squares problem requiring iterative solutions, can be accomplished implicitly by minimising that of the design error, which leads to a linear least-squares problem that can be solved directly. Apropos, the goal of this paper is to take the first step towards proving that as the cardinality of the data set tends towards infinity the observation is indeed true. In this paper we will integrate the synthesis equations in the range between minimum and maximum input values, thereby reposing the discrete approximate synthesis problem as a continuous one. Moreover, we will prove that a lower bound of the Euclidean norm, and indeed of any p-norm, of the design error for planar RRRR function-generating linkages exists and is attained with continuous approximate synthesis.

1. Introduction

Design and structural errors are important performance indicators in the assessment and optimisation of function-generating linkages arising by means of approximate synthesis. The *design error* indicates the error residual incurred by a specific linkage in satisfying its synthesis equations. The *structural error*, in turn, is the difference between the prescribed linkage output value and the actual generated output value for a given input value [1]. From a design point of view it may be successfully argued that the structural error is the one that really matters, for it is directly related to the performance of the linkage.

It was shown in Ref. [2] that as the cardinality of the prescribed discrete input–output (I/O) data-set increases, the corresponding linkages that minimise the Euclidean norms of the design and structural errors tend to converge to the same linkage. The important implication of this observation is that the minimisation of the Euclidean norm of the structural error can be accomplished indirectly via the minimisation of the corresponding norm of the design error, provided that a suitably large number of I/O pairs is prescribed. The importance arises from the fact that the minimisation of the Euclidean norm of the design error leads to a linear least-squares problem whose solution can be obtained directly as opposed to iteratively [3,4], while the minimisation of the same norm of the structural error leads to a nonlinear least-squares problem, and hence, calls for an iterative solution [1].

* Corresponding author.
E-mail address: John.Hayes@carleton.ca (M. Hayes).

http://dx.doi.org/10.1016/j.mechmachtheory.2016.03.012
0094-114X/

Several issues have arisen in the design error minimisation of four-bar linkages. First, the condition number of the synthesis matrix may lead to design parameters that poorly approximate the prescribed function [5]. This problem can be addressed through careful selection of the I/O pairs used to generate the synthesis matrix. It has also been suggested to introduce dial zeros whose values are chosen to minimise the condition number of the synthesis matrix [6]. Second, the identified design parameters have a dependence on the I/O set cardinality. As the number of I/O pairs grows, the magnitude of the design error tends to converge to a lower bound. Hence, the I/O set cardinality might be fixed as soon as the magnitude of the design error reaches some pre-defined minimum value [2].

Diverse interesting and useful optimisation strategies have been proposed recently for structural error minimisation in planar four-bar function-generators. For example, in Ref. [7] the authors define the least squares error between the desired and generated functions as the objective function for a sequential quadratic programming (SQP) approach. The proposed method solves a sequence of optimisation subproblems, each of which optimises a quadratic model of the objective function subject to a linearisation of the constraints based on the distribution of a finite set of precision points. Another novel approach which considers the minimisation of the structural error of the link lengths is described in Ref. [8]. The method treats one of the dyads as having fixed distances between joint centres, while the other dyad has links of variable length. The adjustable link lengths are varied using a discrete set of precision points as benchmarks. A completely different approach is used in Ref. [9] to develop a probabilistic, time-dependent function-generator synthesis method. The authors introduce the concept of "interval reliability synthesis". The dimensions of the link lengths are treated as random variables while their mean values become the design variables, and the probability of failure to produce the function within a prescribed tolerance is minimised over a defined time interval and corresponding position level interval of the function. While these methods achieve excellent results, they do not shed any light on the curious tendency observed in Ref. [2]. What the vast body of literature reporting investigations into function-generator synthesis optimisation is missing is a systematic study of what the implications are of allowing the cardinal number of the I/O data set to tend towards infinity.

Hence, the goal of this paper is to take the first step towards proving that the convergence observed in Ref. [2] is true for planar four-bar function-generators. More precisely, a proof will be given for the design error that as the cardinality of the I/O data set increases from discrete numbers of I/O pairs to an infinite number between minimum and maximum pairs that a lower bound for any p-norm of the design error exists, and corresponds to that of the infinite I/O set, thereby changing the discrete approximate synthesis problem to a continuous approximate synthesis problem. To this end, the design error minimisation occurs in the space of a continuous function possessing an L_p norm defined later in this paper. However, our study is currently restricted to the planar RRRR function-generating linkage, where R denotes *revolute joint*, synthesised using the kinematic model defined in Ref. [10].

2. Design error minimisation: the discrete approximate approach

The synthesis problem of planar four-bar function-generators consists of determining all relevant design parameters such that the mechanism can produce a prescribed finite set of m I/O pairs, $\{\psi_i, \varphi_i\}_1^m$, where ψ_i and φ_i represent the i^{th} input and output variables, respectively, and m is the cardinality of the finite data-set. We define n to be the number of independent design parameters required to fully characterise the mechanism. For planar RRRR linkages, $n = 3$ [10]. If $m = n$, the problem is termed *exact synthesis* and may be considered a special case of approximate synthesis where $m > n$.

We consider the optimisation problem of planar four-bar function-generators as the approximate solution of an overdetermined linear system of equations with the least error. The synthesis equations that are used to establish the linear system for a four-bar function-generator are the *Freudenstein equations* [10]. Consider the mechanism in Fig. 1. The i^{th} configuration is governed by:

$$k_1 + k_2 \cos(\varphi_i) - k_3 \cos(\psi_i) = \cos(\psi_i - \varphi_i), \tag{1}$$

where the k's are the *Freudenstein parameters* , which are the following link length ratios:

$$k_1 = \frac{(a_1^2 + a_2^2 + a_4^2 - a_3^2)}{2a_2a_4}; \quad k_2 = \frac{a_1}{a_2}; \quad k_3 = \frac{a_1}{a_4}. \tag{2}$$

Given a set of three Freudenstein parameters, the corresponding set of link lengths, scaled by a_1, are:

$$a_1 = 1; \quad a_2 = \frac{1}{k_2}; \quad a_4 = \frac{1}{k_3}; \quad a_3 = (1 + a_2^2 + a_4^2 - 2a_2a_4k_1)^{1/2}. \tag{3}$$

The finite set of I/O equations can be written in the following form, using Eq. (1)

$$\mathbf{Sk} = \mathbf{b}, \tag{4}$$

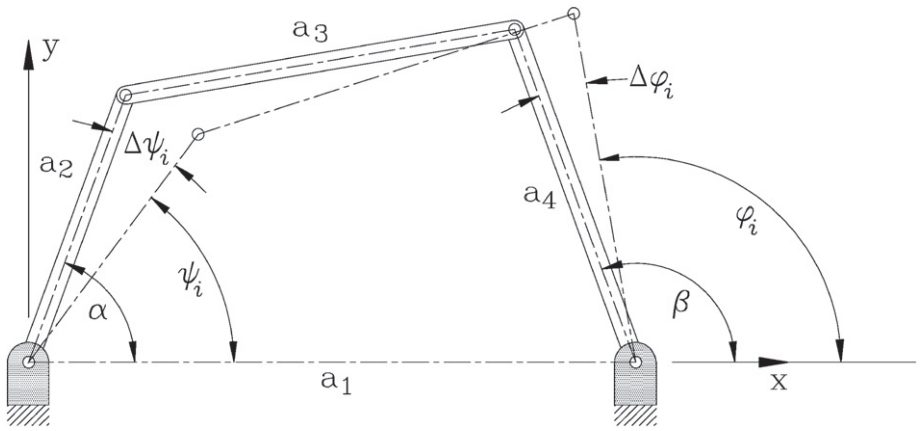

Fig. 1. A four-bar linkage in two configurations.

where $\mathbf{S}$ is the $m \times 3$ *synthesis matrix*, whose i^{th} row is the 1×3 array $\mathbf{s}_i$, $\mathbf{b}$ is an m-dimensional vector, whereas $\mathbf{k}$ is the 3-dimensional vector of design variables called the *Freudenstein parameters* [10]. For the planar RRRR mechanism we have:

$$\mathbf{s}_i = [1 \cos\varphi_i - \cos\psi_i], \quad i = 1, \ldots, m, \tag{5}$$

$$b_i = \cos(\psi_i - \varphi_i), \quad i = 1, \ldots, m, \tag{6}$$

$$\mathbf{k} = [k_1 k_2 k_3]^T. \tag{7}$$

The synthesised linkage will only be capable of generating the desired function approximately. The design error is the algebraic difference of the left-hand side of Eq. (4) less the right-hand side. Because we will be comparing errors associated with different cardinalities, we now include the cardinality m in the definition. The m-dimensional design error vector $\mathbf{d}_m$ for a finite discrete set of $m > 3$ I/O pairs, $\{(\psi_i, \varphi_i)_{i=1\ldots m}\}$, is defined as:

$$\mathbf{d}_m = \mathbf{S}_m \mathbf{k} - \mathbf{b}_m. \tag{8}$$

If the output values prescribed by the functional relationship, $\varphi_{pres,i}$, correspond precisely to the output values generated by the mechanism, i.e., $\varphi_{gen,i}$, then, $\| \mathbf{d}_m \| = 0$. However, for a general prescribed function $\varphi_{pres}(\psi)$, $\| \mathbf{d}_m \| \neq 0$ and we seek the Freudenstein parameter vector that minimises the norm of the design error vector. In general, the weighted Euclidian norm is used:

$$\| \mathbf{d}_m \|^2_{\mathbf{W}_m,2} = \frac{1}{2} \quad \mathbf{d}_m^T \mathbf{W}_m \mathbf{d}_m, \tag{9}$$

where $\mathbf{W}_m$ is an $m \times m$ diagonal matrix with strictly positive elements. In a typical design problem, $\mathbf{W}_m$ is used to adjust the impact on the optimisation of specific I/O pairs. However, for the purposes of this work, $\mathbf{W}_m$ will be set to the identity matrix, $\mathbf{I}_m$. The optimal Freudenstein parameters $\mathbf{k}^*_m$ for this norm are:

$$\mathbf{k}^*_m = \mathbf{S}^+_m \mathbf{b}_m, \tag{10}$$

where $\mathbf{S}^+_m$ is the Moore–Penrose generalised inverse of the synthesis matrix, and the corresponding minimal design error is:

$$\rightarrow \min_{\mathbf{k}} \| \mathbf{d}_m \|_2 = \| \mathbf{d}^*_m \|_2 = \| (\mathbf{I}_m - \mathbf{S}_m \mathbf{S}^+_m) \mathbf{b}_m \|_2. \tag{11}$$

In general, for any matrix, square or rectangular, the condition number κ is a measure of how invertible the matrix is: it is the ratio of the largest to smallest singular values. Consider the system of linear equations represented by $\mathbf{Ax} = \mathbf{b}$. The matrix $\mathbf{A}$ may be viewed as a map from vector space $\mathbf{x}$ to vector space $\mathbf{b}$. A very large condition number of $\mathbf{A}$ implies that the smallest singular value of the matrix is very small, meaning that $\mathbf{b}$ is poorly approximated by $\mathbf{Ax}$. This also implies that $\mathbf{A}^{-1}\mathbf{b}$ very poorly approximates $\mathbf{x}$. Extremely large condition numbers indicate that there is a near linear dependency among some of the rows of $\mathbf{A}$, meaning that one, or more, of its singular values is very close to zero. Such matrices are termed ill-conditioned. The

condition number κ is a property of the matrix **A** and entirely independent of the vector spaces **x** and **b**. For numerical stability considerations, it is always desirable to have a well-conditioned synthesis matrix, otherwise the numerical values of $\mathbf{S}_m^+$ may be significantly distorted by very small singular values, or singular values identically equal to zero, leading to optimised **k** that imply a mechanism which very poorly approximates the function. Hence, the dial zeros α and β, illustrated in Fig. 1, have been introduced to minimise the condition number, κ, of $\mathbf{S}_m$:

$$\psi_i = \alpha + \Delta\psi_i; \quad \varphi_i = \beta + \Delta\varphi_i. \tag{12}$$

When the dial zeros are substituted into Eq. (1), the synthesis equation becomes:

$$k_1 + k_2\cos(\beta + \Delta\varphi_i) - k_3\cos(\alpha + \Delta\psi_i) = \cos(\alpha + \Delta\psi_i - \beta - \Delta\varphi_i), \tag{13}$$

and, the I/O pairs are regarded as a discrete set of incremental angular changes $\{(\Delta\psi_i, \Delta\varphi_i)_{i=0..m}\}$. The arrays $\mathbf{d}_m^*$, $\mathbf{k}_m^*$ and $\mathbf{S}_m$ are now also functions of the dial zeros. With this modification, the design error minimisation problem can be efficiently solved in a least squares sense in two steps:

1. determine the dial zeros to minimise the condition number $\kappa_m(\alpha, \beta)$ of the synthesis matrix $\mathbf{S}_m$;
2. determine the corresponding optimal Freudenstein parameters using Eq. (10).

3. Design error minimisation: the continuous approximate approach

A major issue associated with the discrete approach to the design error minimisation is the appropriate choice for the cardinality of the discrete I/O pair data set such that the minimisation of the structural error is implied. Indeed, the choice of m depends on the prescribed function $\Delta\varphi_{pres}(\Delta\psi)$ and m is generally fixed when some level of convergence is observed. For the example used in Ref. [2] $m = 40$ was observed to be a good choice. We now propose to evaluate the design error over the continuous range between minimum and maximum, or initial and final, input values of the prescribed function, denoted $[\Delta\psi_0, \Delta\psi_f]$. We only consider functions that are continuous over $[\Delta\psi_0, \Delta\psi_f]$, that are defined in a function space, denoted $\mathcal{C}^0([\Delta\psi_0, \Delta\psi_f])$, whereupon the following L_p-norm has been defined for any continuous function f on the closed interval $[\Delta\psi_0, \Delta\psi_f]$:

$$\forall f \in \mathcal{C}^0([\Delta\psi_0, \Delta\psi_f]), \|f\|_p = \left(\int_{\Delta\psi_0}^{\Delta\psi_f} |f(\psi)|^p d\psi\right)^{1/p}, \tag{14}$$

where p is an integer such that $p \geq 1$. Imposing the L_p-norm upon this function space makes $\mathcal{C}^0([\Delta\psi_0, \Delta\psi_f])$ an L_p-space. Such L_p-spaces are defined using a generalisation of the vector norm for finite-dimensional vector spaces [4]. Vector norms are special cases of the family of L_p-norms, often denoted by l_p while L_p is reserved for norms in function spaces [4]. The most common L_p-norms for a continuous function f on a closed interval $[a, b]$, and in fact, the most commonly used vector norms [11], are the *maximum* or *Chebyshev* norm, the Euclidean norm, and the so called Manhattan norm[1] which are respectively defined by:

$$\|f\|_\infty = \max_{x\in[a,b]} |f(x)|; \tag{15}$$

$$\|f\|_2 = \left(\int_a^b f(x)^2 dx\right)^{1/2}; \tag{16}$$

$$\|f\|_1 = \int_a^b |f(x)| dx. \tag{17}$$

The Manhattan and Chebyshev norms are the limiting cases ($p = 1$ and $p = \infty$, respectively) of the family of L_p-norms [4]. The L_p-norms obey the following relationship:

$$\|f\|_\infty \leq \cdots \leq \|f\|_2 \leq \|f\|_1. \tag{18}$$

Typically, the most appropriate norm must be selected to evaluate the magnitude of the objective function for the error minimisation, given a function that is to be approximated by the resulting linkage. However, it turns out that Lawson's

[1] The term Manhattan norm arises because the vector norm corresponds to sums of distances along the basis vector directions, as one would travel along a rectangular street plan.

algorithm [12,13] can be used to sequentially minimise the Chebyshev norm via the minimisation of the Euclidean norm [14]. This means that the continuous approximate approach to the design error minimisation is independent of the L_p-norm because it applies to both the Chebyshev and Euclidean norms, and hence all intermediate ones. Therefore, without loss in generality the Euclidean norm will be used in the example in Section 5, which follows the development of the approach.

Assuming that the prescribed function belongs to $\mathcal{C}^0([\Delta\psi_0, \Delta\psi_f])$, the design error is defined using the Euclidean norm, though any L_p-norm could be used [14]:

$$\| \mathbf{d}(\alpha,\beta)\|_2 = \left(\int_{\Delta\psi_0}^{\Delta\psi_f} (k_1 + k_2\cos(\beta+\Delta\varphi) - k_3\cos(\alpha+\Delta\psi) - \cos(\alpha+\Delta\psi-\beta-\Delta\varphi))^2 d\Delta\psi \right)^{\frac{1}{2}}. \tag{19}$$

After some algebraic manipulation, it can be shown that the square of Eq. (19) is a quadratic function in terms of the Freudenstein parameters:

$$\| \mathbf{d}(\alpha,\beta) \|_2^2 = \mathbf{k}^T\mathbf{A}(\alpha,\beta)\mathbf{k} - 2\mathbf{e}(\alpha,\beta)^T\mathbf{k} + c(\alpha,\beta). \tag{20}$$

The matrix $\mathbf{A}(\alpha,\beta)$ is a 3 × 3 a symmetric positive semidefinite matrix whose six distinct elements a_{ij} are:

$$\begin{aligned}
a_{11} &= \int_{\Delta\psi_0}^{\Delta\psi_f} d\Delta\psi = \Delta\psi_f - \Delta\psi_0;\\
a_{12} &= \int_{\Delta\psi_0}^{\Delta\psi_f} \cos(\beta+\Delta\varphi)d\Delta\psi;\\
a_{13} &= -\int_{\Delta\psi_0}^{\Delta\psi_f} \cos(\alpha+\Delta\psi)d\Delta\psi;\\
a_{22} &= \int_{\Delta\psi_0}^{\Delta\psi_f} \cos^2(\beta+\Delta\varphi)d\Delta\psi\\
a_{23} &= -\int_{\Delta\psi_0}^{\Delta\psi_f} \cos(\beta+\Delta\varphi)\cos(\alpha+\Delta\psi)d\Delta\psi\\
a_{33} &= \int_{\Delta\psi_0}^{\Delta\psi_f} \cos^2(\alpha+\Delta\psi)d\Delta\psi;
\end{aligned}$$

while $\mathbf{e}(\alpha,\beta)$ is a 3-dimensional vector whose elements are:

$$\begin{aligned}
e_1 &= \int_{\Delta\psi_0}^{\Delta\psi_f} \cos(\alpha+\Delta\psi-\beta-\Delta\varphi)d\Delta\psi;\\
e_2 &= \int_{\Delta\psi_0}^{\Delta\psi_f} (\cos(\beta+\Delta\varphi)\cos(\alpha+\Delta\psi-\beta-\Delta\varphi))d\Delta\psi;\\
e_3 &= -\int_{\Delta\psi_0}^{\Delta\psi_f} (\cos(\alpha+\Delta\psi)\cos(\alpha+\Delta\psi-\beta-\Delta\varphi))d\Delta\psi;
\end{aligned}$$

and finally $c(\alpha,\beta)$ is a scalar having the form:

$$c = \int_{\Delta\psi_0}^{\Delta\psi_f} \cos^2(\alpha+\Delta\psi-\beta-\Delta\varphi)d\Delta\psi.$$

When $\mathbf{A}(\alpha,\beta)$ is positive definite, the optimal Freudenstein parameters $\mathbf{k}^*(\alpha,\beta)$ which minimise $\| \mathbf{d}(\alpha,\beta) \|_2^2$ (or equivalently $\|\mathbf{d}(\alpha,\beta) \|_2$) are:

$$\mathbf{k}^*(\alpha,\beta) = \mathbf{A}^{-1}(\alpha,\beta)\mathbf{e}(\alpha,\beta), \tag{21}$$

and the square of the minimal design error is:

$$\min_{\mathbf{k}} \| \mathbf{d}(\alpha,\beta) \|_2^2 = \| \mathbf{d}^*(\alpha,\beta) \|_2^2 = c(\alpha,\beta) - \mathbf{e}(\alpha,\beta)^T\mathbf{A}^{-1}(\alpha,\beta)\mathbf{e}(\alpha,\beta). \tag{22}$$

The assumption of positive definiteness for $\mathbf{A}(\alpha,\beta)$ will be discussed in Section 4. However, a necessary condition for $\mathbf{A}(\alpha,\beta)$ to be positive definite is that it is non-singular. This justifies *a posteriori* why we use the dial zeros. In this case, as in Section 2, the design error minimisation problem is solved in two steps:

1. determine the dial zeros to minimise the condition number $\kappa(\alpha,\beta)$ of $\mathbf{A}(\alpha,\beta)$;
2. determine the corresponding optimal Freudenstein parameters using Eq. (21).

Intuitively, the continuous approximate approach should correspond to the limit of the discrete approximate approach. This is proven to be so in the next section.

4. The design error of the discrete approximate approach is lower bounded by that of the continuous approximate approach

In this section, we assume that $\Delta\varphi_{pres}(\Delta\psi)$ is a continuously differentiable function, however Propositions 1, 2, and 3, which follow, only require continuity. With this assumption and using the notation introduced in the previous sections, the following propositions hold.

Proposition 1. *$\boldsymbol{A}(\alpha,\beta)$ is positive semidefinite, and*

$$\lim_{m\to\infty} \kappa_m(\alpha,\beta) = \kappa(\alpha,\beta).$$

Proposition 2. *If $\boldsymbol{A}(\alpha,\beta)$ possesses full rank, then,*

$$\lim_{m\to\infty} \mathbf{k}_m^*(\alpha,\beta) = \mathbf{k}^*(\alpha,\beta).$$

Recall that $\mathbf{k}^*(\alpha,\beta)$ minimises the design error under the condition that $\mathbf{A}(\alpha,\beta)$ is positive definite. Now, from Proposition 1, we can claim that $\mathbf{A}(\alpha,\beta)$ is at least positive semidefinite. However, the positive definitiveness is not guaranteed and it justifies the need for the assumption in Proposition 2.

Proposition 3. *If $\boldsymbol{A}(\alpha,\beta)$ possesses full rank, then,*

$$\lim_{m\to\infty} \frac{\Delta\psi_f - \Delta\psi_0}{m} \parallel \mathbf{d}_m^*(\alpha,\beta)\parallel_2 = \parallel \mathbf{d}^*(\alpha,\beta)\parallel_2.$$

Proposition 4. *Let (α^*,β^*) be the dial zero pair that minimises $\kappa(\alpha,\beta)$. If the optimal solution (α^*,β^*) is unique, then,*

$$\lim_{m\to\infty} (\alpha_m^*,\beta_m^*) = (\alpha^*,\beta^*).$$

Proposition 5. *If the optimal solution (α^*,β^*) is unique, then,*

$$\lim_{m\to\infty} \kappa_m(\alpha_m,\beta_m) = \kappa(\alpha^*,\beta^*).$$

Moreover, if $\boldsymbol{A}(\alpha^*,\beta^*)$ possesses full rank, then,

$$\lim_{m\to\infty} \mathbf{k}_m^*(\alpha_m,\beta_m) = \mathbf{k}^*(\alpha^*,\beta^*),$$

and

$$\lim_{m\to\infty} \frac{\Delta\psi_f - \Delta\psi_0}{m} \parallel \mathbf{d}_m^*(\alpha_m,\beta_m)\parallel_2 = \parallel \mathbf{d}^*(\alpha^*,\beta^*)\parallel_2.$$

Proposition 5 is our main result. It essentially states that the optimal Freudenstein parameters and the minimal design error for the discrete approach converge to the optimal Freudenstein parameters and the minimal design error for the continuous approach.

4.1. Proofs

Proof of Proposition 1. the proof of Proposition 1 requires the following result.

Proposition 6. *Let f be a continuous function on some interval*$[a,b]$, *then* [4]

$$\lim_{n\to+\infty}\sum_{i=0}^{n-1}\frac{b-a}{n}f(a+i\frac{b-a}{n})=\int_a^b f(x)dx.$$

From Proposition 6, the elements of $\mathbf{A}_m(\alpha,\beta)=\frac{\Delta\psi_f-\Delta\psi_0}{m}\mathbf{S}_m^T(\alpha,\beta)\mathbf{S}_m(\alpha,\beta)$ converge to the elements of $\mathbf{A}(\alpha,\beta)$.

Recall the definitions for positive definiteness and positive semidefiniteness: a real $n\times n$ matrix $\mathbf{A}$ is positive definite if, for all vectors $\mathbf{x}\in\mathbb{R}$, $\mathbf{x}^T\mathbf{A}\mathbf{x}>0$, and positive semidefinite if, for all vectors $\mathbf{x}\in\mathbb{R}$, $\mathbf{x}^T\mathbf{A}\mathbf{x}\geq 0$. Now, from the definitions of the elements a_{ij} of $\mathbf{A}(\alpha,\beta)$ we have

$$\mathbf{A}(\alpha,\beta)=\int_{\Delta\psi_0}^{\Delta\psi_f}\mathbf{B}d\Delta\psi, \tag{23}$$

where $\mathbf{B}$ is a symmetric 3×3 matrix:

$$\mathbf{B}=\begin{bmatrix}1 & \cos(\beta+\Delta\varphi) & -\cos(\alpha+\Delta\psi)\\ \cos(\beta+\Delta\varphi) & \cos^2(\beta+\Delta\varphi) & -\cos(\beta+\Delta\varphi)\cos(\alpha+\Delta\psi)\\ -\cos(\alpha+\Delta\psi) & -\cos(\beta+\Delta\varphi)\cos(\alpha+\Delta\psi) & \cos^2(\alpha+\Delta\psi)\end{bmatrix}. \tag{24}$$

Matrix $\mathbf{B}$ has the special property that it is the vector product of vector $\mathbf{v}$ and its transpose, where

$$\mathbf{v}=\begin{bmatrix}1\\ \cos(\beta+\Delta\varphi)\\ -\cos(\alpha+\Delta\psi)\end{bmatrix}, \tag{25}$$

such that

$$\mathbf{v}\mathbf{v}^T=\mathbf{B}. \tag{26}$$

Then, for each vector $\mathbf{x}=[x_1,x_2,x_3]^T$ in $\mathbb{R}^3$ the function

$$f(\mathbf{x},\Delta\psi)=\mathbf{x}^T\mathbf{B}\mathbf{x}$$

has only non-negative values, as

$$f(\mathbf{x},\Delta\psi)=\mathbf{x}^T\mathbf{B}\mathbf{x}\ =\ \mathbf{x}^T(\mathbf{v}\mathbf{v}^T)\mathbf{x}=\ (\mathbf{x}^T\mathbf{v})^2\geq\ 0.$$

From this result, it necessarily follows that

$$\mathbf{x}^T\mathbf{A}\mathbf{x}=\mathbf{x}^T\left(\int_{\Delta\psi_0}^{\Delta\psi_f}\mathbf{B}d\Delta\psi\right)\mathbf{x}=\ \int_{\Delta\psi_0}^{\Delta\psi_f}(\mathbf{x}^T\mathbf{B}\mathbf{x})d\Delta\psi=\ \int_{\Delta\psi_0}^{\Delta\psi_f}f(\mathbf{x},\Delta\psi)d\Delta\psi\geq\ 0,$$

which completes the proof. Now, given an arbitrary function, the function-generator designer need only check that the eigenvalues of the matrix $\mathbf{A}$ defined by the given function are all greater than zero.

Proof of Proposition 2. the proof of Proposition 2 requires the following proposition.

Proposition 7. *If a sequence of matrices* $\mathbf{M}_n$ *converges to a matrix* $\mathbf{M}$ *and* $\mathbf{M}$ *is invertible then,* $\mathbf{M}_n^{-1}$ *converges to* $\mathbf{M}^{-1}$ [15].

From Proposition 1, $\mathbf{A}_m(\alpha,\beta)$ converges towards $\mathbf{A}(\alpha,\beta)$. $\mathbf{A}(\alpha,\beta)$ possesses full rank by hypothesis, then there must be some index m_0 such that $\forall m\geq m_0$ and $\mathbf{A}_m(\alpha,\beta)$ possesses full rank. Hence, $\forall m\geq m_0\mathbf{S}_m(\alpha,\beta)$ possesses full rank and the pseudo-inverse $\mathbf{S}_m^+(\alpha,\beta)$ is:

$$\mathbf{S}_m^+(\alpha,\beta)=(\mathbf{S}_m^T(\alpha,\beta)\mathbf{S}_m(\alpha,\beta))^{-1}\mathbf{S}_m^T(\alpha,\beta)=\frac{\Delta\psi_f-\Delta\psi_0}{m}\mathbf{A}_m^{-1}(\alpha,\beta)\mathbf{S}_m^T(\alpha,\beta). \tag{27}$$

Eq. (10) then becomes:

$$\mathbf{k}_m^*(\alpha,\beta) = \mathbf{A}_m^{-1}(\alpha,\beta)\left(\frac{\Delta\psi_f - \Delta\psi_0}{m}\mathbf{S}_m^T(\alpha,\beta)\mathbf{b}_m(\alpha,\beta))\right). \tag{28}$$

From Proposition 6, $\left(\frac{\Delta\psi_f-\Delta\psi_0}{m}\mathbf{S}_m^T(\alpha,\beta)\mathbf{b}_m(\alpha,\beta)\right)$ converges to $\mathbf{e}(\alpha,\beta)$. From Proposition 7, $\mathbf{A}_m^{-1}(\alpha,\beta)$ converges towards $\mathbf{A}^{-1}(\alpha,\beta)$, hence $\mathbf{k}_m^*(\alpha,\beta)$ converges towards $\mathbf{A}^{-1}(\alpha,\beta)\mathbf{e}(\alpha,\beta)$ which is equal to $\mathbf{k}^*(\alpha,\beta)$ in Eq. (21). This completes the proof.

Proof of Proposition 3. Eq. (11) can be rewritten:

$$\| \mathbf{d}_m^*(\alpha,\beta) \|_2^2 = \mathbf{b}_m^T(\alpha,\beta)\mathbf{b}_m(\alpha,\beta) - \left(\mathbf{S}_m^T(\alpha,\beta)\mathbf{b}_m(\alpha,\beta)\right)^T \mathbf{k}_m^*(\alpha,\beta). \tag{29}$$

Multiply Eq. (29) by $\frac{\Delta\psi_f-\Delta\psi_0}{m}$. From Proposition 6, $\left(\frac{\Delta\psi_f-\Delta\psi_0}{m}\mathbf{S}_m^T(\alpha,\beta)\mathbf{b}_m(\alpha,\beta)\right)$ converges to $\mathbf{e}(\alpha,\beta)$ and $\left(\frac{\Delta\psi_f-\Delta\psi_0}{m}\mathbf{b}_m^T(\alpha,\beta)\mathbf{b}_m(\alpha,\beta)\right)$ converges to $c(\alpha,\beta)$. From Proposition 2, $\mathbf{k}_m^*(\alpha,\beta)$ converges towards $\mathbf{k}^*(\alpha,\beta)$. This completes the proof.

Proof of Proposition 4. the proof of Proposition 4 requires the following proposition:

Proposition 8. *Letfbe a function continuously differentiable on*$[a,b]$, *then* [16]

$$\left|\int_a^b f(x)dx - \lim_{n\to+\infty}\sum_{i=0}^{n-1}\frac{b-a}{n}f(a+i\frac{b-a}{n})\right| \le \frac{(b-a)\max\{f'(x), x\in[a,b]\}}{n}.$$

The dial zeros are members of a compact set defined by the Cartesian product $K = [-\pi,\pi]\times[-\pi,\pi]$. Hence, the maximum of the first derivative of any entry of $\mathbf{A}_m(\alpha,\beta)$ is bounded uniformly relative to (α,β). From Proposition 8, it follows that the elements of $\mathbf{A}_m(\alpha,\beta)$ converge uniformly relative to (α,β) towards the elements of $\mathbf{A}(\alpha,\beta)$.

The sequence (α_m^*,β_m^*) belongs to K. Hence, there exists a subsequent $(\alpha_{\varphi(m)}^*,\beta_{\varphi(m)}^*)$ which converges to some $(\alpha_\varphi^*,\beta_\varphi^*)$. From the uniform convergence of $\mathbf{A}_m(\alpha,\beta)$, it follows that the elements of $\mathbf{A}_{\varphi(m)}(\alpha_{\varphi(m)}^*,\beta_{\varphi(m)}^*)$ converge towards the elements of $\mathbf{A}(\alpha_\varphi^*,\beta_\varphi^*)$. Following the same arguments used in the proof of Proposition 1, we get:

$$\lim_{m\to\infty}\kappa_{\varphi(m)}(\alpha_{\varphi(m)}^*,\beta_{\varphi(m)}^*) = \kappa(\alpha_\varphi^*,\beta_\varphi^*), \tag{30}$$

or $(\alpha_{\varphi(m)}^*,\beta_{\varphi(m)}^*)$ minimises the condition number of $\mathbf{A}_{\varphi(m)}(\alpha,\beta)$, hence:

$$\forall(\alpha,\beta)\in K, \kappa_{\varphi(m)}(\alpha_{\varphi(m)}^*,\beta_{\varphi(m)}^*) \le \kappa_{\varphi(m)}(\alpha,\beta).$$

From Eq. (30) and Proposition 1, taking the limit on both sides of this inequality gives:

$$\forall(\alpha,\beta)\in K, \kappa(\alpha_\varphi^*,\beta_\varphi^*) \le \kappa(\alpha,\beta).$$

Hence, $(\alpha_\varphi^*,\beta_\varphi^*)$ minimises the condition number of $\mathbf{A}(\alpha,\beta)$. In other words, each convergent (α_m^*,β_m^*) converges to a minimum of the condition number of $\mathbf{A}(\alpha,\beta)$. By hypothesis, this minimum is unique. Hence, $\forall\varphi,(\alpha_\varphi^*,\beta_\varphi^*) = (\alpha^*,\beta^*)$ and the whole sequence (α_m^*,β_m^*) converges to (α^*,β^*). This completes the proof.

Proof of Proposition 5. the first statement of Proposition 5 has been proved in the proof of Proposition 4, see Eq. (30). From the uniform convergence arising from Proposition 8 the convergence in Proposition 2 and Proposition 3 is in fact uniform. The last two statements of Proposition 5 follow. To be completely rigorous, Proposition 7 should be modified to uniform convergence, but doing so introduces no contradictions.

5. Example

The preceding results for continuous approximate synthesis that minimises the design error are now illustrated with an example. Let the prescribed function be the Ackerman steering condition for terrestrial vehicles. The steering condition can be expressed as a trigonometric function whose variables are illustrated in Fig. 2:

$$\sin(\Delta\varphi_{pres} - \Delta\psi) - \rho\sin(\Delta\psi)\sin(\Delta\varphi_{pres}) = 0, \tag{31}$$

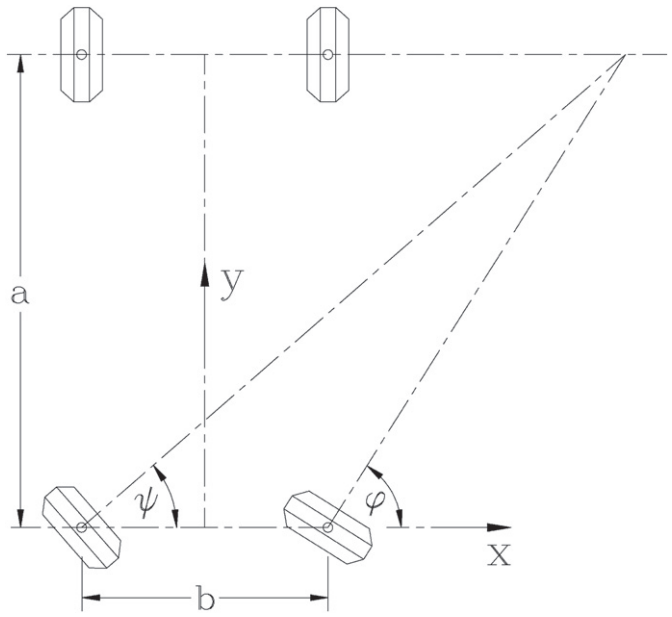

Fig. 2. Graphical illustration of the *Ackerman steering condition*.

with ρ denoting the length ratio b/a, where a is the distance between front and rear axles, and b the distance between the pivots of the wheel-carriers, which are coupled to the chassis. With the dial zeros, the expression for the steering condition becomes:

$$\sin(\beta + \Delta\varphi_{pres} - \alpha - \Delta\psi) - \rho \sin(\alpha + \Delta\psi)\sin(\beta + \Delta\varphi_{pres}) = 0. \tag{32}$$

For our example, $\rho = 0.5$ and $[\Delta\psi_0, \Delta\psi_f] = [-40.00, 30.00]$, where angles are specified in degrees. With these values, the prescribed function, i.e. the steering condition, is continuously differentiable. Hence, Proposition 5 must apply.

5.1. Establishing the optimal dial zeros and Freudenstein parameters

The multi-dimensional Nelder–Mead downhill simplex algorithm [17] is employed to find the optimal values for the dial zeros. Table 1 lists (α^*_m, β^*_m) for different values of m, as well as (α^*, β^*). From the optimal dial zeros obtained in Table 1, it is now possible to compute the optimal Freudenstein parameters. Table 2 lists the optimised Freudenstein parameters, k_i, synthesis matrix condition numbers κ_m, and design error norms which have been normalised by dividing by $\sqrt{m}$ for comparison for different values of m as well as the values using the continuous approach.

Continuous approximate synthesis eliminates the problem of determining an appropriate cardinal number for the data-set because it evaluates the case for $m \to \infty$. Hence there is no need to search for some convergence in order to set the proper value of m, which eliminates a source of error. However, the continuous approach requires numerical integrations, which itself is a source of error. These errors are in fact of the same nature. Indeed, from the development of Section 4, it is clear that discrete approximate synthesis is essentially a numerical integration method itself: Romberg's method for example, which is an extrapolation on the trapezoidal rule [4]. Hence, comparing the errors arising from the discrete approximate synthesis with continuous approximate synthesis is equivalent to comparing the error terms of two different numerical integration methods. The example presented above employed the Matlab function *quadl*, which employs recursive adaptive Lobatto quadrature [18].

Table 1
Optimal dial zeros.

m	α^*_m	β^*_m	α^*	β^*
10	−61.80	67.320	–	–
40	−62.17	68.73	–	–
100	−62.23	69.03	–	–
400	−62.26	69.17	–	–
1000	−62.27	69.20	–	–
∞	–	–	−62.27	69.22

Table 2
Optimised Freudenstein parameters, condition numbers, and normalised design errors.

m	k_1	k_2	k_3	κ_m	κ^*	$\| \mathbf{d}_m \|_2$	$\| \mathbf{d}^* \|_2$
10	−0.993	0.412	−0.429	18.24	–	6.93×10^{-4}	–
40	−1.001	0.406	−0.425	20.79	–	6.44×10^{-4}	–
100	−1.003	0.405	−0.424	21.38	–	6.31×10^{-4}	–
400	−1.003	0.404	−0.424	21.69	–	6.24×10^{-4}	–
1000	−1.004	0.404	−0.424	21.75	–	6.23×10^{-4}	–
∞	−1.004	0.404	−0.424	–	475.03	–	6.23×10^{-4}

6. Conclusions and future work

In this paper a proof has been given that the design error of planar RRRR function-generating linkages synthesised using over-constrained systems of equations established with discrete I/O data sets is bounded by a minimum value established using continuous approximate synthesis between minimum and maximum I/O values. Evaluating the design error over the entire continuous range of the function requires the use of a functional normed space, thereby changing the discrete approximate synthesis problem to a continuous approximate synthesis problem. Assuming that the prescribed function $\Delta\varphi_{pres}(\Delta\psi)$ is continuously differentiable, it is shown that the dial zeros, the optimal Freudenstein parameters, and the minimal design error for discrete approximate synthesis converge towards the dial zeros, the optimal Freudenstein parameters and the minimal design error for continuous approximate synthesis. In other words, the continuous approach corresponds to the discrete approach after setting the cardinality of the I/O set to $m \to \infty$, and represents the bounding optimal values.

The extension of this work is to investigate how the structural error as defined in Ref. [2] bounds the design error. First, it should be determined whether the structural error minimisation problem can be formulated and, more importantly solved, using the continuous approach. Second, it should be investigated whether in this case too, the continuous approach corresponds to the discrete approach with $m \to \infty$. This is certainly much more challenging due to the increased complexity of the continuous structural error minimisation problem, which is a non-linear problem with equality constraints, compared to the continuous design error minimisation problem, which is a quadratic problem without any constraints. Finally, one might ask whether our developments could be applied to other mechanism topologies, such as planar mechanisms possessing prismatic joints, as well as spherical, or spatial linkages.

Acknowledgments

The authors gratefully acknowledge partial financial support for this work provided by a research grant from the *Natural Sciences and Engineering Research Council of Canada* (NSERC) (250012-2011).

References

[1] S.O. Tinubu, K.C. Gupta, Optimal synthesis of function generators without the branch defect, ASME, J. of Mech., Trans., and Autom. in Design 106 (1984) 348–354.
[2] M.J.D. Hayes, K. Parsa, J. Angeles, The effect of data-set cardinality on the design and structural errors of four-bar function-generators, Proceedings of the Tenth World Congress on the Theory of Machines and Mechanisms, Oulu, Finland, 1999, 437–442.
[3] D.J. Wilde, Error synthesis in the least-squares design of function generating mechanisms, ASME, J. of Mechanical Design 104 (1982) 881–884.
[4] G. Dahlquist, Å. Björck, Numerical Methods, translated by Anderson, Prentice-Hall, Inc., U.S.A. 1969.
[5] Z. Liu, J. Angeles, Data conditioning in the optimization of function-generating linkages, Advances in Design Automation: Proc. 19th Annual ASME Design Automation Conference, 1993, 419–426.
[6] Z. Liu, Kinematic Optimization of Linkages, Dept. of Mech. Eng., McGill University, Montréal, QC, Canada, 1993. (Ph.D. thesis)
[7] M. Shariati, M. Norouzi, Optimal synthesis of function generator of four-bar linkages based on distribution of precision points, Mechanica 46 (5) (2011) 1007–1021.
[8] C. Peng, R.S. Sohdi, Optimal synthesis of adjustable mechanisms generating multi-phase approximate paths, Mech. Mach. Theory 45 (7) (2010) 989–996.
[9] J. Zhang, J. Wang, X. Du, Time-dependent probabilistic synthesis for function generator mechanisms, Mech. Mach. Theory 46 (9) (2011) 1236–1250.
[10] F. Freudenstein, Approximate synthesis of four-bar linkages, Trans. ASME 77 (1955) 853–861.
[11] J.E. Gentle, Numerical Linear Algebra for Applications in Statistics, Springer, New York, U.S.A. 1998.
[12] C.L. Lawson, Contributions to the Theory of Linear Least Maximum Approximations, UCLA, Los Angeles, California, U.S.A., 1961. (Ph.D. thesis)
[13] J.R. Rice, K.H. Usow, The Lawson algorithm and extensions, Math. Comput. 22 (101) (December 1967) 118–126.
[14] F. Angeles, J. Angeles, Synthesis of function-generating linkages with minimax structural error: the linear case, Proc. 13th IFToMM World Congress, June 2011.
[15] J. Ercolano, Golden sequences of matrices with application to Fibonacci algebra, The Fibonacci Quarterly 15 (5) (December 1976) 419–426.
[16] N.B. Haaser, J.A. Sullivan, Real Analysis, Van Nostrand Reinhold Co., New York, U.S.A. 1971.
[17] J.A. Nelder, R. Mead, A simplex method for function minimization, Computer Journal 7 (4) (1965) 308–313.
[18] L.F. Shampine, Vectorized adaptive quadrature in MATLAB, J. Comput. Appl. Math. 211 (February 2008) 131–140.

Planar and spherical four-bar linkage v_i-v_j algebraic input-output equations

M. John D. Hayes[a,*], Mirja Rotzoll[a], Quinn Bucciol[a], Zachary A. Copeland[a]

[a] *Carleton University, 1125 Colonel By Drive, Ottawa, ON, K1S 5B6, Canada*

Abstract

The algebraic polynomial input-output (IO) equations relating any two of the relative joint displacement parameters, called v_i and v_j, between any of the six distinct pairs of rigid links in arbitrary planar and spherical four-bar mechanisms are derived. First, the forward kinematics transformation matrices of the corresponding serial kinematic chains are computed in terms of their Denavit-Hartenberg parameters, but with all angles converted to tangent half-angle parameters. These matrices are mapped to their corresponding Study soma coordinates. The serial kinematic chain is closed by equating the soma coordinates to the identity array. Algebraic polynomial elimination methods are then used to obtain a single polynomial in terms of only the design and the selected IO joint displacement parameters. This yields six independent algebraic IO Equations for each of the planar and spherical 4R linkages; the same techniques are applied to derive six additional algebraic IO equations for each of the RRRP and PRRP planar linkages providing a catalogue of 24. The utility of these IO equation sets is demonstrated via discussion of the associated mobility and design parameter spaces.

Keywords: Planar and spherical four-bar linkages, v_i-v_j algebraic input-output equations, algebraic polynomial elimination methods.

1. Introduction

Relative motion between mechanically constrained rigid bodies in the plane, on the surface of a sphere, and in three-dimensional space has fascinated philosophers, mathematicians, and engineers for millennia [1]. The design of predictable motion of a four-bar spherical mechanism appears to have its origins in the development of universal joints based on gimbals, which have also been investigated since antiquity [2]. While there is a substantial volume of archival literature regarding planar and spherical 4R mechanisms, see [3, 4, 5, 6, 7] for a small but

*Corresponding author
Email address: john.hayes@carleton.ca (M. John D. Hayes)

relevant sample, these types of mechanical systems still excite the imagination, see [8, 9, 10, 11, 12] for recent examples.

Eduard Study, 1868-1930, likely inspired by the earlier work of Julius Plücker, 1801-1868, and his Ph.D. student Felix Klein, 1845-1925, on the development of line geometry [13, 14, 15], proposed the theory of mapping the special Euclidean group of rigid body displacements, $SE(3)$, to the points on a six-dimensional hyper-quadric in a seven-dimensional projective space, now known as the Study quadric S_6^2 [16]. The relative displacements of rigid bodies in a plane and on the surface of a sphere map to subspaces of S_6^2. Study called the coordinates of points of this space soma, the Greek word for body. These soma coordinates lead to algebraic polynomials in terms of the joint variables and design parameters for the relative displacements of any particular mechanical system. Study's kinematic mapping image space was notably reintroduced to the research world in [17, 18], and will be relied upon in this paper.

All moveable four-bar linkages generate six distinct functions between the four distinct joint variable parameters taken two at a time, which we abstractly call v_i and v_j. While this is common knowledge in the kinematics community, there do not exist convenient and consistent ways to determine and express these six functions using algebraic means. Moreover, only the v_1-v_4 and v_1-v_3 IO equations can be found in vast body of archival literature, but they are expressed as trigonometric implicit equations, see [3, 8] for standard examples. Hence, we believe this is sufficient justification to present the work on the derivation of the six v_i-v_j algebraic input-output (IO) equations for each of the planar 4R, RRRP, PRRP, and spherical 4R linkages reported herein. The motivation at the foundation of this work is to provide computational tools for mechanism design and analysis that are less cumbersome to use than vector loop methods based on trigonometry. Since our IO equations are algebraic polynomials of degree 4, and 3 or 2 for the PRRP, in two variables with rational coefficients, the full power of the theory of planar algebraic curves [19] can be applied to these 24 distinct algebraic IO curves in their respective v_i-v_j parameter planes. This enables one to observe significantly more and comparatively simple to obtain information regarding all the relative motions generated by the linkage.

In this paper we present a novel algorithm, built on tools from algebraic-geometry, that derives the algebraic polynomials which model the relative displacements of all six IO joint displacement pairs in each class of arbitrary planar and spherical single degree of freedom simple closed kinematic chains. First, the class of open kinematic chains is parameterised using the well known notation for lower-pair kinematic chains of arbitrary architecture: Denavit-Hartenberg (DH) notation [4]. The resulting coordinate transformation matrix describing the forward kinematics of the open chain is equated to the identity matrix to conceptually close the chain [4]. Measures of angle elements in the resulting matrix are converted to their respective tangent half-angle parameters. This modified transformation matrix is then mapped to the coordinates of the seven dimensional projective kinematic image space using the well known definitions of the Study soma coordinates [16, 17, 20, 21]. Next, using an appropriate subset of the soma, elimination theory [22] is used to eliminate undesired variable joint

displacement parameters leaving only the implicit algebraic IO equation for the desired IO parameter pair. The first presentation of a part of the algorithm can be found in [23]. However, in that work we failed to understand how completely general the algorithm is and this work will provide the generalisation. While we have already successfully applied the algorithm to derive the algebraic IO equations for some planar and spherical four-bar linkages [24], here we will derive the six different v_i-v_j IO equations for each of the planar 4R, RRRP, PRRP and spherical 4R linkages, and thereby provide a long needed catalogue of these 24 algebraic IO equations.

2. Planar Four-bar Linkages

We start with a generic 4R open kinematic chain and assign the standard DH coordinate systems and parameters according to [4], see Table 1 and Fig. 1a. The four link lengths are the a_i, and the four joint angles are the θ_i, $i \in \{1, 2, 3, 4\}$. While we do not require them for the planar 4R, there are non-zero link twist angles, τ_i, for the RRRP, PRRP, and spherical 4R linkages, as well as link offsets, d_i, for the RRRP and PRRP linkages. All measures of angle are converted to algebraic parameters using the tangent half-angle substitutions:

$$v_i = \tan\frac{\theta_i}{2} \quad \Rightarrow \quad \cos\theta_i = \frac{1-v_i^2}{1+v_i^2}, \quad \sin\theta_i = \frac{2v_i}{1+v_i^2},$$

$$\alpha_i = \tan\frac{\tau_i}{2} \quad \Rightarrow \quad \cos\tau_i = \frac{1-\alpha_i^2}{1+\alpha_i^2}, \quad \sin\tau_i = \frac{2\alpha_i}{1+\alpha_i^2}.$$

The transformation matrix implied by the algebrised parameters is equated to the identity matrix thereby conceptually closing the kinematic chain. Closing the serial 4R chain by grounding link a_4 means that we may have clockwise (CW) or counter clockwise (CCW) joint index circulation. The CW circulation means that the origins of x_4-y_4 and x_0-y_0 are coincident, but the basis vector directions in each coordinate system are out of phase by π radians. Whereas the CCW circulation means the two coordinate systems are congruent, see Fig. 1b, and we call them the $x_{0/4}$ - $y_{0/4}$ coordinate system. The equations that follow are expressed in that coordinate system.

Table 1: DH parameters for an arbitrary open 4R chain.

axis i	link length a_i	angle θ_i	link offset d_i	twist τ_i
1	a_1	θ_1	0	0
2	a_2	θ_2	0	0
3	a_3	θ_3	0	0
4	a_4	θ_4	0	0

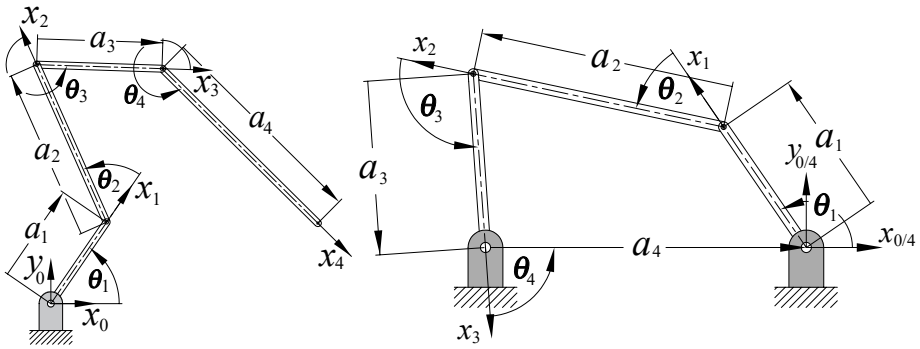

(a) Generic open 4R kinematic chain. (b) Generic closed 4R kinematic chain.

Figure 1: Serial and parallel planar 4R linkages.

Using the definitions found in [23], the DH transformation matrix of the open 4R chain is mapped to the soma array of eight homogeneous coordinates

$$[x_0 : x_1 : x_2 : x_3 : y_0 : y_1 : y_2 : y_3].$$

Since we are only considering the special Euclidean subgroup of direct planar isometries $SE(2)$ generated by planar 4R, RRRP, and PRRP linkages at the moment, four of the soma coordinates always vanish and what remains are

$$\text{planar 4R and RRRP:} \qquad [x_0 : 0 : 0 : x_3 : 0 : y_1 : y_2 : 0]; \tag{1}$$

$$\text{PRRP:} \qquad [x_0 : x_1 : 0 : 0 : 0 : 0 : y_2 : y_3]. \tag{2}$$

Regardless, for a generic representation we use the full Study array here since the 0 elements are also different for spherical linkages [23, 25]. To close the planar serial 4R kinematic chain, the Study array is equated to the identity array thus

$$[x_0 : 0 : 0 : x_3 : 0 : y_1 : y_2 : 0] \quad = \quad [1 : 0 : 0 : 0 : 0 : 0 : 0 : 0]. \tag{3}$$

The Gröbner bases of the ideal generated by the three polynomials $x_3 = 0$, $y_1 = 0$, and $y_2 = 0$ are used to eliminate the two unwanted v_i joint angle parameters leading to the desired v_i-v_j algebraic IO equation. For example, v_2 and v_4 must be eliminated to obtain the v_1-v_3 algebraic IO equation. Because the soma are homogeneous coordinates, and because we are only interested in the kinematic images of real rigid body displacements, we will not use the homogenising coordinate $x_0 = 1$ as a polynomial in our elimination computations.

It is important to note that the IO equations may also be obtained directly on S_6^2. In [26] the DH transformations are expressed as 8×8 matrices and manipulated directly on S_6^2. When equated to the identity array, the IO equation can be obtained with elimination methods. Similarly, in [27] dual quaternions are used to obtain the closure equation of spatial 6R linkages. These methods

could be applied to determine the soma coordinates, but that is not the focus of this paper. What is important is the general unified way to model the kinematic geometry of each of the four classes of four-bar linkage and obtain the six v_i-v_j algebraic IO equations from the associated soma coordinates for each of the planar 4R, RRRP, PRRP, and spherical 4R linkages.

2.1. Derivation of the Six Planar 4R Linkage v_i-v_j IO Equations

Let the input angle parameter be v_1 and the output angle parameter be v_4. In [23] two elimination steps were applied to the Gröbner bases of the ideal generated by the soma coordinates x_3, y_1 and y_2 to eliminate the angle parameters v_2 and v_3 from the equations yielding the algebraic IO equation relating the v_1 and v_4 angle parameters, which we call the v_1-v_4 IO equation. It has the form

$$Av_1^2v_4^2 + Bv_1^2 + Cv_4^2 - 8a_1a_3v_1v_4 + D = 0, \tag{4}$$

where

$$\begin{aligned}
A = A_1A_2 &= (a_1 - a_2 + a_3 - a_4)(a_1 + a_2 + a_3 - a_4),\\
B = B_1B_2 &= (a_1 + a_2 - a_3 - a_4)(a_1 - a_2 - a_3 - a_4),\\
C = C_1C_2 &= (a_1 - a_2 - a_3 + a_4)(a_1 + a_2 - a_3 + a_4),\\
D = D_1D_2 &= (a_1 + a_2 + a_3 + a_4)(a_1 - a_2 + a_3 + a_4),\\
v_1 &= \tan\frac{\theta_1}{2},\\
v_4 &= \tan\frac{\theta_4}{2}.
\end{aligned}$$

This algebraic equation is of degree 4 in the v_1 and v_4 variable parameters, while the coefficients labelled A, B, C, and D are each products of two bilinear factors which can be viewed as eight distinct planes treating the four a_i link lengths as homogeneous coordinates. See Section 5.2 for a detailed description of this design parameter space.

In the approach used in [23] to obtain this IO equation from the ideal $\langle x_3, y_1, y_2\rangle$ both v_2 and v_3 are eliminated by first computing the Gröbner bases of the ideal using the Maple 2021 "`tdeg`" monomial ordering with the list sequence (v_3, v_2, v_4, v_1). This is *graded reverse lexicographic order*, also known as *degrevlex* in the literature [28], with indeterminate ordering $v_3 > v_2 > v_4 > v_1$. This monomial ordering sorts the terms by total degree before breaking ties between terms with identical degree by comparing the smallest indeterminate first and considering a higher degree as smaller in the term ordering. The execution of this step is immediate on a standard computer with an Intel Core i7-7700 CPU @ 3.60 GHz. In this case, 12 bases are computed, all functions of all four v_i. We eliminate v_2 and v_3 by computing the bases of these 12 with the reverse monomial ordering by using "`plex`", which is the *pure lexicographic order*, also known as *lex* [28]. This results in 8 new bases, with one that is a function of

only v_1 and v_4 and the four a_i, which represents the IO equation we are looking for.

However, we have since discovered that a single application of the elimination monomial ordering called "`lexdeg`" in Maple 2021 leads directly to the desired planar 4R v_1-v_4 IO equation. When the ideal generated by the system of polynomials contains coefficients that are not too large or complicated, as for the planar 4R linkages, this elimination monomial ordering is very efficient, in the sense that it does not compute an entire "`plex`" basis. For the two disjoint lists of variables, those to be eliminated and those to be retained, the "`lexdeg`" ordering is equivalent to a product order which uses "`tdeg`" on each of the two disjoint lists of variables. All six of the distinct IO equations for each of the planar 4R, RRRP, and PRRP kinematic architectures are easily computed using the "`lexdeg`" elimination monomial ordering. This is how the IO equations for these planar four-bar linkages have been derived. For the planar 4R, the five remaining v_i-v_j IO equations each contain all eight of the bilinear factors of the coefficients labelled $A_1, A_2, B_1, B_2, C_1, C_2, D_1$, and D_2 in Eq. (4), but in different permutations. This means that the design parameter space, as defined in [29], is the same for all six of these IO equations. The execution of the code is immediate for all six IO equations for each of the three kinematic architectures.

By applying the "`lexdeg`" monomial term orderings to the planar 4R variables in the appropriate disjoint lists, the v_1-v_2, v_1-v_3, v_2-v_3, v_2-v_4, and v_3-v_4 IO equations are obtained and listed as follows.

$$A_1B_2v_1^2v_2^2 + A_2B_1v_1^2 + C_1D_2v_2^2 - 8a_2a_4v_1v_2 + C_2D_1 = 0, \tag{5}$$

$$A_1B_1v_1^2v_3^2 + A_2B_2v_1^2 + C_2D_2v_3^2 + C_1D_1 = 0, \tag{6}$$

$$A_1D_2v_2^2v_3^2 + B_2C_1v_2^2 + B_1C_2v_3^2 - 8a_1a_3v_2v_3 + A_2D_1 = 0, \tag{7}$$

$$A_1C_1v_2^2v_4^2 + B_2D_2v_2^2 + A_2C_2v_4^2 + B_1D_1 = 0, \tag{8}$$

$$A_1C_2v_3^2v_4^2 + B_1D_2v_3^2 + A_2C_1v_4^2 + 8a_2a_4v_3v_4 + B_2D_1 = 0. \tag{9}$$

Eqs. (4), (5), (7), and (9) all contain a bilinear quadratic term because they relate adjacent angle pairs, while Eqs. (6) and (8) relate opposite angle pairs, and hence do not possess a bilinear quadratic term.

Each of these six IO equations is of degree 4 in the two variable angle parameters, defining quartic curves in the planes spanned by the different v_i-v_j angle parameter pairs. They also all have genus 1 meaning that there is a maximum number of two assembly modes. This is so because of a theorem on algebraic curves proved by Axel Harnack in 1876 [30] which relates the circuits of an algebraic curve to its genus. Each of the v_i-v_j algebraic IO equations are quartic curves of genus 1, therefore, following Harnack, each can have at most two circuits. Each circuit of a particular v_i-v_j IO curve corresponds to one of the mechanisms assembly modes. In essence, Harnack's theorem states that an algebraic curve of genus n can have at most $n + 1$ circuits. One may therefore immediately conclude that a planar 4R mechanism can never have more than two assembly modes.

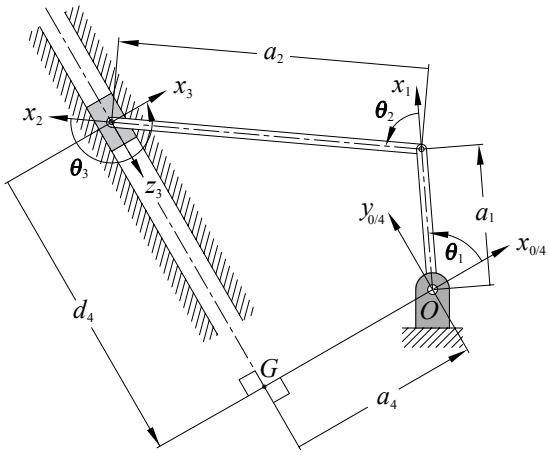

Figure 2: Planar RRRP linkage with Denavit-Hartenberg coordinate system and parameter assignments.

2.2. Six Planar RRRP Linkage v_i-v_j IO Equations

Next we shall list the six algebraic IO equations for planar RRRP mechanisms obtained using our technique employing the "`lexdeg`" elimination monomial ordering. An arbitrary RRRP linkage is illustrated in Fig. 2. The P-pair z_3-axis induces the two link twist angles and a link offset listed in Table 2.

Table 2: DH parameters for the RRRP.

i	θ_i	d_i	a_i	τ_i	α_i
1	θ_1	0	a_1	0	0
2	θ_2	0	a_2	0	0
3	θ_3	0	0	$\pi/2$	1
4	0	d_4	a_4	-$\pi/2$	-1

Applying the methods in [23] to the DH parameters by algebraising the angle parameters with tangent half-angle equivalents, projecting the DH closure equation into Study's kinematic mapping image space as soma coordinates, then eliminating the intermediate joint variable parameters v_2 and v_3 using "`lexdeg`" leads to the RRRP v_1-d_4 algebraic IO equation:

$$v_1^2 d_4^2 + R v_1^2 + d_4^2 - 4 a_1 v_1 d_4 + S = 0, \tag{10}$$

where

$$R = R_1 R_2 = (a_1 + a_2 - a_4)(a_1 - a_2 - a_4),$$
$$S = S_1 S_2 = (a_1 + a_2 + a_4)(a_1 - a_2 + a_4),$$
$$v_1 = \tan \frac{\theta_1}{2}.$$

The four bilinear factors R_1, R_2, S_1, and S_2 can be regarded as four planes intersecting in the faces of a four-sided pyramid in the design parameter space orthogonally spanned by the three lengths a_1, a_2, and a_4, see [31] for a detailed description.

Using the same approach, the five remaining joint variable parameter pairings lead to the following five additional RRRP algebraic IO equations:

$$R_2 v_1^2 v_2^2 + R_1 v_1^2 - S_2 v_2^2 + 4a_2 v_1 v_2 - S_1 = 0; \tag{11}$$
$$R_1 v_1^2 v_3^2 + R_2 v_1^2 - S_2 v_3^2 - S_1 = 0; \tag{12}$$
$$S_2 v_2^2 v_3^2 - R_2 v_2^2 - R_1 v_3^2 - 4a_1 v_2 v_3 + S_1 = 0; \tag{13}$$
$$v_2^2 d_4^2 - R_2 S_2 v_2^2 + d_4^2 - R_1 S_1 = 0; \tag{14}$$
$$v_3^2 d_4^2 - R_1 S_2 v_3^2 + d_4^2 + 4a_2 v_3 d_4 - R_2 S_1 = 0. \tag{15}$$

All six of the RRRP algebraic IO equations are of degree 4, representing quartic curves in the respective joint variable parameter planes. These six IO equations also all possess genus 1 meaning again that there is a maximum number of two assembly modes.

For the RRRP linkages that are rocker-sliders, each distinct circuit of the IO curve also contains two branches, one for each working mode. When the input angle reaches minimum or maximum values the mechanism instantaneously stops moving as the coupler becomes perpendicular to the direction of travel of the P-pair. In this singular configuration, unless mechanical constraints are imposed, the slider may move in one of two directions as the rocker input link begins to move again in the opposite sense. These are defined as the working modes of the particular assembly mode. Each working mode traces a distinct branch in the particular circuit of the IO curve. Together, both branches cover the entire circuit.

2.3. Six Planar PRRP Linkage v_i-v_j IO Equations

An identical approach is used for the planar PRRP linkages. Referring to Fig. 3, it is to be seen that general PRRP elliptical trammel linkages have but two design parameters, namely a_2 and τ_4, the coupler length, and the twist angle between the two P-pairs. The twist angle is typically $\tau_4 = \pi/2$, though it can be any other value. The DH parameters for an arbitrary PRRP are listed in Table 3. Again we apply the methods in [23] and the "`lexdeg`" monomial ordering to the DH parameters of the PRRP by algebraising the angle parameters with tangent half-angle equivalents, projecting the DH closure equation into

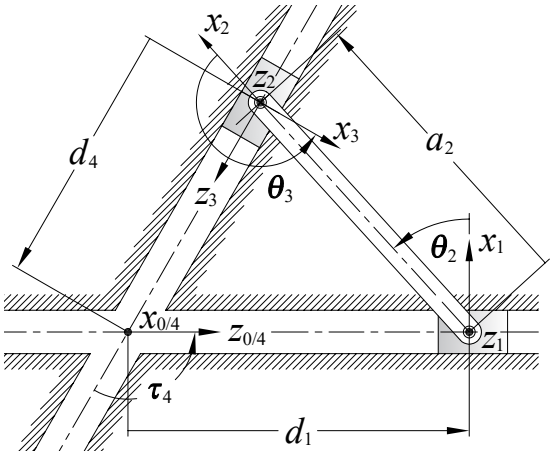

Figure 3: Planar PRRP linkage with Denavit-Hartenberg coordinate systems and parameter assignments.

Table 3: DH parameters for the PRRP.

i	θ_i	v_i	d_i	a_i	τ_i	α_i
1	$-\pi/2$	-1	d_1	0	$-\pi/2$	-1
2	θ_2	v_2	0	a_2	0	0
3	θ_3	v_2	0	0	$\pi/2$	1
4	$\pi/2$	1	d_4	0	τ_4	α_4

Study's kinematic mapping image space as soma coordinates, then eliminating the intermediate joint variable parameters leading to the PRRP algebraic IO equations. The symmetry of the six algebraic IO equations is clearly revealed when we define the following three coefficients:

$$\begin{aligned} T &= a_2^2(\alpha_4^2+1); \\ U &= a_2(\alpha_4^2-1); \\ V &= a_2(\alpha_4^2+1). \end{aligned}$$

Using these coefficients the six algebraic IO equations are:

$$(\alpha_4^2+1)(d_1^2+d_4^2)-2(\alpha_4^2-1)d_1d_4-T=0; \tag{16}$$

$$2\alpha_4 d_1 v_2^2+Uv_2^2+2\alpha_4 d_1-4a_2\alpha_4 v_2-U=0; \tag{17}$$

$$2\alpha_4 d_1 v_3^2-Vv_3^2+2\alpha_4 d_1+V=0; \tag{18}$$

$$\alpha_4 v_2 v_3-v_2-v_3-\alpha_4=0; \tag{19}$$

$$2\alpha_4 v_2^2 d_4+Vv_2^2+2\alpha_4 d_4-V=0; \tag{20}$$

$$2\alpha_4 v_3^2 d_4-Uv_3^2+4a_2\alpha_4 v_3+2\alpha_4 d_4+U=0. \tag{21}$$

It is to be seen that Eqs. (17), (18), (20), and (21) are of degree 3, representing cubic curves in their respective joint variable parameter planes, while Eqs. (16) and (19) are of degree 2, and are different conics. When the respective quadratic forms are diagonalised it is easy to show that Eq. (16) is an ellipse, while Eq. (19) is an hyperbola which depends only on the link twist α_4. Moreover, each of the six PRRP algebraic IO equations, Eqs. (16-21) possess genus 0, unlike the planar 4R and RRRP IO equations. According to Harnak's theorem we conclude that the PRRP linkage has at most one assembly mode since each IO equation has a single circuit.

3. Spherical 4R Linkages

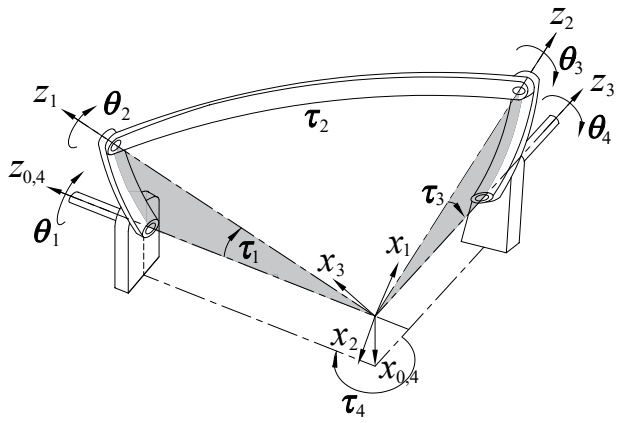

Figure 4: Spherical 4R DH reference frames and parameters.

Consider the arbitrary spherical 4R linkage illustrated in Fig. 4. The general IO equation expresses the implicit functional relationship between the input and output angles, θ_i and θ_j, in terms of the constant twist angles between the four R-pair centres, τ_i. For a unit sphere, the twist angles are equivalent to the corresponding arc lengths. The derivation of the algebraic form of the

spherical IO equation [23] also makes use of the original Denavit-Hartenberg (DH) parametrisation of the kinematic geometry [32].

The forward kinematics of an arbitrary serial 4R spherical kinematic chain is obtained as a linear transformation matrix in terms of the DH parameters. This linear transformation can then be mapped to the corresponding eight Study soma coordinates [23]. For spherical kinematic chains there are also only four homogeneous soma coordinates since the displacement group contains only rotations about a fixed point. The corresponding Study array is:

$$[x_0 : x_1 : x_2 : x_3 : 0 : 0 : 0 : 0]. \tag{22}$$

The ideal generated by the three non-trivial soma that equate to zero, namely x_1, x_2, and x_3 are used to derive the algebraic IO equations relating the six distinct edges of an arbitrary spherical quadrangle.

Algebrising the joint angles and link twists with the tangent half-angle parameters $v_i = \tan(\theta_i/2)$ and $\alpha_i = \tan(\tau_i/2)$ leads to the algebraic form of each v_i-v_j IO equation. The v_1-v_4 algebraic IO equation is

$$Av_1^2v_4^2 + Bv_1^2 + Cv_4^2 + 8\alpha_1\alpha_3\left(\alpha_4^2+1\right)\left(\alpha_2^2+1\right)v_1v_4 + D = 0, \tag{23}$$

where

$$\begin{aligned}
A \;=\; A_1A_2 \;&=\; (\alpha_1\alpha_2\alpha_3 - \alpha_1\alpha_2\alpha_4 + \alpha_1\alpha_3\alpha_4 - \alpha_2\alpha_3\alpha_4 + \alpha_1 - \alpha_2 + \alpha_3 - \alpha_4)\\
&\quad\;(\alpha_1\alpha_2\alpha_3 - \alpha_1\alpha_2\alpha_4 - \alpha_1\alpha_3\alpha_4 - \alpha_2\alpha_3\alpha_4 - \alpha_1 - \alpha_2 - \alpha_3 + \alpha_4),\\
B \;=\; B_1B_2 \;&=\; (\alpha_1\alpha_2\alpha_3 + \alpha_1\alpha_2\alpha_4 - \alpha_1\alpha_3\alpha_4 - \alpha_2\alpha_3\alpha_4 + \alpha_1 + \alpha_2 - \alpha_3 - \alpha_4)\\
&\quad\;(\alpha_1\alpha_2\alpha_3 + \alpha_1\alpha_2\alpha_4 + \alpha_1\alpha_3\alpha_4 - \alpha_2\alpha_3\alpha_4 - \alpha_1 + \alpha_2 + \alpha_3 + \alpha_4),\\
C \;=\; C_1C_2 \;&=\; (\alpha_1\alpha_2\alpha_3 - \alpha_1\alpha_2\alpha_4 - \alpha_1\alpha_3\alpha_4 + \alpha_2\alpha_3\alpha_4 - \alpha_1 + \alpha_2 + \alpha_3 - \alpha_4)\\
&\quad\;(\alpha_1\alpha_2\alpha_3 - \alpha_1\alpha_2\alpha_4 + \alpha_1\alpha_3\alpha_4 + \alpha_2\alpha_3\alpha_4 + \alpha_1 + \alpha_2 - \alpha_3 + \alpha_4),\\
D \;=\; D_1D_2 \;&=\; (\alpha_1\alpha_2\alpha_3 + \alpha_1\alpha_2\alpha_4 + \alpha_1\alpha_3\alpha_4 + \alpha_2\alpha_3\alpha_4 - \alpha_1 - \alpha_2 - \alpha_3 - \alpha_4)\\
&\quad\;(\alpha_1\alpha_2\alpha_3 + \alpha_1\alpha_2\alpha_4 - \alpha_1\alpha_3\alpha_4 + \alpha_2\alpha_3\alpha_4 + \alpha_1 - \alpha_2 + \alpha_3 + \alpha_4).
\end{aligned}$$

The coefficients A, B, C, and D all have two bicubic factors. It can be shown that when the radius of the sphere is infinite then Eqs. (23) and (4) are functionally identical [23], hence the same coefficient names A, B, C, and D are used. While the derivation of this algebraised v_1-v_4 IO equation is novel and far from intuitive, the algebraic form of this fourth degree polynomial in the v_1-v_4 IO angle parameters is not. The earliest derivations of similar equations representing manipulatable octahedra, identical in form, are due to Raoul Bricard in 1897 [33]. This fascinating similarity between movable octahedral and spherical linkage algebraic IO equations is not at all a coincidence, as will be illustrated in Section 5.2.

4. Derivation of the Six Spherical v_i-v_j IO Equations

Using the eight bicubic coefficient definitions from Eq. (23), the remaining five v_i-v_j equations contain all eight of the bicubic coefficients, but in different

permutations:

$$A_1B_2v_1^2v_2^2+A_2B_1v_1^2+C_1D_2v_2^2+8\alpha_2\alpha_4\big(\alpha_1^2+1\big)\big(\alpha_3^2+1\big)v_1v_2+C_2D_1=0; \quad (24)$$

$$A_1B_1v_1^2v_3^2 + A_2B_2v_1^2 + C_2D_2v_3^2 + C_1D_1 = 0; \quad (25)$$

$$A_1D_2v_2^2v_3^2+B_2C_1v_2^2+B_1C_2v_3^2-8\alpha_1\alpha_3\big(\alpha_2^2+1\big)\big(\alpha_4^2+1\big)\,v_2v_3+A_2D_1=0; \quad (26)$$

$$A_1C_1v_2^2v_4^2 + B_2D_2v_2^2 + A_2C_2v_4^2 + B_1D_1 = 0; \quad (27)$$

$$A_1C_2v_3^2v_4^2+B_1D_2v_3^2+A_2C_1v_4^2+8\alpha_2\alpha_4\big(\alpha_1^2+1\big)\big(\alpha_3^2+1\big)\,v_3v_4+B_2D_1=0. \quad (28)$$

As for the planar 4R and RRRP linkage algebraic IO equations, we see that Eqs. (25) and (27) do not contain a bilinear quadratic term because they relate angle parings between the spherical quadrangle edges that intersect in opposite vertices. Each of Eqs. (23)-(28) has genus 1.

The v_1-v_4 IO Equation. The soma coordinates representing the forward kinematics of the spherical 4R are polynomials containing coefficients are already to complicated to efficiently use the "`lexdeg`" elimination monomial ordering. To obtain this IO equation from the ideal generated by the three soma coordinates that equate to zero, both v_2 and v_3 are eliminated by first computing the Gröbner bases using the Maple 2021 "`tdeg`" monomial ordering with the list sequence (v_3, v_2, v_4, v_1), meaning that the indeterminate ordering is $v_3 > v_2 > v_4 > v_1$. In this case, 12 bases are computed, all functions of all four v_i. We eliminate v_2 and v_3 by computing the bases of these 12 with the reverse monomial ordering by using "`plex`". This results in 10 new bases, with one that is a function of only v_1 and v_4 and the four α_i, which represents the IO equation we are looking for. This polynomial splits into three factors. The first two are $(1 + v_1^2)(1 + v_4^2)$, a product that is always greater than zero, and can be safely factored out, leaving us with Eq. (23). This, and some of the other spherical 4R IO equations are computable in one application of the "`lexdeg`" elimination monomial ordering, but the computation time is more than an order of magnitude greater, about 3500 s, than the 120 s for the sequential application of "`tdeg`" and "`plex`" on an Intel Core i7-7700 CPU @ 3.60 GHz.

It is important to note that we are using the standard Denavit-Hartenberg [32] relative joint angle parameters, which are each a measure of the relative angle a link makes with the previous link in the kinematic chain. This fact enables us to derive the remaining five IO equations such that the same eight bicubic coefficient factors characterise all six IO equations. This is generally not the case when vector loop methods are used together with trigonometry, see [34] for a detailed example.

The v_1-v_2 IO Equation. The derivation steps are precisely the same as for the v_1-v_4 IO equation. Eliminating v_3 and v_4 from the same three soma coordinates, the resulting v_1-v_2 IO equation splits into three similar factors. The first two, $(1 + v_1^2)(1 + v_2^2)$, can be safely factored out, leaving us with Eq. (24).

The v_1-v_3 IO Equation. The derivation steps are precisely the same as for

the previous two IO equations. But, after the elimination of v_2 and v_4 from the same three soma coordinates, the resulting v_1-v_3 IO equation splits into five factors. The first two are $(1+v_1^2)(1+v_3^2)$, and can be safely factored out. The next two are

$$(\alpha_2^2\alpha_3^2+2\alpha_2\alpha_3+1)v_3^2+\alpha_2^2\alpha_3^2-2\alpha_2\alpha_3+1, \tag{29}$$

$$(\alpha_2^2-2\alpha_2\alpha_3+\alpha_3^2)v_3^2+\alpha_2^2+2\alpha_2\alpha_3+\alpha_3^2. \tag{30}$$

In order for either, or both, of Eqs. (29) or (30) to be identically zero the arc length parameters α_2 and α_3 must be complex. This means these two factors may also eliminated since we are only interested in real linkages, leaving us with Eq. (25).

The v_2-v_3 IO Equation. To derive this IO equation using elimination methods on the three soma coordinates we have been using requires a very different approach. We were successful by first applying the graded reverse lexicographical order "`tdeg`" to the three soma coordinates using the list sequence (v_1, v_4, v_2, v_3), then applying *graded lexicographic order* using "`grlex`" to the bases identified with "`tdeg`". After each computation we obtain 12 bases, all in terms of the four α_i and the four v_i, with the exception of one in the graded lexicographic order set of bases, which is in terms of the four α_i, but only v_1, v_2, and v_3, and is used in the elimination steps. Next, resultants are used to eliminate v_4 first, then v_1. We obtain a v_2-v_3 IO equation that splits into nine factors.

The first five of these factors are simple to divide out since they are trivially non-zero: the first is -1; the other four are the squares of a single α_i added to a positive integer. The next three factors are functions of v_2 and v_3, but only α_1, α_2, and α_3:

$$\begin{aligned}(\alpha_1\alpha_2-\alpha_1\alpha_3+\alpha_2\alpha_3+1)^2v_2^2v_3^2+(\alpha_1\alpha_2+\alpha_1\alpha_3-\alpha_2\alpha_3+1)^2v_2^2+\\ 8\alpha_1\alpha_3(\alpha_2^2+1)v_2v_3+(\alpha_1\alpha_2-\alpha_1\alpha_3-\alpha_2\alpha_3-1)^2v_3^2+(\alpha_1\alpha_2+\alpha_1\alpha_3+\alpha_2\alpha_3-1)^2;\end{aligned} \tag{31}$$

$$\begin{aligned}(\alpha_1\alpha_2\alpha_3+\alpha_1-\alpha_2+\alpha_3)^2v_2^2v_3^2+(\alpha_1\alpha_2\alpha_3-\alpha_1+\alpha_2+\alpha_3)^2v_2^2-\\ 8\alpha_1\alpha_3(\alpha_2^2+1)v_2v_3+(\alpha_1\alpha_2\alpha_3+\alpha_1+\alpha_2-\alpha_3)^2v_3^2+(\alpha_1\alpha_2\alpha_3-\alpha_1-\alpha_2-\alpha_3)^2;\end{aligned} \tag{32}$$

$$\begin{aligned}\alpha_3(\alpha_1\alpha_2+1)(\alpha_1-\alpha_2)v_2^2+2\alpha_1\alpha_3(\alpha_2^2+1)v_2v_3-\alpha_1(\alpha_2\alpha_3+1)(\alpha_2-\alpha_3)v_3^2+\\ \alpha_2(\alpha_1+\alpha_3)(\alpha_1\alpha_3-1).\end{aligned} \tag{33}$$

In order for Eqs. (31), (32), and/or (33) to be identically zero the arc length parameters α_1, α_2, and/or α_3 must be complex numbers, so we may safely divide these three factors out, leaving only Eq. (26) as the desired IO equation.

The v_2-v_4 IO Equation. The derivation steps for the v_2-v_4 IO equation are the same as those for the v_1-v_4, v_1-v_2, and v_1-v_3 IO equations. The the second set of Gröbner bases computed using the pure lexicographic order with list sequence (v_3, v_1, v_2, v_4) lead to an IO equation that splits into five factors, the first two are trivial. The next two are

$$(\alpha_1^2\alpha_2^2+2\alpha_1\alpha_2+1)v_2^2+\alpha_1^2\alpha_2^2-2\alpha_1\alpha_2+1, \tag{34}$$

$$(\alpha_1^2-2\alpha_1\alpha_2+\alpha_2^2)v_2^2+\alpha_1^2+2\alpha_1\alpha_2+\alpha_2^2. \tag{35}$$

For either, or both of Eqs. (34) and (35) to equate to zero, it requires both α_1 and α_2 to be complex. We can therefore factor both of these out, leaving only the desired v_2-v_4 IO, Eq. (27).

The v_3-v_4 IO Equation. Finally, the derivation steps for the v_3-v_4 IO equation are precisely the same as for the v_2-v_4 IO equation. After the elimination of v_1 and v_2 from the same three soma coordinates, the resulting v_3-v_4 IO equation splits into three factors. The first two are safely divided out, leaving us with Eq. (28).

5. Applications

5.1. Mobility Classification

Treating each pair of v_i-v_j to be coordinate axes in the plane spanned by the two, then each IO equation for a pair of joint angle parameters contains two double points at infinity[1], one on each of the v_i and v_j axes. The double points at infinity belonging to each of the four distinct v_i coordinate axes together with the type of points at $v_i = 0$ completely define the mobility limits, if they exist, between each v_i-v_j angle parameter pair. For a planar algebraic curve to possess a double point, it's degree must be $n > 3$. Hence, this analysis does not apply to PRRP linkages, but it does apply to the R-pairs in an RRRP linkage. The double point at infinity on the d_4 axis is always an acnode independent of the lengths of the links and offsets, which is reassuring as this means the travel of the prismatic slider is always finite. But, for R-pairs, the nature of the double points determine if extreme orientations exist that are implied by the v_i where the two corresponding links can align. Hence, the examination of these two points is sufficient to determine whether a particular joint enables a crank, a rocker, a π-rocker, or a 0-rocker relative link motion [35, 36].

For example, let us determine the double points for the v_1-v_4 IO curve for a planar 4R. First homogenise Eq. (4) using the homogenising coordinate v_0, then redefine the IO equation as

$$k \;:=\; Av_1^2v_4^2 + Bv_0^2v_1^2 + Cv_0^2v_4^2 - 8a_1a_3v_0^2v_1v_4 + Dv_0^4 \;=\; 0. \tag{36}$$

Then compute the partial derivatives of k with respect to the three homogeneous coordinates, giving

$$\frac{\partial k}{\partial v_0} \;:=\; 2Bv_0v_1^2 + 2Cv_0v_4^2 - 16a_1a_3v_0v_1v_4 + 4Dv_0^3 \;=\; 0, \tag{37}$$

$$\frac{\partial k}{\partial v_1} \;:=\; 2Av_1v_4^2 + 2Bv_0^2v_1 - 8a_1a_3v_0^2v_4 \;=\; 0, \tag{38}$$

$$\frac{\partial k}{\partial v_4} \;:=\; 2Av_1^2v_4 + 2Cv_0^2v_4 - 8a_1a_3v_0^2v_1 \;=\; 0. \tag{39}$$

[1] The maximum number of double points for a planar algebraic curve of degree n is $\frac{(n-1)(n-2)}{2}$.

Finally solve the system of four equations (36)-(39) for v_0, v_1, and v_4. In this case, similar for all the IO equations, there are two solutions which are independent of the design parameters a_1, a_2, a_3, and a_4. These two solutions are double points at infinity on the v_1 and v_4 axes, named DP_1 and DP_2:

$$DP_1 = \{v_0 = 0, v_1 = v_1, v_4 = 0\}; \tag{40}$$
$$DP_2 = \{v_0 = 0, v_1 = 0, v_4 = v_4\}. \tag{41}$$

One possibility to determine the type of double point, i.e., whether it is a crunode (regular double point), acnode (isolated double point), or cusp, is to evaluate whether the double point has a pair of real, or complex conjugate tangents. If the double point has two real distinct tangents, it is a crunode; if it has two real coincident tangents, it is a cusp; and if the tangents are both complex conjugates, the double point is an acnode [21, 37]. Thus, after homogenising each v_i-v_j angle pair IO equation using the homogenising coordinate v_0, leading to IO_h, the following discriminant yields information on the double point at infinity on the v_j axis:

$$\Delta := \left(\frac{\partial^2 IO_h}{\partial v_i \partial v_0}\right)^2 - \frac{\partial^2 IO_h}{\partial v_i^2}\frac{\partial^2 IO_h}{\partial v_0^2} \begin{cases} > 0 \Rightarrow \text{crunode;} \\ = 0 \Rightarrow \text{cusp;} \\ < 0 \Rightarrow \text{acnode.} \end{cases} \tag{42}$$

Proceeding with the double point analysis of all six v_i-v_j equations, the points at infinity on each axis result in 12 discriminants. However, as the v_i-v_j equations are all dependent on each other, only four are distinct. Each one describes the nature of the double point at infinity of each v_i for $i \in \{1...4\}$:

$$\begin{aligned} \Delta_{v_1} = {} & -4(a_1 + a_2 - a_3 - a_4)(a_1 + a_2 + a_3 - a_4) \\ & (a_1 - a_2 + a_3 - a_4)(a_1 - a_2 - a_3 - a_4); \end{aligned}$$

$$\begin{aligned} \Delta_{v_2} = {} & -4(a_1 - a_2 - a_3 + a_4)(a_1 - a_2 + a_3 + a_4) \\ & (a_1 - a_2 + a_3 - a_4)(a_1 - a_2 - a_3 - a_4); \end{aligned}$$

$$\begin{aligned} \Delta_{v_3} = {} & -4(a_1 - a_2 + a_3 + a_4)(a_1 + a_2 - a_3 + a_4) \\ & (a_1 + a_2 - a_3 - a_4)(a_1 - a_2 + a_3 - a_4); \end{aligned}$$

$$\begin{aligned} \Delta_{v_4} = {} & -4(a_1 + a_2 - a_3 + a_4)(a_1 - a_2 - a_3 + a_4) \\ & (a_1 - a_2 + a_3 - a_4)(a_1 + a_2 + a_3 - a_4). \end{aligned}$$

Using the bilinear factors defined by Eq. (4) these discriminants can be rewritten compactly as

$$\Delta_{v_1} = -4\ A_1 A_2 B_1 B_2, \tag{43}$$
$$\Delta_{v_2} = -4\ A_1 B_2 C_1 D_2, \tag{44}$$
$$\Delta_{v_3} = -4\ A_1 B_1 C_2 D_2, \tag{45}$$
$$\Delta_{v_4} = -4\ A_1 A_2 C_1 C_2. \tag{46}$$

From these conditions we can extract the following information. If $\Delta_{v_1} \geq 0$, then the double point at infinity on the v_1 axis is either a crunode or a cusp. Knowing that $v_1 = \infty$ corresponds to $\theta_1 = 180°$, which implies that the link a_1 can physically reach the extreme position where a_1 aligns with and overlays the previous link a_4. Similarly, if $\Delta_{v_1} < 0$, then the double point at $v_1 = \infty$ is an acnode which in turn indicates that a_1 can not physically reach the extreme position where a_1 aligns with and overlays a_4. Analogous conclusions can be drawn from Equations (44), (45), and (46).

As previously mentioned, to fully understand the mobility of every link, it equally requires the analysis of whether the other extremes where the link under investigation aligns with, but does not overlay, the previous link. We need to investigate whether the linkage is assemblable at $v_i = 0$. Clearly, one possibility to obtain a condition with this information can be derived using the six v_i-v_j equations by substituting $v_i = 0$ and solving for v_j. Again, due to the equations' dependencies, we obtain four distinct conditions, one for each v_i:

$$\begin{aligned}
\Omega_{v_1} &= [-(a_1 - a_2 - a_3 + a_4)(a_1 - a_2 + a_3 + a_4) \\
&\quad (a_1 + a_2 - a_3 + a_4)(a_1 + a_2 + a_3 + a_4)]^{\frac{1}{2}}; \\
\Omega_{v_2} &= [-(a_1 + a_2 - a_3 - a_4)(a_1 + a_2 + a_3 - a_4) \\
&\quad (a_1 + a_2 - a_3 + a_4)(a_1 + a_2 + a_3 + a_4)]^{\frac{1}{2}}; \\
\Omega_{v_3} &= [-(a_1 + a_2 + a_3 - a_4)(a_1 - a_2 - a_3 - a_4) \\
&\quad (a_1 - a_2 - a_3 + a_4)(a_1 + a_2 + a_3 + a_4)]^{\frac{1}{2}}; \\
\Omega_{v_4} &= [-(a_1 - a_2 - a_3 - a_4)(a_1 + a_2 - a_3 - a_4) \\
&\quad (a_1 - a_2 + a_3 + a_4)(a_1 + a_2 + a_3 + a_4)]^{\frac{1}{2}}.
\end{aligned}$$

Using the bilinear factors from Eq. 4 these expressions can be rewritten compactly as:

$$\Omega_{v_1} = \sqrt{-C_1 C_2 D_1 D_2}; \tag{47}$$
$$\Omega_{v_2} = \sqrt{-A_2 B_1 C_2 D_1}; \tag{48}$$
$$\Omega_{v_3} = \sqrt{-A_2 B_2 C_1 D_1}; \tag{49}$$
$$\Omega_{v_4} = \sqrt{-B_1 B_2 D_1 D_2}. \tag{50}$$

With this information we can establish a completely generic classification scheme to determine the relative mobilities of every link in the simple closed kinematic chain. Using the bilinear factors the classification can be constructed according to Tables 4-7. The beauty of this classification scheme lies in its completely generic nature, covering both positive and negative values for the a_i. This result requires the a_i to be considered as directed line segments. For

example $a_1 > 0$ means that it is directed from the join with a_4 to a_2, $a_1 < 0$ means a_1 points in the opposite direction. Moreover, the classification scheme is directly linked to the algebraic IO equations. We are now able to explain the different spatial sections that are spanned by the linear factors in the design parameter space reported in [36].

Table 4: Mobility of a_1 relative to a_4.

$A_1A_2B_1B_2$	$C_1C_2D_1D_2$	mobility of a_1
≤ 0	≤ 0	crank
≤ 0	> 0	π-rocker
> 0	≤ 0	0-rocker
> 0	> 0	rocker

Table 5: Mobility of a_2 relative to a_1.

$A_1B_2C_1D_2$	$A_2B_1C_2D_1$	mobility of a_2
≤ 0	≤ 0	crank
≤ 0	> 0	π-rocker
> 0	≤ 0	0-rocker
> 0	> 0	rocker

Table 6: Mobility of a_3 relative to a_2.

$A_1B_1C_2D_2$	$A_2B_2C_1D_1$	mobility of a_3
≤ 0	≤ 0	crank
≤ 0	> 0	π-rocker
> 0	≤ 0	0-rocker
> 0	> 0	rocker

Table 7: Mobility of a_4 relative to a_3.

$A_1A_2C_1C_2$	$B_1B_2D_1D_2$	mobility of a_4
≤ 0	≤ 0	crank
≤ 0	> 0	π-rocker
> 0	≤ 0	0-rocker
> 0	> 0	rocker

It is straightforward to use this same analysis applied to the spherical 4R as well as the planar RRRP linkages to determine the relative mobility conditions for each link in the chain. However, in the interest if brevity, we will not include these results in this paper.

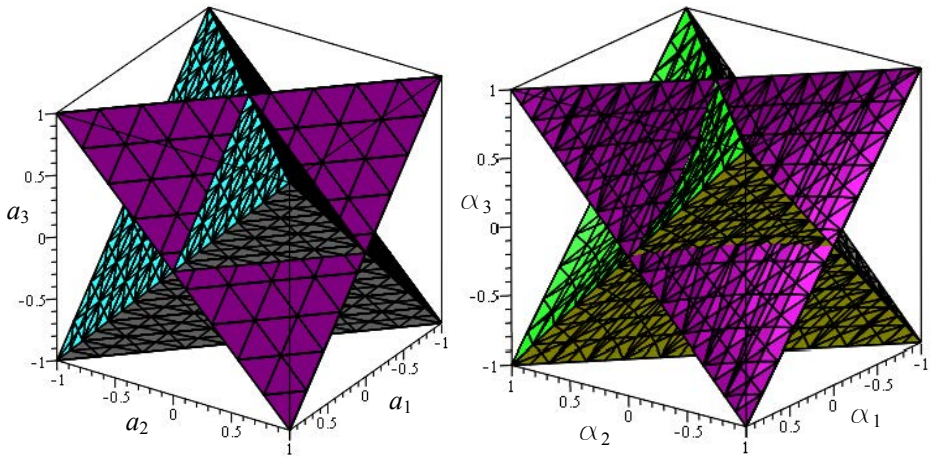

(a) Planar 4R stellated octahedron. (b) Spherical 4R degenerate bicubic surfaces.

Figure 5: Planar and spherical 4R design parameter spaces.

5.2. Design Parameter Spaces

The first graphical representation of the design parameter space of planar and spherical 4R linkages can be found in [38, 39, 40]. In the case of the planar 4R it reveals plane bound regions in a three-space having the Freudenstein parameters as mutually orthogonal basis vectors. However, the full symmetry of the group of planar 4R linkages is obscured by the trigonometric description of the IO equation. The symmetries of the algebraic IO equations for the spherical and planar 4R and the planar RRRP and PRRP linkages are fully revealed graphically when one considers the link lengths a_i, link offsets d_i, and link twist angle parameters α_i as design parameters, see [25, 36, 31]. For planar and spherical 4R function generators the scale of the linkage is irrelevant. We can consider these four a_i and four α_i design parameters as homogeneous coordinates, and assign a_4 and α_4 to normalise the four coordinates, thereby setting $a_4 = 1$ for the planar and $\alpha_4 = 1$ as the spherical design space parameter coordinates and treat the remaining three lengths or twist angles as mutually orthogonal basis vectors.

In the planar 4R design parameter three-space, each of the distinct eight bilinear factors in Eqs. (4)-(9) represent eight distinct planes. These eight planes intersect in 12 lines which are the edges of a setllated octahedron having order 48 octahedral symmetry [41], which Johannes Kepler named "stella octangula", which is Latin for "eight-pointed star", referring to the eight vertices, see Fig. 5a. In the entire universe of polytopes, it is the only regular compound of two tetrahedra [41]: two tetrahedra which intersect in an octahedron! Each distinct point in the design parameter space represents a distinct planar 4R linkage. The eight planes segment the design parameter space into regions that represent the mobility of the linkages contained in that region [36, 42].

For the spherical 4R, the eight bicubic factors in the four coefficients A, B, C,

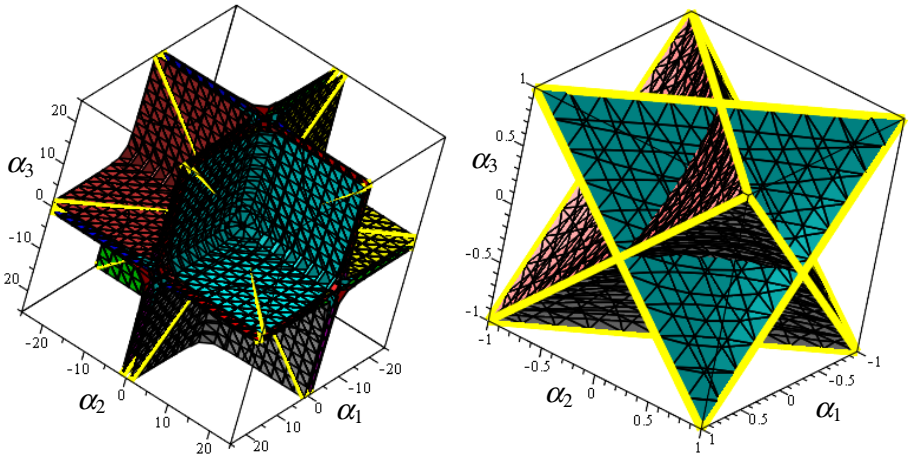

(a) In the range $-25 \leq \alpha_i \leq 25$.

(b) In the range $-1 \leq \alpha_i \leq 1$.

Figure 6: Eight cubic surfaces in the spherical 4R design parameter space.

and D in Eq. (23) are symmetric singular cubic surfaces, see Fig. 5b, which each possess three distinct finite lines and three common lines at infinity [25]. Note that a cubic surface can contain as many as 27 lines [43]; those that contain less than 27 are called *singular*, while those that contain exactly 27 are *non-singular*. Each of these cubic surfaces possess three ordinary double points [25]. It is also shown in [43] that a cubic surface possessing three ordinary double points can have, at most, 12 lines, which is the case for these eight cubic surfaces. Of these 12 lines on each surface, six are complex and six are real. Of the six real lines three are at infinity. The remaining three lines on each surface intersect each other in an equilateral triangle.

Different pairs of the eight cubic surfaces have one finite line in common, meaning there are 12 distinct finite lines among the eight surfaces. The finite lines contain the twelve edges of another stellated octahedron. The faces of the same stellated octahedron are also found in the design parameter space of planar 4R linkages. The edges of this regular double tetrahedron can be regarded as the intersection of the bilinear factors of the coefficients of the planar 4R and the singular cubic surfaces formed by the coefficients of the spherical 4R IO equations in the design parameter spaces. This is as remarkable as it is fascinating! Fig. 6 illustrates the eight cubic surfaces and the three finite lines on each. This illustrates the connection between Bricard's movable octahedra mentioned at the end of Section 3 and the intersection of the spherical 4R and planar 4R design parameter spaces.

With the six algebraic v_i-v_j equations, and the previously identified mobility classification using double points and discriminants, it becomes evident that the planes containing the faces of the stellated octahedron contain even more mobility information than stated in [36], namely, information on the relative mobility of every link in the chain! In fact, the stellated octahedron face planes

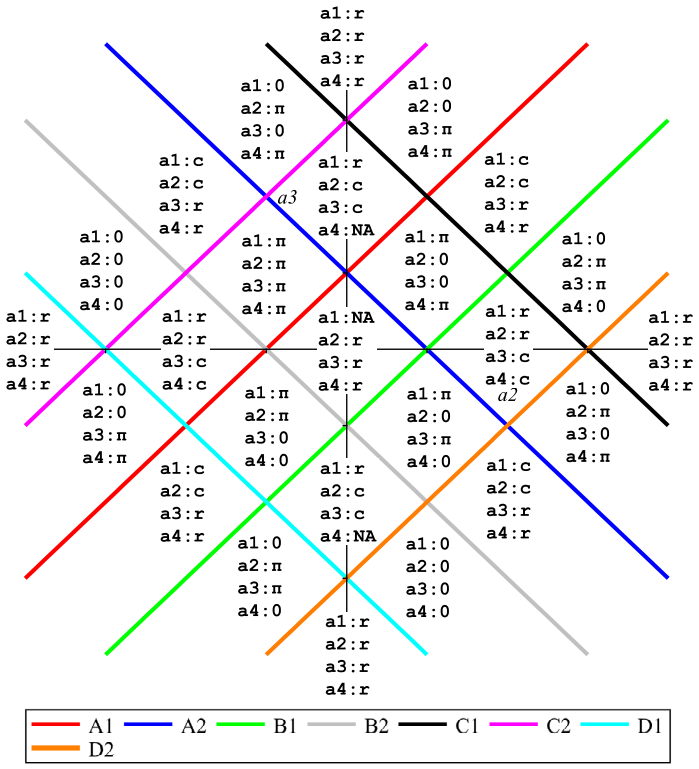

Figure 7: Intersection of the planar 4R stellated octahedron in the design parameter space with the plane $a_1 = 0.5$.

segment the design parameter space into distinct regions which each describes the relative mobility of a_1, a_2, a_3 and a_4. Since a complete analysis of the design parameter space would go well beyond the scope of this paper, we will limit the discussion herein to one short example as follows.

Consider the intersection traces of the bilinear factors in the parameter plane $a_1 = 0.5$ spanned by a_2 and a_3 in the design parameter space where a_2 and a_3 are the horizontal and vertical axes, respectively. Here the bilinear factors are parallel and orthogonal plane trace lines. Together with Tabs. 4-7, the mobility of all a_2 and a_3 of any length can now be identified, resulting in Fig. 7 where **r** indicates that the corresponding link is a rocker, **c** a crank, π a π-rocker, and **0** a 0-rocker, while NA indicates the linkage is not assemblable. This analysis can be conducted for every area separated by the bilinear factors in the design parameter space, resulting in a complete geometric mobility classification of planar four bar linkages which is directly linked to the six algebraic v_i-v_j IO equations.

6. Conclusions

In this paper we have derived the six possible planar 4R, RRRP, PRRP, and spherical 4R algebraic IO equations that describe the relative input and output joint displacement parameters between different pairs of edges of planar and spherical quadrangles providing a catalogue of 24 IO equations. They were derived using Study's soma coordinates that represent the displacement space of all kinematic chains, and polynomial elimination methods to reveal the desired algebraic IO equations. We showed that these algebraic polynomials define design parameter spaces, where distinct points represent distinct four-bar linkages. The location of the point in that space determines the linkage mobility characteristics. We showed that evaluating the nature of the double points at infinity in each of the v_i-v_j planes gives conditions on the relative mobility of each link in the kinematic chain.

Acknowledgements

The authors acknowledge the financial support of the Natural Sciences and Engineering Research Council of Canada (NSERC).

[1] M. Ceccarelli (Ed.), Distinguished Figures in Mechanism and Machine Science, Their Contributions and Legacies Part 1., Springer, NY, U.S.A., 2007.

[2] R. Willis, Principles of Mechanism, *2nd edition*, Cambridge University Press, Cambridge, England, 1841.

[3] F. Freudenstein, Design of four-link mechanisms, Ph.D. thesis, Columbia University, New York, NY, U.S.A (1954).

[4] J. Denavit, R. S. Hartenberg, A Kinematic Notation for Lower-pair Mechanisms Based on Matrices, Trans ASME J. Appl. Mech. 22 (2) (1955) 215–221.

[5] M. Savage, A. S. Hall, Unique Descriptions of All Spherical Four-bar Linkages., ASME J. Eng. Ind. 92 (3) (August 1970) 559–563.

[6] C. R. Barker, J. Lo, Classification of Spherical Four-bar Mechanisms., *Proceedings of the 1986 ASME Mechanisms Conference*, Columbus, OH, USA., 1986.

[7] C. H. Chiang, Kinematics of Spherical Mechanisms, Krieger Publishing Company, Malabar, FL, U.S.A., 2000.

[8] S. S. Balli, S. Chand, Transmission Angle in Mechanisms (Triangle in Mech), Mechanism and Machine Theory 37 (2) (2002) 175–195.

[9] H.-P. Schröcker, M. Husty, J. M. McCarthy, Kinematic Mapping Based Evaluation of Assembly Modes for Planar Four-bar Synthesis, ASME, Journal of Mechanical Design 129 (9) (2007) 924–929.

[10] S. Deshpande, A. Purwar, A Machine Learning Approach to Kinematic Synthesis of Defect-free Planar Four-bar Linkages, Journal of Computing and Information Science in Engineering 17 (2) (2019).

[11] Q. J. Ge, A. Purwar, Zhao, P., S. Deshpande, A Task-driven Approach to Unified Synthesis of Planar Four-bar Linkages Using Algebraic Fitting of a Pencil of G-manifolds, Journal of Computing and Information Science in Engineering 17 (2) (2019).

[12] S. Moazami, H. Zargarzadeh, S. Palanki, Kinematics of Spherical Robots Rolling Over 3D Terrains, Complexity 2019 (2019) https://doi.org/10.1155/2019/7543969.

[13] J. Plücker, "über ein neues Coordinatensystem", Journal für die reine und angewandte Mathematik (Crelle's Journal) vol. 5 (1830) pages 1–36.

[14] J. Plücker, "On a New Geometry of Space", Philosophical Transactions of the Royal Society of London vol. 155 (1865) pages 725–791.

[15] F. Klein, "Vergleichende Betrachtungen über neuere geometrische Forschungen, Erlangen", *reprinted in 1893*, Mathematische Annalen vol. 43 (1872) pages 63–100.

[16] E. Study, Geometrie der Dynamen, Teubner Verlag, Leipzig, Germany, 1903.

[17] O. Bottema, B. Roth, Theoretical Kinematics, Dover Publications, Inc., New York, N.Y., 1990.

[18] M. L. Husty, An Algorithm for Solving the Direct Kinematics of General Stewart-Gough Platforms, Mechanism and Machine Theory 31 (4) (1996) 365–379.

[19] E. J. F. Primrose, Planar Algebraic Curves, MacMillan, New York, NY, U.S.A., 1955.

[20] F. Klein, Elementary Mathematics from an Advanced Standpoint: Geometry, Dover Publications, Inc., New York, NY, U.S.A., 1939.

[21] M. L. Husty, A. Karger, H. Sachs, W. Steinhilper, Kinematik und Robotik, Springer-Verlag Berlin, Heidelberg, New York, 1997.

[22] D. Cox, J. Little, D. O'Shea, Ideals, Varieties, and Algorithms: an Introduction to Computational Algebraic Geometry and Commutative Algebra, 2nd Edition, Springer-Verlag, Berlin, Germany, 1997.

[23] M. Rotzoll, M. J. D. Hayes, M. L. Husty, M. Pfurner, A General Method for Determining Algebraic Input-Output Equations for Planar and Spherical 4R Linkages, in: J. Lenarčič, B. Siciliano (Eds.), Advances in Robotic Kinematics 2020, Springer International Publishing, Cham, Switzerland, 2021, pp. 90–97. doi:10.1007/978-3-030-50975-0_12.

[24] M. Rotzoll, M. J. D. Hayes, A General Method for Determining Algebraic Input-output Equations for the Slider-crank and the Bennett Linkage, 11th CCToMM Symposium on Mechanisms, Machines, and Mechatronics, eds. S. Nokleby, and P. Cardou, Ontario Tech University, Oshawa, ON, Canada, June 3-4, 2021.

[25] M. J. D. Hayes, M. Rotzoll, C. Ingalls, M. Pfurner, Design Parameter Space of Spherical Four-bar Linkages, in: C. B. Pisla, D., C. Vaida (Eds.), New Trends in Mechanism and Machine Science, EuCoMeS, Springer Nature Switzerland AG.

[26] M. Pfurner, Analysis of spatial serial manipulators using kinematic mapping, Ph.D. thesis, University of Innsbruck, Innsbruck, Austria (2006).

[27] A. Shabani, J. M. Porta, F. Thomas, A Branch-and-prune Method to Solve Closure Equations in Dual Quaternions, Mechanism and Machine Theory 164. doi:https://doi.org/10.1016/j.mechmachtheory.2021.104424.

[28] W. Adams, P. Loustaunau, An Introduction to Gröbner Bases, Vol. 3, American Mathematical Society, Graduate Studies in Mathematics, 1994.

[29] M. J. D. Hayes, M. Rotzoll, M. L. Husty, Design parameter space of planar four-bar linkages, in: T. Uhl (Ed.), Advances in Mechanism and Machine Science, Springer Nature, Cham, Switzerland, 2019, pp. 229–238.

[30] A. Harnack, Über die Vieltheiligkeit der ebenen algebraischen Curven, Mathematische Annalen 10 (1876) 189–198.

[31] A. Nichol, M. Rotzoll, M. J. D. Hayes, Planar RRRP Mechanism Design Parameter Space, 11th CCToMM Symposium on Mechanisms, Machines, and Mechatronics, eds. S. Nokleby, and P. Cardou, Ontario Tech University, Oshawa, ON, Canada, June 3-4, 2021.

[32] R. S. Hartenberg, J. Denavit, Kinematic Synthesis of Linkages, McGraw-Hill, Book Co., New York, NY, U.S.A., 1964.

[33] R. Bricard, Mémoire sur la théorie de l'octaèdre articulé, J. Math. Pures Appl. 3 (1897) 113–148.

[34] M. J. D. Hayes, M. Rotzoll, A. Iraei, A. Nichol, Q. Bucciol, Algebraic Differential Kinematics of Planar 4R Linkages, 20th International Conference on Advanced Robotics, ICAR 2021, Ljubljana, Slovenia, 2021.

[35] A. P. Murray, P. M. Larochelle, A Classification Scheme for Planar $4R$, Spherical $4R$, and Spatial $RCCR$ Linkages to Facilitate Computer Animation, *Proceedings of 1998 ASME Design Engineering Technical Conferences (DETC'98)*, Atlanta, Georgia, U.S.A., September 13-16, 1998.

[36] M. J. D. Hayes, M. Rotzoll, M. L. Husty, M. Pfurner, "Design Parameter Space of Planar Four-bar Linkages", Proceedings of the 15^{th} IFToMM World Congress, June 30-July 4, 2019.

[37] R. Cipolla, P. Giblin, Visual Motion of Curves and Surfaces, Cambridge University Press, Cambridge, U.K., 2000.

[38] C. M. Gosselin, J. Angeles, Representation graphique de la region de mobilite des mecanismes plans et spheriques a barres articulees, Mechanism and Machine Theory 22 (6) (1987) 557–562. doi:https://doi.org/10.1016/0094-114X(87)90050-4.
URL https://www.sciencedirect.com/science/article/pii/0094114X87900504

[39] C. M. Gosselin, J. Angeles, Mobility Analysis of Planar and Spherical Linkages, Computers in Mechanical Engineering.

[40] C. M. Gosselin, J. Angeles, Optimization of Planar and Spherical Function Generators as Minimum-defect Linkages, Mechanism and Machine Theory 24 (4) (1989) 293–307.

[41] H. S. M. Coxeter, Regular Polytopes, 3^{rd} Edition, Dover Publications, Inc., New York, NY, U.S.A., 1973.

[42] M. Rotzoll, Q. Bucciol, M. J. D. Hayes, Algebraic Input-output Angle Equation Derivation Algorithm for the Six Distinct Angle Pairings in Arbitrary Planar 4R Linkages, in: 20th International Conference on Advanced Robotics, ICAR 2021, *Ljubljana, Slovenia*, 2021.

[43] B. Segre, The Non-singular Cubic Surfaces; a New Method of Investigation with Special Reference to Questions of Reality, Oxford, The Clarendon Press, 1942.

Kinematic geometry of spatial RSSR mechanisms

Mirja Rotzoll[a], Margaret H. Regan[b], Manfred L. Husty[c], M. John D. Hayes[a,*]

[a] *Carleton University, 1125 Colonel By Drive, Ottawa, ON K1S 5B6, Canada*
[b] *Duke University, 120 Science Drive Physics 117, Durham, NC 27708, U.S.A.*
[c] *University of Innsbruck, Technikerstraße 13, 6020 Innsbruck, Austria*

Abstract

Two different novel methods to derive the input-output (IO) equation of arbitrary RSSR linkages are described. Both methods share some common elements, i.e., they use the standard Denavit-Hartenberg notation to first describe the linkage as an open kinematic chain, and Study's kinematic mapping to describe the displacement of the coordinate frame attached to the end-effector of the chain with respect to the relatively non-moving base frame. The kinematic closure equation is obtained in the seven-dimensional projective kinematic mapping image space by equating the eight Study soma coordinates to the identity array. Then two methods are successfully applied to eliminate the intermediate joint angle parameters leading to the degree four biquadratic implicit algebraic IO equation: a) the linear implicitisation algorithm, which can be applied after rearranging the closure equation such that the linkage can be viewed as two serial RS chains, and b) numerical elimination theory using pseudowitness sets. Both approaches lead to the same IO equation. The utility of this algebraic form of the IO equation is illustrated with three detailed application examples.

Keywords: RSSR linkage, Study soma coordinates, algebraic input-output equation, linear implicitisation algorithm.

1. Introduction

The RSSR mechanism has been investigated since 1955 [1], if not earlier. It has been broadly used in modern applications ranging from hinging to landing gear deployment systems so there has long been a need for design tools for synthesis and analysis. The earliest works considering mobility limits date from as early as 1969, see [2, 3, 4, 5]. Displacement and dynamic analysis of the RSSR dates from 1972, if not earlier [6, 7]. Optimal synthesis of RSSR linkages for various objectives can be traced to the early 1980s [8], but there is also modern interest, see [9] for example. Rigid body motion synthesis using Study's kinematic mapping [10] was elegantly developed for planar four-bar

*Corresponding Author
Email address: john.hayes@carleton.ca (M. John D. Hayes)

linkages in [11]. Motivated by this, a derivation algorithm that describes the linkage using Denavit Hartenberg (DH) parameters, projects the displacement transformation matrix into Study's kinematic image space, and manipulates the resulting equations via Gröbner bases to obtain the algebraic input-output (IO) equation for planar, spherical, and Bennett linkages has been investigated with results reported in the literature by the authors of this paper. A natural extension of this algorithm to general motion in three dimensional space is to apply it to another well-investigated spatial linkage, the RSSR, which will be the main focus of this paper. In addition, the results obtained using the polynomial elimination method [12] are supported by a numerical method [13] leading to an identical algebraic IO equation, as well as a verification of the equation using an animated example linkage that was created in the GeoGebra software.

It is important to note that we make no claims regarding the relative ease or difficulty of the method presented in this paper for deriving the RSSR algebraic IO equation compared to any existing method, we simply claim that it is different. However, to underscore the utility of this form of the algebraic RSSR IO equation as the cornerstone for development of powerful novel mechanical design tools for synthesis and analysis, three detailed example applications are presented: continuous approximate synthesis for function generation minimising the design and structural errors; mobility limits; and extreme values of angular velocity and acceleration.

The RSSR linkage consists of two revolute (R) and two spherical (S) joints and following the Kutzbach criterion, possesses 2 degrees of freedom (dof). However, one dof that does not influence the IO equation corresponds to the rotation of the coupler link between the two spherical joints about its own longitudinal axis. This so-called idle dof can have a positive effect on the durability of the linkage in engineering applications, as it helps to evenly wear the S joints. Generally, the IO equation of the RSSR is much more involved compared to the planar, and spherical ones, as in addition to the link lengths between the four joints, the linkage further possesses three additional design parameters between the revolute joints, i.e., two link offsets and a link twist. Previous trigonometric derivations of the RSSR IO equation are available, for example, in [1, 14, 15]. Hartenberg and Denavit's derivation of the IO equation [14] uses their well-known parameters and trigonometric relations, while the derivation in [15] leads to an equation that resembles a more complex version of the Freudenstein equation [16]. This is not entirely surprising given that the planar four-bar is a special case of the RSSR linkage.

2. Denavit-Hartenberg (DH) Parametrisation

The literature contains many variations of the original Denavit-Hartenberg (DH) coordinate system and parameter assignment convention. For example, subtly different coordinate frame attachment rules and parameter definitions have been devised for mechanical system calibration, dynamic analysis, accounting for misalignment of joint axis directions, etc., see [17, 18, 19, 20] for several

different examples. Therefore, it is important to precisely define the convention used in this work to avoid confusion and misinterpretation since the corresponding coordinate transformations are all different from those of Denavit and Hartenberg.

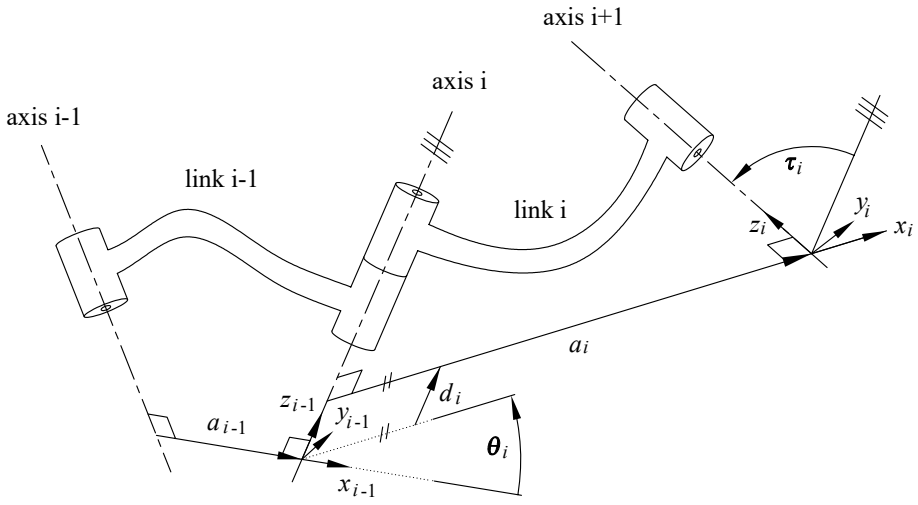

Figure 1: DH parameters in a general serial 3R kinematic chain.

To visualise the four DH parameters, consider two arbitrary sequential neighbouring links, $i-1$ and i. Two such links are illustrated, together with their DH coordinate systems and parameters, in Fig. 1. The DH parameters [21] are defined in the following way.

θ_i, joint angle: the angle from x_{i-1} to x_i measured about z_{i-1}.

d_i, link offset: the distance from x_{i-1} to x_i measured along z_{i-1}.

τ_i, link twist: the angle from z_{i-1} to z_i measured about x_i.

a_i, link length: the directed distance from z_{i-1} to z_i measured along x_i.

Each of the two S joints of the RSSR can be modelled as three R joints whose rotation axes are mutually orthogonal and intersect at the sphere centre. Hence, eight coordinate frames are attached to the linkage. The chosen coordinate systems are illustrated in Fig. 2 and the corresponding DH parameters are to be found in Table 1. Note that the only link twist that is a design parameter is τ_8. The twists between the three mutually orthogonal R joint axes comprising the S joints are $\pm\pi$. We arbitrarily use the positive value, as the sign has no impact on the resulting algebraic IO equation.

In the remainder of this paper, the tangent half angle substitutions for the angle parameters $v_i = \tan(\theta_i/2)$ and $\alpha_i = \tan(\tau_i/2)$ will be used in order to

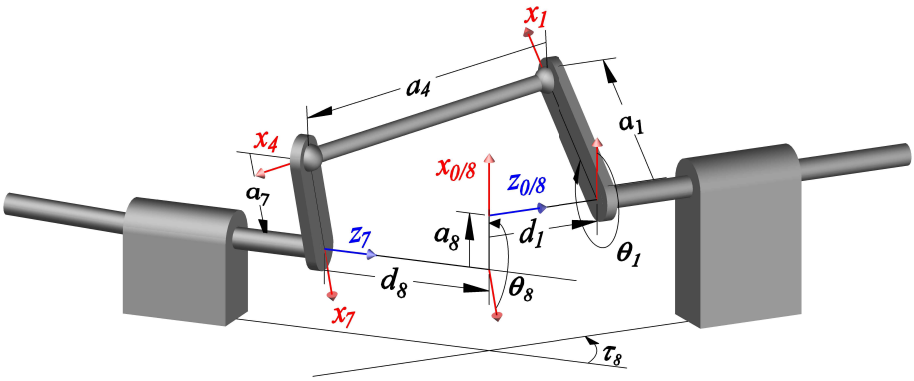

Figure 2: An arbitrary RSSR mechanism.

Table 1: DH parameters for the RSSR mechanism.

joint axis i	joint angle θ_i	link offset d_i	link length a_i	link twist τ_i
1	θ_1	d_1	a_1	0
2	θ_2	0	0	$\pi/2$
3	θ_3	0	0	$\pi/2$
4	θ_4	0	a_4	0
5	θ_5	0	0	$\pi/2$
6	θ_6	0	0	$\pi/2$
7	θ_7	0	a_7	0
8	θ_8	d_8	a_8	τ_8

algebraise the transformations. This implies that

$$\cos\theta_i = \frac{1-v_i^2}{1+v_i^2}, \quad \sin\theta_i = \frac{2v_i}{1+v_i^2}, \tag{1}$$

$$\cos\tau_i = \frac{1-\alpha_i^2}{1+\alpha_i^2}, \quad \sin\tau_i = \frac{2\alpha_i}{1+\alpha_i^2}. \tag{2}$$

We begin with a serial RSSR kinematic chain and determine the forward kinematics following [21]. The required multiplication of the individual DH transformation matrices from one coordinate frame to another yields the overall homogeneous transformation matrix that describes the relationship between the first and last coordinate frames. To close the kinematic chain, we want the first and last coordinate systems to align in both their orientation and origin. Algebraically, this is specified using the kinematic closure equation, where the

overall transformation equates to the identity [21]

$$\prod_{i=1}^{8} {}_{i}^{i-1}\mathbf{T} = \mathbf{I}. \tag{3}$$

The elements of this algebraic DH transformation matrix are then directly mapped into Study's kinematic image space where the constraint manifold could be analysed as it has already been successfully demonstrated for the planar 4R, spherical 4R, and Bennett linkage by the authors. However, applying Gröbner bases or other elimination methods to the eight Study soma coordinates to symbolically obtain the IO equation for the RSSR linkage is computationally too demanding for an algebraic geometry approach. While very computationally demanding, a numerical approach that uses the forward kinematics of the serial RSSR chain mapped to the eight soma coordinates, described in Section 5, using pseudowitness sets leads directly to the desired IO equation. Still, there are algebraic approaches.

A well known algebraic geometry approach to obtain an expression for the forward and inverse kinematics of a serial kinematic chain is to split it into two subchains, thereby conceptually splitting the closure equation in two by multiplying both sides by the inverses of half of the DH transformations. In the case of the RSSR, the closure equation becomes

$${}_{1}^{0}\mathbf{T}\ {}_{2}^{1}\mathbf{T}\ {}_{3}^{2}\mathbf{T}\ {}_{4}^{3}\mathbf{T} = \mathbf{I}\ {}_{8}^{7}\mathbf{T}^{-1}\ {}_{7}^{6}\mathbf{T}^{-1}\ {}_{6}^{5}\mathbf{T}^{-1}\ {}_{5}^{4}\mathbf{T}^{-1}. \tag{4}$$

This step essentially divides the linkage into two serial chains joined at the 4th coordinate frame located in the second S joint, i.e., one serial chain between the coordinate frames 0 and 4, and one serial chain between the coordinate frames 4 and 8, which correspond to the expressions on the left and right sides of Eq. (4), respectively, which we call the left RS and right RS dyads. Eq. (4) will be used in Section 4 to obtain the algebraic IO equation by projecting it to the image space. However, before we proceed we will briefly recall Study's kinematic mapping [10].

3. Study's Kinematic Mapping

The homogeneous transformation matrices in Eqs. (3) and (4) represent a subgroup of the group of spatial Euclidean displacements, $SE(3)$, with respect to a relatively non-moving coordinate frame. There are several possibilities to parameterise this rigid body displacement group, one of them being the kinematic mapping that was originally formulated by Eduard Study and reported in an appendix of his book "Geometrie der Dynamen" [10] in 1903. It defines every distinct Euclidean displacement as a distinct point on a six-dimensional quadric hyper-surface in a seven-dimensional projective space $\mathbb{P}^7$ now known as the Study quadric, S_6^2. A point on S_6^2 consists of eight homogeneous coordinates, not all zero, $[x_0 : x_1 : x_2 : x_3 : y_0 : y_1 : y_2 : y_3]$ which Study called a "soma", a

Greek word meaning "body". The hyper-surface is a seven-dimensional bilinear hyper-quadratic equation given by

$$x_0y_0 + x_1y_1 + x_2y_2 + x_3y_3 = 0, \tag{5}$$

excluding the *exceptional generator*, which we call A_∞, where $x_0 = x_1 = x_2 = x_3 = 0$, having the parametric representation

$$[0 : 0 : 0 : 0 : y_0 : y_1 : y_2 : y_3].$$

A_∞ does not represent any real displacement, but it nonetheless plays an important role as a generator space. For a soma to represent a real displacement in $SE(3)$, it must satisfy two conditions: the first being Eq. (5); the second being the inequality

$$x_0^2 + x_1^2 + x_2^2 + x_3^2 \quad \neq \quad 0. \tag{6}$$

Eq. (5) contains only bilinear cross terms. This implies that the quadric has been rotated out of its standard position, or normal form. It is straightforward to diagonalise the quadratic form of Eq. (5) which reveals that this six-dimensional quadric in $\mathbb{P}^7$ has the normal form

$$x_0^2 + x_1^2 + x_2^2 + x_3^2 - y_0^2 - y_1^2 - y_2^2 - y_3^2 = 0, \tag{7}$$

which is analogous to the Plücker quadric, P_4^2, of line geometry. The normal form of S_6^2 shows that it is a six-dimensional hyperboloid of one sheet doubly-ruled by special 3-space generators in two opposite reguli, which we call A-planes and B-planes, after [22].

It can be shown that lines on S_6^2 represent either a one parameter set of translations or rotations. The lines which contain the 1×8 identity array $[1 : 0 : 0 : \ldots : 0]$, which Study called the "protosoma", are either the one parameter rotation or translation subgroups. The exceptional generator A_∞ is an A-plane. In general, two different A-planes do not intersect, nor do two different B-planes, but there are exceptions [23]. An A-plane corresponds to $SO(3)$ if it contains the identity and its intersection with A_∞ is the empty set, and to $SE(2)$ if it contains the identity and intersects A_∞ in a line. These two types of A-planes intersect each other in lines on S_6^2. Each of these lines represent rotations about the line orthogonal to the plane of the planar displacement and through the centre point of the spherical displacement [23, 24]. The only B-planes that intersect A_∞ correspond to the subgroup of all translations, while in general the intersection of an A-plane and a B-plane is either a point, or a two dimensional plane [25].

Given a homogeneous transformation matrix $\mathbf{T}$ whose 3×3 rotation submatrix elements are denoted as $\mathbf{A} = (a_{ij})$ with $i, j \in \{1, 2, 3\}$ and whose translation vector elements are denoted as t_k with $k \in \{1, 2, 3\}$, then the corresponding Study soma coordinates, also known as Study parameters, are obtained in the following way. The homogeneous quadruple $x_0 : x_1 : x_2 : x_3$ can be obtained

from at least one of the following ratios:

$$\begin{aligned} x_0 : x_1 : x_2 : x_3 = & \ 1 + a_{11} + a_{22} + a_{33} : a_{32} - a_{23} : a_{13} - a_{31} : a_{21} - a_{12}; \\ = & \ a_{32} - a_{23} : 1 + a_{11} - a_{22} - a_{33} : a_{12} + a_{21} : a_{31} + a_{13}; \\ = & \ a_{13} - a_{31} : a_{12} + a_{21} : 1 - a_{11} + a_{22} - a_{33} : a_{23} + a_{32}; \\ = & \ a_{21} - a_{12} : a_{31} + a_{13} : a_{23} + a_{32} : 1 - a_{11} - a_{22} + a_{33}. \end{aligned} \quad (8)$$

The remaining four coordinates $y_0 : y_1 : y_2 : y_3$ are linear combinations of the x_i and t_i and are computed as

$$\begin{aligned} y_0 &= \tfrac{1}{2}(t_1x_1 + t_2x_2 + t_3x_3), & y_1 &= \tfrac{1}{2}(-t_1x_0 + t_3x_2 - t_2x_3), \\ y_2 &= \tfrac{1}{2}(-t_2x_0 - t_3x_1 + t_1x_3), & y_3 &= \tfrac{1}{2}(-t_3x_0 + t_2x_1 - t_1x_2). \end{aligned} \quad (9)$$

Study developed the method to compute the four x_i parameters directly from the 3×3 rotation submatrix $\mathbf{A}$ via one of the four sets of ratios expressed in Eq. (8). In general each of the four yield the same ratios. But in certain instances, for example when $\mathbf{A}$ describes a rotation through angle π, one or more of the four ratios in Eq. (8) result in $x_0 : x_1 : x_2 : x_3 = 0 : 0 : 0 : 0$, the exceptional generator. But for every rotation matrix $\mathbf{A}$ at least one of the four ratios does not result in four zeros. Study also showed that the mapping is bijective, meaning that for each point on S_6^2 there is one and only one Euclidean displacement represented by the homogeneous 4×4 transformation matrix $\mathbf{T}$:

$$\mathbf{T} = \frac{1}{\delta}\begin{bmatrix} x_0^2 + x_1^2 + x_2^2 + x_3^2 & 0 & 0 & 0 \\ 2(-x_0y_1 + x_1y_0 - x_2y_3 + x_3y_2) & x_0^2 + x_1^2 - x_2^2 - x_3^2 & 2(-x_0x_3 + x_1x_2) & 2(x_0x_2 + x_1x_3) \\ 2(-x_0y_2 + x_1y_3 + x_2y_0 - x_3y_1) & 2(x_0x_3 + x_1x_2) & x_0^2 - x_1^2 + x_2^2 - x_3^2 & 2(-x_0x_1 + x_2x_3) \\ 2(-x_0y_3 - x_1y_2 + x_2y_1 + x_3y_0) & 2(-x_0x_2 + x_1x_3) & 2(x_0x_1 + x_2x_3) & x_0^2 - x_1^2 - x_2^2 + x_3^2 \end{bmatrix}$$

where $\delta = x_0^2 + x_1^2 + x_2^2 + x_3^2$. The first column is the associated translation of the Euclidean displacement and the elements of the lower right 3×3 submatrix are the nine a_{ij} of the associated rotation matrix $\mathbf{A}$. Hence, the mechanical constraints imposed by the type of joints used in the kinematic chains of the RSSR are mapped onto Study's quadric. The result is a parametric representation in terms of Study soma coordinates of the constraint manifold.

The image of the overall DH transformation matrix $\mathbf{T}$ of the RSSR linkage, Eq. (3), in terms of Study parameters yields

$$\begin{aligned} x_0 &= 2v_1v_2v_3v_4v_5v_6v_7v_8 - 2v_1v_2v_3v_4v_5v_6 + ... + 2\alpha_8v_6v_8 + 2v_7v_8 - 2, \\ x_1 &= 2\alpha_8v_1v_2v_3v_4v_5v_6v_7v_8 - 2\alpha_8v_1v_2v_3v_4v_5v_6 + ... + 2\alpha_8v_7v_8 - 2\alpha_8, \\ x_2 &= -2\alpha_8v_1v_2v_3v_4v_5v_6v_7 - 2\alpha_8v_1v_2v_3v_4v_5v_6v_8 + ... - 2\alpha_8v_7 - 2\alpha_8v_8, \\ x_3 &= -2v_1v_2v_3v_4v_5v_6v_7 - 2v_1v_2v_3v_4v_5v_6v_8 + ... + 2\alpha_8v_6 - 2v_7 - 2v_8, \\ y_0 &= -a_1\alpha_8v_1v_2v_3v_4v_5v_6v_7v_8 + a_4\alpha_8v_1v_2v_3v_4v_5v_6v_7v_8 + ... - \alpha_8a_8, \\ y_1 &= a_1v_1v_2v_3v_4v_5v_6v_7v_8 - a_4v_1v_2v_3v_4v_5v_6v_7v_8 + ... + a_1 + a_4 + a_7 + a_8, \\ y_2 &= -\alpha_8d_1v_1v_2v_3v_4v_5v_6v_7v_8 - \alpha_8d_8v_1v_2v_3v_4v_5v_6v_7v_8 + ... + \alpha_8d_8, \\ y_3 &= -d_1\alpha_8v_1v_2v_3v_4v_5v_6v_7v_8 - d_8v_1v_2v_3v_4v_5v_6v_7v_8 + ... + d_1 + d_8. \end{aligned} \quad (10)$$

As these polynomials are extremely large, each containing 128 very large terms, only the beginning and end of the expressions sorted using graded lexicographic ordering with $v_1 > v_2 > \ldots > v_8$ are displayed here. These polynomials will be solved numerically in Section 5, but are otherwise too cumbersome to deal with using algebraic geometry and computer algebra software, such as Maple 2021. For this we require a different approach.

As mentioned earlier, one well known different approach involves conceptually splitting the RSSR into two serial RS chains. In this way, mapping the left hand side of Eq. (4), the left RS chain, into Study's kinematic image space yields eight significantly smaller polynomials

$$
\begin{aligned}
x_0 &= 4v_1v_2v_3v_4 - 4v_1v_3 - 4v_2v_3 - 4v_3v_4,\\
x_1 &= -4v_1v_2 + 4v_1v_4 + 4v_2v_4 + 4,\\
x_2 &= 4v_1v_2v_4 + 4v_1 + 4v_2 - 4v_4,\\
x_3 &= -4v_1v_2v_3 - 4v_1v_3v_4 - 4v_2v_3v_4 + 4v_3,\\
y_0 &= -2d_1v_1v_2v_3 - 2d_1v_1v_3v_4 - 2d_1v_2v_3v_4 + 2a_1v_1v_2 - 2a_4v_1v_2 - 2a_1v_1v_4\\
&\quad + 2a_4v_1v_4 + 2a_1v_2v_4 + 2a_4v_2v_4 + 2d_1v_3 + 2a_1 + 2a_4,\\
y_1 &= 2a_1v_1v_2v_3v_4 - 2a_4v_1v_2v_3v_4 + 2d_1v_1v_2v_4 - 2a_1v_1v_3 + 2a_4v_1v_3 + 2a_1v_2v_3\\
&\quad + 2a_4v_2v_3 + 2a_1v_3v_4 + 2a_4v_3v_4 + 2d_1v_1 + 2d_1v_2 - 2d_1v_4,\\
y_2 &= 2a_1v_1v_2v_3 + 2a_4v_1v_2v_3 + 2a_1v_1v_3v_4 + 2a_4v_1v_3v_4 - 2a_1v_2v_3v_4 + 2a_4v_2v_3v_4\\
&\quad + 2d_1v_1v_2 - 2d_1v_1v_4 - 2d_1v_2v_4 + 2a_1v_3 - 2a_4v_3 - 2d_1,\\
y_3 &= -2d_1v_1v_2v_3v_4 + 2a_1v_1v_2v_4 + 2a_4v_1v_2v_4 + 2d_1v_1v_3 + 2d_1v_2v_3 + 2d_1v_3v_4\\
&\quad + 2a_1v_1 + 2a_4v_1 - 2a_1v_2 + 2a_4v_2 + 2a_1v_4 - 2a_4v_4.
\end{aligned}
\tag{11}
$$

And finally, mapping the right hand side of Eq. (4), the right RS chain, into Study's kinematic image space yields eight additional smaller polynomials

$$
\begin{aligned}
x_0 &= 4v_5v_6v_7v_8 - 4v_5v_6 - 4\alpha_8v_5v_7 - 4\alpha_8v_5v_8 - 4v_6v_7 - 4v_6v_8 + 4\alpha_8v_7v_8 - 4\alpha_8,\\
x_1 &= -4\alpha_8v_5v_6v_7v_8 + 4\alpha_8v_5v_6 - 4v_5v_7 - 4v_5v_8 + 4\alpha_8v_6v_7 + 4\alpha_8v_6v_8 + 4v_7v_8 - 4,\\
x_2 &= 4\alpha_8v_5v_6v_7 + 4\alpha_8v_5v_6v_8 + 4v_5v_7v_8 + 4\alpha_8v_6v_7v_8 - 4v_5 - 4\alpha_8v_6 + 4v_7 + 4v_8,\\
x_3 &= 4v_5v_6v_7 + 4v_5v_6v_8 - 4\alpha_8v_5v_7v_8 + 4v_6v_7v_8 + 4\alpha_8v_5 - 4v_6 - 4\alpha_8v_7 - 4\alpha_8v_8,\\
y_0 &= -2a_7\alpha_8v_5v_6v_7v_8 + 2a_8\alpha_8v_5v_6v_7v_8 - 2d_8v_5v_6v_7 - 2d_8v_5v_6v_8 - 2\alpha_8d_8v_5v_7v_8\\
&\quad - 2d_8v_6v_7v_8 - 2a_7\alpha_8v_5v_6 - 2a_8\alpha_8v_5v_6 + 2a_7v_5v_7 + 2a_8v_5v_7 - 2a_7v_5v_8\\
&\quad + 2a_8v_5v_8 - 2a_7\alpha_8v_6v_7 - 2a_8\alpha_8v_6v_7 + 2a_7\alpha_8v_6v_8 - 2a_8\alpha_8v_6v_8 + 2a_7v_7v_8\\
&\quad - 2a_8v_7v_8 + 2\alpha_8d_8v_5 + 2d_8v_6 - 2\alpha_8d_8v_7 - 2\alpha_8d_8v_8 + 2a_7 + 2a_8,\\
y_1 &= -2a_7v_5v_6v_7v_8 + 2a_8v_5v_6v_7v_8 + 2\alpha_8d_8v_5v_6v_7 + 2\alpha_8d_8v_5v_6v_8 - 2d_8v_5v_7v_8\\
&\quad + 2\alpha_8d_8v_6v_7v_8 - 2a_7v_5v_6 - 2a_8v_5v_6 - 2a_7\alpha_8v_5v_7 - 2a_8\alpha_8v_5v_7 + 2a_7\alpha_8v_5v_8\\
&\quad - 2a_8\alpha_8v_5v_8 - 2a_7v_6v_7 - 2a_8v_6v_7 + 2a_7v_6v_8 - 2a_8v_6v_8 - 2a_7\alpha_8v_7v_8\\
&\quad + 2a_8\alpha_8v_7v_8 + 2d_8v_5 - 2\alpha_8d_8v_6 - 2d_8v_7 - 2d_8v_8 - 2a_7\alpha_8 - 2a_8\alpha_8,\\
y_2 &= 2\alpha_8d_8v_5v_6v_7v_8 - 2a_7v_5v_6v_7 - 2a_8v_5v_6v_7 + 2a_7v_5v_6v_8 - 2a_8v_5v_6v_8\\
&\quad - 2a_7\alpha_8v_5v_7v_8 + 2a_8\alpha_8v_5v_7v_8 + 2a_7v_6v_7v_8 - 2a_8v_6v_7v_8 - 2\alpha_8d_8v_5v_6
\end{aligned}
\tag{12}
$$

$$
\begin{aligned}
&- 2d_8v_5v_7 - 2d_8v_5v_8 - 2\alpha_8d_8v_6v_7 - 2\alpha_8d_8v_6v_8 + 2d_8v_7v_8 - 2a_7\alpha_8v_5 \\
&- 2a_8\alpha_8v_5 + 2a_7v_6 + 2a_8v_6 + 2a_7\alpha_8v_7 + 2a_8\alpha_8v_7 - 2a_7\alpha_8v_8 + 2a_8\alpha_8v_8 - 2d_8, \\
y_3 = {} & 2d_8v_5v_6v_7v_8 + 2a_7\alpha_8v_5v_6v_7 + 2a_8\alpha_8v_5v_6v_7 - 2a_7\alpha_8v_5v_6v_8 + 2a_8\alpha_8v_5v_6v_8 \\
&- 2a_7v_5v_7v_8 + 2a_8v_5v_7v_8 - 2a_7\alpha_8v_6v_7v_8 + 2a_8\alpha_8v_6v_7v_8 - 2d_8v_5v_6 \\
&+ 2\alpha_8d_8v_5v_7 + 2\alpha_8d_8v_5v_8 - 2d_8v_6v_7 - 2d_8v_6v_8 - 2\alpha_8d_8v_7v_8 - 2a_7v_5 - 2a_8v_5 \\
&- 2a_7\alpha_8v_6 - 2a_8\alpha_8v_6 + 2a_7v_7 + 2a_8v_7 - 2a_7v_8 + 2a_8v_8 + 2\alpha_8d_8.
\end{aligned}
$$

The polynomials of Eqs. (11) and (12) will be manipulated in Section 4 using the linear implicitisation algorithm [12] to reveal the algebraic RSSR IO equation.

4. Algebraic Geometry Approach

To obtain the RSSR algebraic IO equation, the parametric equations of the Study coordinates of Eqs. (11) and (12) need to be expressed implicitly as a single polynomial equation in the desired motion parameters v_1 and v_8 in the seven-dimensional kinematic mapping image space. This requires an algorithm that eliminates the unwanted motion parameters v_i where $i \in \{2, \ldots, 7\}$. One implicitisation algorithm that allows for the transformation from the explicit parametric Study representation into a set of implicit polynomial equations is known as the linear implicitisation algorithm. The resulting constraint equations are implicit polynomials that form an algebraic variety in $\mathbb{P}^7$ and can be manipulated with different tools to obtain the IO equation. A detailed description of the linear implicitisation algorithm, together with illustrative examples is to be found in [12, 26].

The two serial RS chains of the RSSR linkage consist of one revolute and one spherical joint each. Clearly, the S joint spherical displacements, $SO(3)$, are completely contained on sub-spaces of the Study quadric as there is no translation involved and thus, all four y_i Study coordinates are identically zero. In other words, the displacements constrained by the S joints form special A-planes on the Study quadric. Further, the R joint in the serial RS chain rotates the S joint in a planar displacement thereby moving this special A-plane on S_6^2. It is well known that a 3-space can be represented by the intersection of four hyperplanes in the kinematic image space. To determine the RSSR algebraic IO equation we must identify these hyperplanes, one set for each serial RS chain. To obtain their implicit equations the linear implicitisation algorithm will be employed. The main goal of the linear implicitisation algorithm is to find the minimal number of implicit equations that describe the mechanical constraints in the image space. It allows for the elimination of motion parameters which, in the case of the RSSR, correspond to the variables $v_2, v_3, \ldots, v_7$. On the other hand, the design parameters a_i, d_i and α_i are fixed values that depend on the chosen linkage. However, to obtain the implicit polynomials for the spherical special 3-spaces v_1 and v_8 are temporarily also considered as design parameter constants.

To begin, we assume that the resulting variety is defined by linear constraint equations, and hence a general linear ansatz polynomial can be written, using

the graded reverse lexicographic monomial ordering [27], as

$$C_1y_3 + C_2y_2 + C_3y_1 + C_4y_0 + C_5x_3 + C_6x_2 + C_7x_1 + C_8x_0 = 0. \tag{13}$$

This linear ansatz polynomial has eight unknown coefficients C_i, $i \in \{1, \cdots, 8\}$. In the case of the left hand side of the RSSR chain, Eq. (11) is substituted into Eq. (13) and after reorganising such that the variable angle parameters of the spherical displacement are collected, yields

$$\begin{aligned}
&(-2C_1d_1v_1 + 2C_3a_1v_1 - 2C_3a_4v_1 + 4C_8v_1 - 2C_4d_1 - 2C_2a_1 + 2C_2a_4 - 4C_5)v_2v_3v_4 \\
&+ (2C_2a_1v_1 + 2C_2a_4v_1 - 2C_4d_1v_1 - 4C_5v_1 + 2C_1d_1 + 2C_3a_1 + 2C_3a_4 - 4C_8)v_2v_3 \\
&+ (2C_1a_1v_1 + 2C_1a_4v_1 + 2C_3d_1v_1 + 4C_6v_1 - 2C_2d_1 + 2C_4a_1 + 2C_4a_4 + 4C_7)v_2v_4 \\
&+ (2C_2d_1v_1 + 2C_4a_1v_1 - 2C_4a_4v_1 - 4C_7v_1 - 2C_1a_1 + 2C_1a_4 + 2C_3d_1 + 4C_6)v_2 \\
&+ (2C_2a_1v_1 + 2C_2a_4v_1 - 2C_4d_1v_1 - 4C_5v_1 + 2C_1d_1 + 2C_3a_1 + 2C_3a_4 - 4C_8)v_3v_4 \\
&+ (2C_1d_1v_1 - 2C_3a_1v_1 + 2C_3a_4v_1 - 4C_8v_1 + 2C_2a_1 - 2C_2a_4 + 2C_4d_1 + 4C_5)v_3 \\
&+ (-2C_2d_1v_1 - 2C_4a_1v_1 + 2C_4a_4v_1 + 4C_7v_1 + 2C_1a_1 - 2C_1a_4 - 2C_3d_1 - 4C_6)v_4 \\
&+ (2C_1a_1v_1 + 2C_1a_4v_1 + 2C_3d_1v_1 + 4C_6v_1 - 2C_2d_1 + 2C_4a_1 + 2C_4a_4 + 4C_7) = 0.
\end{aligned} \tag{14}$$

To fulfil this equation, the coefficients of the motion parameters in Eq. (14) must vanish since the v_2, v_3, and v_4 orientation angle parameters are, in general non-zero. In matrix form, this can be expressed as

$$\begin{bmatrix}
2a_1v_1 + 2a_4v_1 & -2d_1 & 2d_1v_1 & 2a_1 + 2a_4 & 0 & 4v_1 & 4 & 0 \\
-2d_1v_1 & -2a_1 + 2a_4 & 2a_1v_1 - 2a_4v_1 & -2d_1 & -4 & 0 & 0 & 4v_1 \\
-2a_1 + 2a_4 & 2d_1v_1 & 2d_1 & 2a_1v_1 - 2a_4v_1 & 0 & 4 & -4v_1 & 0 \\
2a_1v_1 + 2a_4v_1 & -2d_1 & 2d_1v_1 & 2a_1 + 2a_4 & 0 & 4v_1 & 4 & 0 \\
2d_1 & 2a_1v_1 + 2a_4v_1 & 2a_1 + 2a_4 & -2d_1v_1 & -4v_1 & 0 & 0 & -4 \\
2d_1 & 2a_1v_1 + 2a_4v_1 & 2a_1 + 2a_4 & -2d_1v_1 & -4v_1 & 0 & 0 & -4 \\
2d_1v_1 & 2a_1 - 2a_4 & -2a_1v_1 + 2a_4v_1 & 2d_1 & 4 & 0 & 0 & -4v_1 \\
2a_1 - 2a_4 & -2d_1v_1 & -2d_1 & -2a_1v_1 + 2a_4v_1 & 0 & -4 & 4v_1 & 0
\end{bmatrix}
\begin{bmatrix} C_1 \\ C_2 \\ C_3 \\ C_4 \\ C_5 \\ C_6 \\ C_7 \\ C_8 \end{bmatrix} =
\begin{bmatrix} 0 \\ 0 \\ 0 \\ 0 \\ 0 \\ 0 \\ 0 \\ 0 \end{bmatrix}.$$

Solving for the unknown C_i and back-substituting their solutions into the general linear ansatz polynomial Eq. (13) reveals all four hyperplanes that satisfy the variety in $\mathbb{P}^7$. The solution shows that C_1, C_3, C_4, and C_8 are all free parameters with arbitrary values while C_2, C_5, C_6, and C_7 are expressions containing only v_1 and the design parameters and, after simplifying, are each linear in four of the Study parameters, and therefore hyperplanes. These four hyperplanes collected in terms of the Study parameters are

$$\begin{aligned}
0 &= (a_1^2v_1^2 - a_4^2v_1^2 + d_1^2v_1^2 + a_1^2 - a_4^2 + d_1^2)x_3 + (-2d_1v_1^2 - 2d_1)y_0 \\
&\quad + 4a_1v_1y_1 + (2a_1v_1^2 - 2a_4v_1^2 - 2a_1 - 2a_4)y_2, \qquad (15) \\
0 &= (a_1^2v_1^2 - a_4^2v_1^2 + d_1^2v_1^2 + a_1^2 - a_4^2 + d_1^2)x_2 - 4a_1v_1y_0 + (-2d_1v_1^2 - 2d_1)y_1 \\
&\quad + (-2a_1v_1^2 + 2a_4v_1^2 + 2a_1 + 2a_4)y_3, \qquad (16) \\
0 &= (a_1^2v_1^2 - a_4^2v_1^2 + d_1^2v_1^2 + a_1^2 - a_4^2 + d_1^2)x_1 + (2a_1v_1^2 + 2a_4v_1^2 - 2a_1 + 2a_4)y_0 \\
&\quad + (2d_1v_1^2 + 2d_1)y_2 - 4a_1v_1y_3, \qquad (17)
\end{aligned}$$

$$0 = (a_1^2v_1^2 - a_4^2v_1^2 + d_1^2v_1^2 + a_1^2 - a_4^2 + d_1^2)x_0 + (-2a_1v_1^2 - 2a_4v_1^2 + 2a_1 - 2a_4)y_1 + 4a_1v_1y_2 + (2d_1v_1^2 + 2d_1)y_3. \tag{18}$$

The same procedure can be done with the right hand side of the RSSR by substituting Eq. (12) in the general linear ansatz polynomial, Eq. (13). In this case, the motion parameters to be eliminated are v_5, v_6 and v_7. Solving the resulting homogeneous matrix equation for the new unknown C_i yields the following four hyperplanes in a similar way. They are

$$\begin{aligned}0 = {} & (a_7^2\alpha_8^2v_8^2 - 2a_7a_8\alpha_8^2v_8^2 + a_8^2\alpha_8^2v_8^2 + \alpha_8^2d_8^2v_8^2 + a_7^2v_8^2 - 2a_8a_7v_8^2 \\ & + a_8^2v_8^2 + d_8^2v_8^2 + \alpha_8^2a_7^2 + 2a_7a_8\alpha_8^2 + a_8^2\alpha_8^2 + \alpha_8^2d_8^2 + a_7^2 + 2a_7a_8 + a_8^2 + d_8^2)x_3 \\ & + (-2\alpha_8^2d_8v_8^2 + 2d_8v_8^2 + 8a_7\alpha_8v_8 - 2\alpha_8^2d_8 + 2d_8)y_0 \\ & + (-4d_8\alpha_8v_8^2 - 4\alpha_8^2a_7v_8 + 4a_7v_8 - 4d_8\alpha_8)y_1 \\ & + (-2a_7\alpha_8^2v_8^2 + 2\alpha_8^2a_8v_8^2 - 2a_7v_8^2 + 2a_8v_8^2 + 2a_7\alpha_8^2 + 2\alpha_8^2a_8 + 2a_7 + 2a_8)y_2,\end{aligned} \tag{19}$$

$$\begin{aligned}0 = {} & (a_7^2\alpha_8^2v_8^2 - 2a_7a_8\alpha_8^2v_8^2 + a_8^2\alpha_8^2v_8^2 + \alpha_8^2d_8^2v_8^2 + a_7^2v_8^2 - 2a_8a_7v_8^2 \\ & + a_8^2v_8^2 + d_8^2v_8^2 + \alpha_8^2a_7^2 + 2a_7a_8\alpha_8^2 + a_8^2\alpha_8^2 + \alpha_8^2d_8^2 + a_7^2 + 2a_7a_8 + a_8^2 + d_8^2)x_2 \\ & + (4d_8\alpha_8v_8^2 + 4\alpha_8^2a_7v_8 - 4a_7v_8 + 4d_8\alpha_8)y_0 \\ & + (-2\alpha_8^2d_8v_8^2 + 2d_8v_8^2 + 8a_7\alpha_8v_8 - 2\alpha_8^2d_8 + 2d_8)y_1 \\ & + (2a_7\alpha_8^2v_8^2 - 2\alpha_8^2a_8v_8^2 + 2a_7v_8^2 - 2a_8v_8^2 - 2a_7\alpha_8^2 - 2\alpha_8^2a_8 - 2a_7 - 2a_8)y_3,\end{aligned} \tag{20}$$

$$\begin{aligned}0 = {} & (a_7^2\alpha_8^2v_8^2 - 2a_7a_8\alpha_8^2v_8^2 + a_8^2\alpha_8^2v_8^2 + \alpha_8^2d_8^2v_8^2 + a_7^2v_8^2 - 2a_8a_7v_8^2 \\ & + a_8^2v_8^2 + d_8^2v_8^2 + \alpha_8^2a_7^2 + 2a_7a_8\alpha_8^2 + a_8^2\alpha_8^2 + \alpha_8^2d_8^2 + a_7^2 + 2a_7a_8 + a_8^2 + d_8^2)x_1 \\ & + (-2a_7\alpha_8^2v_8^2 + 2\alpha_8^2a_8v_8^2 - 2a_7v_8^2 + 2a_8v_8^2 + 2a_7\alpha_8^2 + 2\alpha_8^2a_8 + 2a_7 + 2a_8)y_0 \\ & + (2\alpha_8^2d_8v_8^2 - 2d_8v_8^2 - 8a_7\alpha_8v_8 + 2\alpha_8^2d_8 - 2d_8)y_2 \\ & + (4d_8\alpha_8v_8^2 + 4\alpha_8^2a_7v_8 - 4a_7v_8 + 4d_8\alpha_8)y_3,\end{aligned} \tag{21}$$

$$\begin{aligned}0 = {} & (a_7^2\alpha_8^2v_8^2 - 2a_7a_8\alpha_8^2v_8^2 + a_8^2\alpha_8^2v_8^2 + \alpha_8^2d_8^2v_8^2 + a_7^2v_8^2 - 2a_8a_7v_8^2 \\ & + a_8^2v_8^2 + d_8^2v_8^2 + \alpha_8^2a_7^2 + 2a_7a_8\alpha_8^2 + a_8^2\alpha_8^2 + \alpha_8^2d_8^2 + a_7^2 + 2a_7a_8 + a_8^2 + d_8^2)x_0 \\ & + (2a_7\alpha_8^2v_8^2 - 2\alpha_8^2a_8v_8^2 + 2a_7v_8^2 - 2a_8v_8^2 - 2a_7\alpha_8^2 - 2\alpha_8^2a_8 - 2a_7 - 2a_8)y_1 \\ & + (-4d_8\alpha_8v_8^2 - 4\alpha_8^2a_7v_8 + 4a_7v_8 - 4d_8\alpha_8)y_2 \\ & + (2\alpha_8^2d_8v_8^2 - 2d_8v_8^2 - 8a_7\alpha_8v_8 + 2\alpha_8^2d_8 - 2d_8)y_3.\end{aligned} \tag{22}$$

Solving Eqs. (15), ..., (18) for the four y_i and substituting these expressions into Eqs. (19), ..., (22) leaves four equations in the four unknown Study parameters x_i. This suggests solving the system of four equations for the four unknown x_i. However, doing so leads only to the trivial solution $x_i = y_i = 0$, $i \in \{0, 1, 2, 3\}$, which we call the null point. This result can be explained geometrically in $\mathbb{P}^7$ as follows: the two special 3-spaces representing the displacements of the S joints are two $SO(3)$ A-planes that are moved around on S_6^2 under the action of the two R joints, and only ever intersect in the null point.

But, there is a solution. Further inspection of the four equations shows that the equations form a homogeneous system of linear equations. Expressing this linear homogeneous system in matrix-vector form $\mathbf{Cx} = \mathbf{0}$, we know that this system only has a nontrivial solution when the determinant of the 4×4 coefficient matrix $\mathbf{C}$ with respect to the x_i vanishes [28]. Thus, after computing the determinant and omitting the factors that can never vanish, the general algebraic IO equation of the RSSR linkage arises directly from the determinant as

$$\begin{gathered} Av_1^2v_8^2 + 8d_1\alpha_8a_7v_1^2v_8 + 8d_8\alpha_8a_1v_1v_8^2 + Bv_1^2 \\ +8a_1a_7(\alpha_8 - 1)(\alpha_8 + 1)v_1v_8 + Cv_8^2 + 8d_8\alpha_8a_1v_1 + 8d_1\alpha_8a_7v_8 + D = 0, \end{gathered} \tag{23}$$

where

$$\begin{aligned} A &= (\alpha_8^2 + 1)A_1A_2 + R, \\ B &= (\alpha_8^2 + 1)B_1B_2 + R, \\ C &= (\alpha_8^2 + 1)C_1C_2 + R, \\ D &= (\alpha_8^2 + 1)D_1D_2 + R, \end{aligned}$$

and

$$\begin{aligned} A_1 &= (a_1 - a_4 + a_7 - a_8), & A_2 &= (a_1 + a_4 + a_7 - a_8), \\ B_1 &= (a_1 + a_4 - a_7 - a_8), & B_2 &= (a_1 - a_4 - a_7 - a_8), \\ C_1 &= (a_1 - a_4 - a_7 + a_8), & C_2 &= (a_1 + a_4 - a_7 + a_8), \\ D_1 &= (a_1 + a_4 + a_7 + a_8), & D_2 &= (a_1 - a_4 + a_7 + a_8), \end{aligned}$$

with

$$R = (d_1 - d_8)^2\alpha_8^2 + (d_1 + d_8)^2.$$

Eq. (23) is an implicit biquadratic algebraic curve of degree 4 in the joint angle parameters v_1 and v_8, as one would expect.

5. Numerical Approach

The degree four algebraic IO equation for the RSSR expressed as Eq. (23) will be compared to the result from a concomitant numerical method. The aim for the numerical method is to compute an eliminant with the general approach of numerical elimination theory [29, Ch. 16]. This involves performing computations using the given polynomial system from Eq. (10) and geometrically projecting points via pseudowitness sets [30]. For this problem, the pseudowitness set provided that the degree of the eliminant is 8 in 9 variables $(v_1, v_8, \alpha_8, a_1, a_4, a_7, a_8, d_1, d_8)$. Since there are a total of $\binom{9+8}{8} = 24310$ monomials of degree at most 8 in 9 variables, the approach is to use the pseudowitness set to generate at least 24310 sample points and then to use interpolation to

recover the eliminant [31, Ch. 6]. To gather these sample points, one randomly fixes values of the parameters $\alpha_8, a_1, a_4, a_7, a_8, d_1, d_8$, and solves for the angle parameter values, v_1 and v_8 using any of a variety of sampling methods within numerical algebraic geometry [32, Sec. 2.3]. This yields precisely the same IO equation as the linear implicitisation approach, Eq. (23).

6. Geometric Verification

To verify both the algebraic and numerical results, the IO equation of an arbitrary linkage was animated in GeoGebra. The model enabled measurement of the output angle for any given input angle. Tracing the locus of each input-output pair results in a curve which is compared with the herein derived IO equation, Eq. (23). The chosen design parameters for the example linkage are $a_1 = 3$, $a_4 = 5$, $a_7 = 9$, $a_8 = 11$, $d_1 = 1$, $d_8 = 3$, and $\tau_8 = 60°$. While the

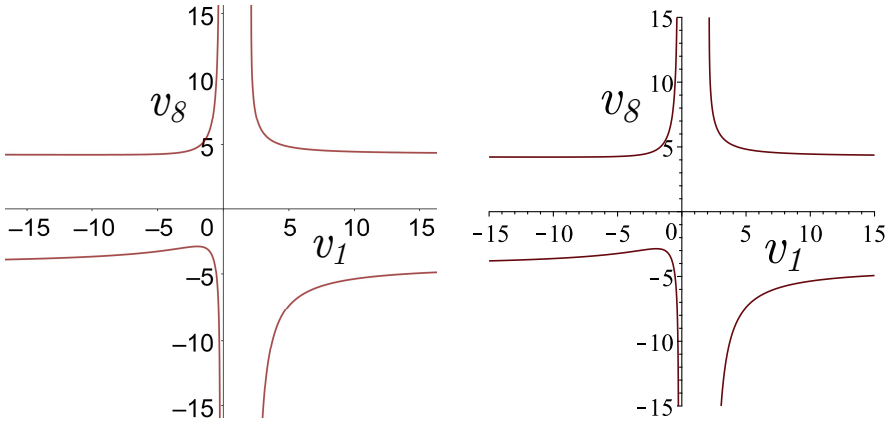

(a) IO equation generated in GeoGebra. (b) Derived IO equation according to Eq. (23).

Figure 3: Example RSSR function generator with $a_1 = 3$, $a_4 = 5$, $a_7 = 9$, $a_8 = 11$, $d_1 = 1$, $d_8 = 3$, and $\tau_8 = 60°$.

result of the GeoGebra file is displayed in Fig. 3a, substituting the same design parameters into Eq. (23) yields the curve in Fig. 3b. As can be seen, the curves are congruent which further suggests that Eq. (23) is indeed correct.

7. Applications

To demonstrate how the form of the algebraic IO equation for the RSSR linkage that has been obtained by the methods outlined in this paper is particularly useful for mechanical design by way of synthesis and analysis of RSSR mechanisms, several applications will be summarised and illustrated with examples. While it must be acknowledged that the IO equation itself is not new, see the 1955 book by J.S. Beggs for example [1], the algebraic form leads to computationally efficient and mathematically elegant tools for synthesis and analysis

of RSSR linkages that are entirely new, and will be reported for the first time in what follows.

7.1. Continuous Approximate Synthesis of RSSR Function Generators Minimising the Design and Structural Errors

For an RSSR function generator linkage, the synthesis equation will contain six of the seven DH design parameters a_1, a_4, a_7, d_1, and d_8, all normalised by $a_8 = 1$, along with the twist parameter α_8. Exact synthesis results in a linkage that precisely generates the prescribed function, but only for the six precision IO pairs, which are used to generate a set of six synthesis equations linear in the six unknown DH link design parameters. In a highly relevant paper from 1973 [15], the trigonometric form of the RSSR IO equation is derived in the style of Freudenstein for the first time, leading to a synthesis equation with all seven of the DH design parameters which was successfully applied to exact function generator synthesis.

Whereas, approximate synthesis uses $n > 7$ precision IO pairs to create an overconstrained set of synthesis equations leading to a linkage that generates the desired function, in general, but only approximately over the desired displacement range due to errors induced by the number of precision pairs as well as their spacing. *Design* and *structural* errors [14] are important performance indicators used in the assessment and optimisation of mechanical systems intended as function generating linkages designed by means of approximate synthesis. The design error is the residual of the identified linkage in satisfying the synthesis equation [16], and is evaluated at each of $n > 7$ precision points in a discrete set satisfying the prescribed function. Minimising the Euclidean norm of the design error leads to a linear least-squares problem. The structural error, on the other hand, is defined as the difference between the prescribed output angle, and the output angle that is generated by the linkage at each precision point [33]. This problem is typically solved by minimising the norm of the array of the structural error evaluated at each precision point using some form of Gauss-Newton non-linear minimisation, requiring an iterative solution procedure that terminates when a desired minimum norm threshold is obtained. The structural error is arguably the metric that truly matters since it is directly related to the physical performance of the linkage.

However, it was observed in [34] that as the cardinality of the data set used to compute the design error minimising linkage becomes large, on the order of $n \geq 40$, the design error minimising linkage tends to converge to the structural error minimising linkage. Hence, one may avoid the non-linear structural error computation provided a sufficient number of precision points are specified. Continuous approximate synthesis eliminates the problem of determining an appropriate cardinality for the data-set because it evaluates the case for $n \to \infty$. Hence there is no need to search for some convergence in order to set an appropriate value of n, which eliminates a source of error. Unfortunately, while it was demonstrated in [35] that this extension is possible through the integration of the trigonometric Freudenstein equation for planar 4R linkages, the generalisation of the process is computationally prohibitive and any advantage obtained

through the elimination of the need for an explicit solution to the non-linear structural error problem is lost to the numerical complexity of the integration. The planar 4R continuous approximate synthesis example presented in [35] employed the Matlab function *quadl*, which employs recursive adaptive Lobatto quadrature [36], and the computation time to approximately evaluate the integral required more than four hours on an Intel 32-bit dual-core x86 CPU @ 3.10 GHz. The relative complexity involved in integrating the trigonometric RSSR IO equation would likely require an order of magnitude more computation time than that required to integrate that of the 4R IO equation.

While there are many algebraic, meaning non-trigonometric, methods for approximate synthesis in the vast body of literature, see [37] for but one example, there are none which integrate the synthesis equations, thereby making the cardinality of the IO data set tend towards infinity. The following method integrates the square of Eq. (23) between the lower and upper input angular range limits generating a continuous infinite set of IO angle pairs. We partition the result into a 25x1 array of angle parameters which we call the synthesis array $\mathbf{s}$, and a 25x1 array of the seven associated DH link coefficients of $a_1, a_4, a_7, a_8, d_1, d_8$ and the twist parameter α_8, which we call the design parameter array $\mathbf{p}$. Substitute the prescribed function $v_8 = f(v_1)$ into the synthesis array, $\mathbf{s}$. To establish the synthesis equation, which is now a function of only v_1, take the Euclidean inner product of $\mathbf{p}$ with the integral of $\mathbf{s}$ over the prescribed bounds for v_1. The result of this inner product is then minimised over the real numbers. The output of this method is the seven link DH parameters that minimise both the design and structural errors for the RSSR linkage in generating the prescribed $v_8 = f(v_1)$ function, which is summarised by

$$\min_{(a_1,a_4,a_7,a_8,d_1,d_8,\alpha_8)\in\mathbb{R}} \left(\mathbf{p} \cdot \int_{v_{1_{\min}}}^{v_{1_{\max}}} \mathbf{s}(v_1, f(v_1)) dv_i \right) = 0. \tag{24}$$

The *Minimize* command used in Maple 2021 to solve the problem computes a local minimum of an objective function subject to constraints. If the problem is convex, as when the objective function and constraints are linear, for example, the solution will also be a global minimum. The algorithms that this command use assume the objective function and constraints are twice continuously differentiable. In this context, the Euclidean norm of the structural error over every point in the generated function is nothing more than the area between the prescribed function and the generated function in the variable angle parameter plain, which is equivalent to the design error.

An example will now be considered. Let the prescribed function be

$$v_8 = 2 + \tan\left(\frac{v_1}{{v_1}^2 + 1}\right), \quad 0 \leq v_1 \leq 2. \tag{25}$$

The first step is to compute Eq. (24). Then, to obtain a reasonable initial guess for the *Minimize* command used in Maple 2021, six IO pairs $[v_1, v_8]$ were

specified for the exact synthesis problem with $a_8 = 1$ as

$$[0, 2], \left[\frac{1}{5}, \frac{6560}{2989}\right], \left[\frac{1}{4}, \frac{30055}{13419}\right], \left[\frac{1}{3}, \frac{31661}{3710}\right], \left[\frac{1}{2}, \frac{49597}{0471}\right], \left[1, \frac{64699}{25409}\right].$$

The exact synthesis results are listed in Table 2. Using those design parameters as initial guesses for the *Minimize* command lead to the parameter values also listed in Table 2. The run time needed by Maple 2021 to integrate Eq. (24) on a 64-bit Intel Core i7-7700 CPU @ 3.60 GHz was 9.23 seconds, while the time required to run the *Minimize* command was less than 0.01 seconds. This runtime is impressive given that the computations were preformed using symbolic computer algebra compared to the 4 hours to run the numerical integration for a planar 4R linkage using Matlab; granted that this computation was performed on a much older Intel 32-bit dual-core x86 CPU @ 3.10 GHz. Regardless, the trigonometric integration required three orders of magnitude more computation time for the planar 4R synthesis compared to time required for the spatial RSSR synthesis.

Table 2: Synthesis results.

DH parameters	Exact synthesis	Continuous approximate synthesis
a_1	-0.5469961643	-0.481883141397214
a_4	3.760575070	3.76405010790231
a_7	1.349675373	1.35343558991690
a_8	1	0.957062422213279
α_8	0.8098696692	0.807467792413472
d_1	-4.899249807	-4.89575807959238
d_8	1.499319150	1.58161616407823

Table 3: Structural error generating Eq. (25).

Structural error	Exact synthesis	Continuous approximate synthesis
	0.011635738	-0.000261858

A comparison of the prescribed function Eq. (25) with the exact and continuous approximate synthesis generated functions in the v_1-v_8 plane are shown in Fig. 4. The structural and design errors are simply the difference of the areas under the IO curves. It is to be seen that the structural error for the continuous approximate synthesis linkage is two orders of magnitude smaller that the structural error for the linkage generated using exact synthesis, see Table 3.

7.2. Mobility Limits

With the algebraic IO equation, it is a very simple matter to determine general conditions for the relative mobility of the two ground fixed links. Treating the v_1-v_8 IO pair to be coordinate axes in the plane spanned by the two, then

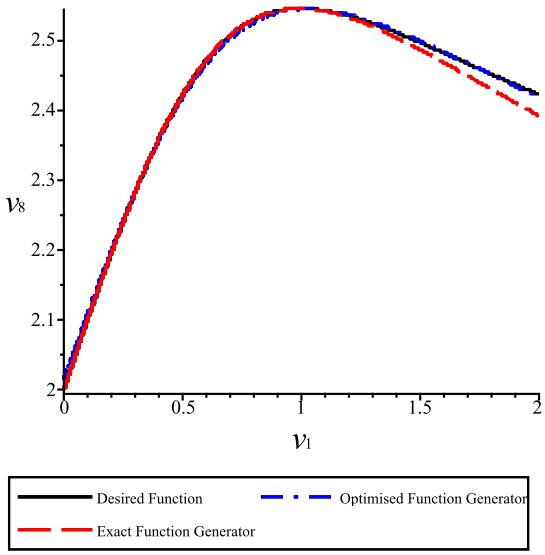

Figure 4: The prescribed, exact, and continuous synthesis approximation of Eq. (25) in the v1-v8 plane.

the IO equation contains two double points at infinity on the v_1 and v_8 axes. The double points at infinity belonging to each of the coordinate axes together with the ability of links a_1 and a_7 to reach $v_1 = 0$ and $v_8 = 0$ completely define the mobility limits, if they exist, between the v_1-v_8 angle parameter pair. The examination of this is sufficient to determine whether a particular joint enables a crank, a rocker, a π-rocker, or a 0-rocker link motion. See [4] from 1971 for the first double point analysis of the RSSR, but only for a simplified special case, where mobility criteria, though incomplete, are reported.

We proceed by evaluating whether each double point has a pair of real, or complex conjugate tangents. If the double point has two real distinct tangents, it is a crunode; if it has two real coincident tangents, it is a cusp; and if the tangents are both complex conjugates, the double point is an acnode. Thus, after homogenising the v_1-v_8 IO equation using the homogenising coordinate v_0, leading to IO_h, the following discriminant yields information on the double point at infinity on the v_i axis:

$$\Delta_{v_i} = \left(\frac{\partial^2 IO_h}{\partial v_j \partial v_0}\right)^2 - \frac{\partial^2 IO_h}{\partial v_j^2}\frac{\partial^2 IO_h}{\partial v_0^2} \begin{cases} > 0 \Rightarrow \text{crunode;} \\ = 0 \Rightarrow \text{cusp;} \\ < 0 \Rightarrow \text{acnode.} \end{cases} \tag{26}$$

The values for Δ_{v_1} and Δ_{v_8} are obtained by substituting values for the seven variable link DH design parameters into the following two discriminants:

$$\Delta_{v_1} = 32a_7^2\alpha_8^2 d_1^2 - AB; \tag{27}$$

and

$$\Delta_{v_8} = 32a_1^2\alpha_8^2 d_8^2 - AC, \tag{28}$$

Table 4: Mobility of a_1 and a_7.

Δ_{v_1}	Ω_{v_1}	mobility of a_1	Δ_{v_8}	Ω_{v_8}	mobility of a_7
≥ 0	≥ 0	crank	≥ 0	≥ 0	crank
≥ 0	< 0	π-rocker	≥ 0	< 0	π-rocker
< 0	≥ 0	0-rocker	< 0	≥ 0	0-rocker
< 0	< 0	rocker	< 0	< 0	rocker

where A, B, and C are all defined in Eq. (23).

From these conditions we can extract information on the ability of the input and output links to rotate through π. For example, if $\Delta_{v_1} \geq 0$, then the double point at $v_1 = \infty$ is either a crunode or a cusp. Knowing that $v_1 = \infty$ corresponds to $\theta_1 = 180^\circ$, this implies that the link a_1 can rotate through π. Similarly, if $\Delta_{v_1} < 0$, then the double point at $v_1 = \infty$ is an acnode which in turn indicates that a_1 has a rotation limit less than π.

It is equally required to investigate whether the linkage is assemblable at $v_i = 0$. Clearly, one possibility to obtain a condition with this information can be derived using the v_1-v_8 equation by substituting $v_i = 0$ and solving for v_j. For each of v_1 and v_8 we obtain a radicand Ω_v whose value must be $\Omega_v \geq 0$ if the link can rotate through 0:

$$\begin{aligned}\Omega_{v_1} \;=\;& -\alpha_8^2\left(d_1-d_8\right)^2\left(\alpha_8^2\left(d_1-d_8\right)^2+2\left(d_1+d_8\right)^2\right)-\left(d_1+d_8\right)^4+\\ & 2\big(a_1^2+2a_1a_8-a_4^2+a_7^2+a_8^2\big)\big[4d_8\big(\alpha_8^4d_1-\alpha_8^2d_8-d_1\big)-\big(d_1^2+d_8^2\big)\left(\alpha_8^4+1\right)\big]+\\ & 4\left(a_1^2+2a_1a_8-a_4^2-3a_7^2+a_8^2\right)\alpha_8^2d_1^2-C_1C_2D_1D_2\left(\alpha_8^2+1\right)^2; \qquad (29)\end{aligned}$$

$$\begin{aligned}\Omega_{v_8} \;=\;& -\alpha_8^2\left(d_1-d_8\right)^2\left(\alpha_8^2\left(d_1-d_8\right)^2+2\left(d_1+d_8\right)^2\right)-\left(d_1+d_8\right)^4+\\ & 2\big(a_1^2-a_4^2+a_7^2+2a_7a_8+a_8^2\big)\big[4d_1\big(d_8\alpha_8^4-\alpha_8^2d_1-d_8\big)-\big(d_1^2+d_8^2\big)\left(\alpha_8^4+1\right)\big]+\\ & 4\left(3a_1^2+a_4^2-a_7^2-2a_7a_8-a_8^2\right)\alpha_8^2d_8^2-B_1B_2D_1D_2\left(\alpha_8^2+1\right)^2; \qquad (30)\end{aligned}$$

where B_1, B_2, C_1, C_2, D_1, and D_2 are all defined in Eq. (23). With this information we have a completely general classification scheme to determine the relative mobilities of the RSSR, see Table 4.

We will verify the mobility classification with an example. Let the DH parameters be $a_1 = 1/8$, $a_4 = 4$, $a_7 = 1$, $a_8 = 1/8$, $\alpha_8 = \tan((60\pi/180)/2)$, $d_1 = 2$, $d_8 = 2$. Evaluating the discriminants with these DH link design parameters reveals that $\Delta_{v_1} = 10.6667$ and $\Omega_{v_1} = 6.437500000$, indicating that a_1 has no mobility limits while $\Delta_{v_8} = -36$ and $\Omega_{v_8} = -12.6667$, indicating that a_7 is a rocker in each assembly mode. It is a simple matter to determine the configuration and the extreme values of v_8 by evaluating the appropriate derivatives

of Eq. (23) for each assembly mode. The corresponding IO curves in both the v_1-v_8 and θ_1-θ_8 planes are illustrated in Fig. 5 which validates the classification.

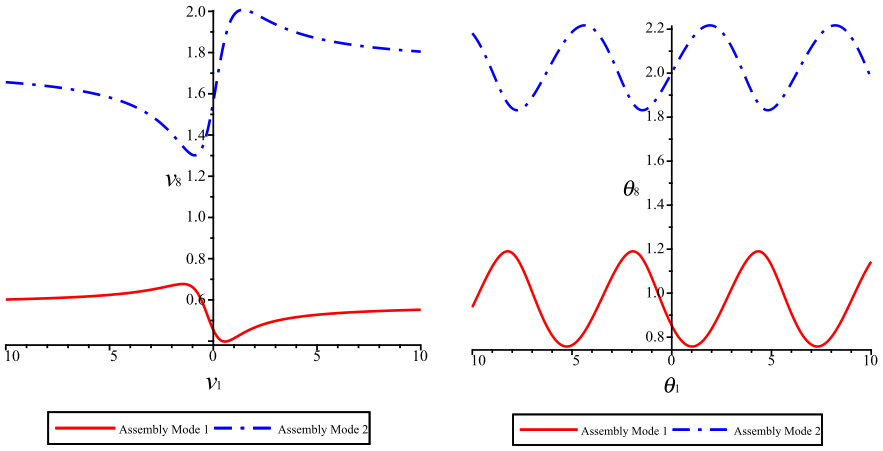

(a) IO curve in v_1-v_8 plane.

(b) IO curve in θ_1-θ_8 plane.

Figure 5: RSSR mobility for $a_1 = 1/8$, $a_4 = 4$, $a_7 = 1$, $a_8 = 1/8$, $\alpha_8 = \tan((60\pi/180)/2)$, $d_1 = 2$, $d_8 = 2$.

7.3. Differential Kinematics

Finally, we will determine the extreme output angular velocities and accelerations for a constant input angular velocity. These are important for bearing sizing, among other design considerations that are vital to robust mechanical design of RSSR linkages. While there have been some investigations in the literature examining the dynamics of the RSSR, there are no straightforward methods to be found that give explicit algebraic equations for computing the angular velocity and acceleration extrema for the RSSR, see [6, 38] for example. In [6] the time derivatives of the Cartesian coordinates of the joint centres are used instead of the angles that define the orientation of the links, meaning the equations are not IO equations per se. We therefore believe that the algebraic RSSR IO equation derived in this paper is best suited for such computations. However, to identify extreme angular velocity and acceleration outputs for a constant input angular velocity requires that the angle parameters be transformed back into angles. While $\dot{\theta}_1$ may be constant the corresponding parameter $\dot{v}_1$ is not since it is configuration dependent. That is

$$\dot{v}_1 = \frac{d\tan(\theta_1/2)}{dt} = \frac{\dot{\theta}_1\left(\tan^2(\theta_1/2)+1\right)}{2} = \frac{\dot{\theta}_1(v_1^2+1)}{2}. \quad (31)$$

The first step is to take the first two time derivatives of Eq. (23), which will not be listed here in the interest of brevity. The extreme angular velocities and accelerations, along with the configurations in which they occur in both

assembly modes can be easily obtained computationally with the following two algorithms.

Extreme RSSR angular velocity algorithm.

If values for a_1, a_4, a_7, a_8, d_1, d_8, and α_8 are specified and the input angular velocity is a constant specified value, we wish to determine the critical values $\theta_{1_{\text{crit}}}$ that result in $\dot{\theta}_{8_{\text{min/max}}}$, so we need to eliminate θ_8 from both the position and angular velocity IO equations.

1. Convert v_1 and v_8 in the IO equation to angles as $v_i = \tan(\theta_i/2)$ and solve for θ_8.
2. Substitute the expression for θ_8 from Step 1 into the $\dot{\theta}_1$-$\dot{\theta}_8$ equation and solve for $\dot{\theta}_8$, which gives $\dot{\theta}_8 = f(\theta_1)$ since $\dot{\theta}_1$ is a specified constant.
3. Solve $\dfrac{d\dot{\theta}_8}{d\theta_1} = 0$ for $\theta_{1_{\text{crit}}}$ and determine the values of $\dot{\theta}_{8_{\text{min/max}}}$ corresponding to each distinct value of $\theta_{1_{\text{crit}}}$.

Extreme RSSR angular acceleration algorithm.

If values for a_1, a_4, a_7, a_8, d_1, d_8, and α_8 are specified and the input angular velocity is a constant specified value, we wish to determine the critical values $\theta_{1_{\text{crit}}}$ that result in $\ddot{\theta}_{8_{\text{min/max}}}$, so we need to eliminate θ_8 and $\dot{\theta}_8$ from the position, angular velocity, and acceleration IO equations.

1. Convert v_1 and v_8 in the IO equation to angles as $v_i = \tan(\theta_i/2)$ and solve for θ_8.
2. Substitute the expression for θ_8 from Step 1 into the $\dot{\theta}_1$-$\dot{\theta}_8$ equation and solve for $\dot{\theta}_8$, which gives $\dot{\theta}_8 = f(\theta_1)$ since $\dot{\theta}_1$ is a specified constant.
3. Substitute the expressions for θ_8 and $\dot{\theta}_8$ into the $\ddot{\theta}_1$-$\ddot{\theta}_8$ equation.
4. Solve the resulting equation for $\ddot{\theta}_8$, which gives $\ddot{\theta}_8 = f(\theta_1)$ since $\ddot{\theta}_1 = 0$.
5. Solve $\dfrac{d\ddot{\theta}_8}{d\theta_1} = 0$ for $\theta_{1_{\text{crit}}}$ and determine the values of $\ddot{\theta}_{8_{\text{min/max}}}$ corresponding to each distinct value of $\theta_{1_{\text{crit}}}$.

For an example, again let the DH parameters be $a_1 = 1/8$, $a_4 = 4$, $a_7 = 1$, $a_8 = 1/8$, $\alpha_8 = \tan((60\pi/180)/2)$, $d_1 = 2$, $d_8 = 2$ and the constant input angular velocity be $\dot{\theta}_1 = 10$ rad/s. Using the two algorithms above the output angular velocity and acceleration are expressed in terms of the input angle, see Figs. 6. To the best of the authors collective knowledge, the extreme angular accelerations for an RSSR linkage have not been reported in the literature until now. Even if this is not precisely so, it is clear that the algebraic form of the RSSR equation in the form presented herein has distinct advantages for computation compared to any other representation. The extreme angular accelerations $\ddot{\theta}_{8_{\text{min/max}}}$ and critical input angles are computed and listed in Table 5.

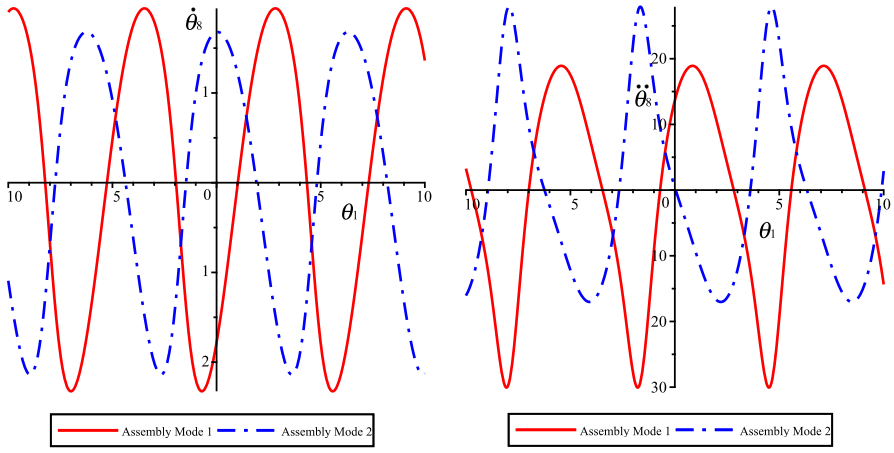

(a) RSSR angular velocity profile.

(b) RSSR angular acceleration profile.

Figure 6: RSSR angular velocity and acceleration profiles for $a_1 = 1/8$,$a_4 = 4$, $a_7 = 1$, $a_8 = 1/8$, $\alpha_8 = \tan((60\pi/180)/2)$, $d_1 = 2$, $d_8 = 2$, $\dot{\theta}_1 = 10$ rad/s.

Table 5: $\ddot{\theta}_{8_{\min/\max}}$ and $\theta_{1_{\text{crit}}}$ for $\dot{\theta}_1 = 10$ rad/s.

Assembly Mode	$\ddot{\theta}_{8_{\min/\max}}$ rad/s^2	$\theta_{1_{\text{crit}}}$ rad
1	-30.06554948	4.506090280
	18.91834314	0.8463167974
2	-17.03055542	2.201742476
	27.91274981	4.631288097

8. Conclusions

Recently it has been shown that Study's kinematic image space and elimination theory provide an excellent, straight forward tool to derive algebraic IO equations for planar, spherical, and Bennett linkages. In this paper, the same method was extended to arbitrary spatial RSSR four-bar linkages. After describing the linkage with standard DH parameters and mapping the closure equation into Study's kinematic image space, the intermediate motion parameters were eliminated with two concomitant methods: algebraically using the linear implicitisation algorithm; and numerically using pseudowitness sets to generate points and then interpolation to recover the eliminant. Both methods lead to the same IO equation containing four more complicated coefficients of the input and output angles compared to the planar 4R, but clearly containing the algebraic IO equation of planar 4R linkages as a subset. This IO equation was additionally verified using a geometric animation in GeoGebra. Finally, three applications were discussed and illustrated with examples to underscore

the utility of the RSSR algebraic IO equation as derived in this paper for four-bar synthesis and analysis.

Acknowledgements

The authors thank Jonathan Hauenstein for helpful discussions regarding numerical computation methods. Martin Pfurner is also acknowledged for thoughtful contributions to our understanding of S_6^2. The authors also acknowledge the financial support of the Natural Sciences and Engineering Research Council of Canada (NSERC) via Grant No. RGPIN-2017-06327.

[1] J. Beggs, Mechanism, McGraw-Hill, New York, NY, U.S.A., 1955.

[2] H. Nolle, Ranges of Motion Transfer by the R-G-G-R Linkage, Journal of Mechanisms 4 (1) (1969) 145–157.

[3] F. Sticher, Mobility Limit Analysis of R-S-S-R Mechanisms by "Ellipse Diagram", Journal of Mechanisms 5 (1) (1970) 393–414.

[4] O. Bottema, The Motion of the Skew Four-bar, Journal of Mechanisms 6 (1) (1971) 69–79.

[5] F. Freudenstein, E. Primrose, On the Criteria for the Rotability of the Cranks of a Skew Four-bar Linkage, ASME Journal of Engineering for Industry 98 (4) (1976) 1285–1288.

[6] S. Molian, Kinematics and Dynamics of the RSSR Mechanism, Journal of Mechanisms 6 (1) (1971) 69–79.

[7] J. Duffy, M. Gilmartin, Displacement Analysis of the Generalised RSSR Mechanism, Mechanism and Machine Theory 13 (5) (1978) 533–541.

[8] A. Wilhelm, R. Sodhi, Design of RSSR Function Generator by Curve Matching, in: Unknown Host Publication Title, Japan Soc of Precision Engineers, 1984, pp. 118–123.

[9] C. Mazzotti, M. Troncossi, V. Parenti-Castelli, Dimensional Synthesis of the Optimal RSSR Mechanism for a Set of Variable Design Parameters, Meccanica 52 (1) (2017) 2439–2447.

[10] E. Study, Geometrie der Dynamen, Teubner Verlag, Leipzig, Germany, 1903.

[11] B. Ravani, B. Roth, Motion Synthesis Using Kinematic Mappings, ASME J. Mech., Trans., and Automation 105 (3) (1983) 460–467.

[12] D. R. Walter, M. L. Husty, On Implicitization of Kinematic Constraint Equations, Machine Design & Research (CCMMS 2010) 26 (2010) 218–226.

[13] A. J. Sommese, C. W. Wampler, The Numerical Solution Of Systems Of Polynomials Arising In Engineering And Science, World Scientific Publishing Co. Pte. Ldt., Hackensack, NJ, U.S.A., 2005.

[14] R. S. Hartenberg, J. Denavit, Kinematic Synthesis of Linkages, McGraw-Hill, New York, NY, U.S.A, 1964.

[15] A. V. M. Rao, G. N. Sandor, D. Kohli, A. H. Soni, Closed Form Synthesis of Spatial Function Generating Mechanism for the Maximum Number of Precision Points, ASME J. Eng. Ind. 95 (3) (1973) 725–736.

[16] F. Freudenstein, Design of Four-link Mechanisms, Ph.D. thesis, Columbia University, New York, NY, U.S.A. (1954).

[17] J. Craig, Introduction to Robotics, Mechanics and Control, 4th Edition, Addison-Wesley Publishing Co., Reading, MA, U.S.A., 2017.

[18] B. Mooring, Z. Roth, M. Driels, Fundamentals of Manipulator Calibration, John Wiley & Sons, Inc., New York, NY, U.S.A., 1991.

[19] C. H. An, C. G. Atkeson, J. M. Hollerbach, Model-based Control of a Robot Manipulator, The MIT Press, Cambridge, MA, U.S.A., 1988.

[20] S. Hayati, Robot Arm Geometric Link Parameter Estimation, Proc. 22nd IEEE Conf. on Decision and Control, San Antonio, TX, U.S.A. (1983) 1477–1483.

[21] J. Denavit, R. S. Hartenberg, A Kinematic Notation for Lower-Pair Mechanisms Based on Matrices, ASME J. Appl. Mech. 22 (2) (1955) 215–221. doi:10.1115/1.4011045.

[22] J. M. Selig, Geometric Fundamentals of Robotics, 2nd Edition, Springer Science + Business Media Inc, New York, NY, U.S.A., 2005.

[23] J. M. Selig, On the Geometry of the Homogeneous Representation for the Group of Proper Rigid-body Displacements, Rom. J. Techn. Sci. – Appl. Mechanics 58 (1-2) (2013) 153–176.

[24] M. Pfurner, The Family of Two Generator 3-Space Rulings of the Study Quadric, Private Communication (August 25, 2022).

[25] M. L. Husty, H.-P. Schröcker, Kinematics and Algebraic Geometry, in: J. M. McCarthy (Ed.), 21st Century Kinematics, Springer-Verlag, London, 2013, pp. 85–123. doi:10.1007/978-1-4471-4510-3_4.

[26] M. L. Husty, D. R. Walter, Mechanism Constraints and Singularities - the Algebraic Formulation, CISM International Centre for Mechanical Sciences 589, Springer International Publishing, Cham, Switzerland, 2019, pp. 101–180. doi:10.1007/978-3-030-05219-5_4.

[27] D. A. Cox, J. Little, D. O'Shea, Using Algebraic Geometry, 2nd Edition, Springer Science + Business Media Inc., New York, NY, U.S.A., 2004.

[28] A. Dresden, Solid Analytic Geometry and Determinants, John Wiley & Sons, Inc., New York, NY, U.S.A., 1930.

[29] D. J. Bates, A. J. Sommese, J. D. Hauenstein, C. W. Wampler, Numerically Solving Polynomial Systems with Bertini, SIAM, Philadelphia, PA, U.S.A., 2013. doi:10.1137/1.9781611972702.

[30] J. D. Hauenstein, A. J. Sommese, Witness Sets of Projections, Applied Mathematics and Computation 217 (7) (2010) 3349–3354. doi:10.1016/j.amc.2010.08.067.

[31] D. Kincaid, W. Cheney, Numerical Analysis: Mathematics of Scientific Computing, American Mathematical Society, Provedince, RI, U.S.A., 2002.

[32] D. A. Cox, Applications of Polynomial Systems, Vol. 134, CBMS Regional Conference Series in Mathematics, American Mathematical Society, Providence, RI, U.S.A., 2020.

[33] S. Tinubu, K. Gupta, Optimal Synthesis of Function Generators Without the Branch Defect, ASME, J. of Mech., Trans., and Autom. in Design 106 (3) (1984) 348–354.

[34] M. Hayes, K. Parsa, J. Angeles, The Effect of Data-set Cardinality on the Design and Structural Errors of Four-bar Function-generators, in: Proceedings of the Tenth World Congress on the Theory of Machines and Mechanisms, *Oulu, Finland*, 1999, pp. 437–442.

[35] A. Guigue, M. Hayes, Continuous Approximate Synthesis of Planar Function-generators Minimising the Design Error, Mechanism and Machine Theory 101 (2016) 158–167.

[36] L. F. Shampine, "Vectorized Adaptive Quadrature in MATLAB", Journal of Computational and Applied Mathematics 211 (February 2008) 131–140.

[37] A. Perez, J. M. McCarthy, Dual Quaternion Synthesis of Constrained Robotic Systems, ASME Journal of Mechanical Design 125 (5) (2004) 425–435.

[38] G. S. Sutherland, Quality of Motion and Force Transmission, Mechanism and Machine Theory 16 (1981) 221–225.

Multi-modal Continuous Approximate Synthesis of Planar Four-bar Function Generators

Zachary A. Copeland and M. John D. Hayes*

Department Mechanical and Aerospace Engineering,
Carleton University,
Ottawa, ON, Canada
E-mail: zackcopeland@cmail.carleton.ca
E-mail: johnhayes@cunet.carleton.ca
*Corresponding author

Abstract: This paper introduces a novel multi-modal continuous approximate synthesis algorithm for planar four-bar function generators. Multi-modal in this sense means concurrently synthesising multiple functions between different joint variable parameter pairs in a four-bar linkage over the desired continuous input-output ranges between different pairs of variables. These are not competing functions, rather perturbed functions. The continuous multi-modal synthesis equation is the sum of the squared input-output equations integrated over the different prescribed input variable parameter ranges. Every planar four-bar mechanism explicitly generates six distinct functions each uniquely determined by one set of link parameter constants. We will examine the simultaneous continuous approximate synthesis of two related perturbed functions between different pairs of joint variables that, in general, require different link constants to generate. The optimisation involves identifying the best *compromise* link constants to approximately generate the two prescribed functions. Planar 4R and RRRP examples are presented where two different functions, one primary and the other perturbed secondary, are generated over continuous ranges between the specified input variable parameter and the associated output variable parameter. We evaluate the continuous multi-modal synthesis results by comparing the areas between the generated degree 4 planar algebraic curves in the parameter planes of the input and output joint variables to those of the prescribed input-output functions over their continuous ranges, thereby simultaneously evaluating a measure of the Euclidean norm of both the design and structural errors. The work presented herein is preliminary, and intended only as a proof-of-concept.

Keywords: Planar four-bar mechanisms; algebraic input-output (IO) equations; continuous approximate synthesis; multi-modal continuous approximate synthesis.

Reference to this paper should be made as follows: Copeland, Z.A. and Hayes, M.J.D. (2023) 'Multi-modal Continuous Approximate Synthesis of Planar Four-bar Function Generators', *Int. J. Mechanisms and Robotic Systems*, Vol. 5, No. 3, pp. 246-269.

Biographical notes: Zachary A. Copeland received his BEng (2015), and M.A.Sc (2017) in Mechanical Engineering from Carleton University, Ottawa, ON, Canada. He is currently a PhD candidate in Mechanical Engineering developing continuous approximate synthesis theory and techniques at Carleton. His interests also include manufacturing and production technologies, as well as the theory of machines and mechanisms. He enjoys manufacturing and implementation, as well as software design.

M. John D. Hayes received his BEng (1995), MEng (1996), and PhD (1999) degrees all from McGill University in Montreal, QC, Canada. He is currently a Full Professor in the Department of Mechanical and Aerospace Engineering at Carleton University in Ottawa, ON, Canada. His research interests include computational kinematics, algebraic geometry, and optimisation as they apply to mechanical systems design, analysis, calibration, and simulation.

1 Introduction

The study of planar four-bar linkages involves a large variety of problems: guiding a point along a specific curve or path, known as coupler curve or path generation; guiding a rigid body through a sequence of positions and orientations, known as the Burmester, or rigid body guidance problem [1]; guiding a rigid body along a time-dependent sequence of positions and orientations, usually called trajectory generation [2]; problems concerning the transmission of forces and torques [3]; or designing an optimally balanced linkage [4]. An additional important subset of this gamut is the function generation problem [5]. It consists of identifying a mechanism which is able to approximate, in some sense, a mathematical function between an input and output (IO) pair of joint variables for a given planar linkage kinematic architecture comprising RR-, RP-, PR-, or PP-dyads. In this context R and P indicate revolute and prismatic joints connecting a pair of rigid links, also known as R- and P-pairs. A great number of examples of planar function generator synthesis, addressing many different issues, are to be found in the literature, see [6, 7, 8, 9, 10, 11, 12] for a small sample.

The function generation problem is the focus of this paper. All movable mechanical systems generate functions between all of the joint variables as they move. Figure 1 illustrates one such planar four-bar 4R linkage where the reference coordinate systems, length and angle parameters have been assigned strictly according to the Denavit-Hartenberg (DH) parameter assignment rules [1, 13]. If links a_1 and a_3 are the input and output links, respectively, the IO function is specified as $\theta_4 = f(\theta_1)$. Once the four a_i link lengths are identified which approximately generate the prescribed function, the corresponding mechanism generates five additional functions, one for each of the five other distinct angle pairings $\theta_j = f(\theta_i)$. All six of these functions are determined by the identified values for the link lengths that approximately generate the lone prescribed function.

Exact synthesis results in a linkage that precisely generates the prescribed function, but only for the three precision IO pairs that generate the desired output for three prescribed input parameters creating a set of three synthesis equations in three unknown link length ratios. Whereas, approximate synthesis uses $n > 3$ precision IO pairs to create an overconstrained set of synthesis equations leading to a linkage that generates the desired function, in general, but only approximately over the desired displacement range due to errors induced by the synthesis. *Design* and *structural* errors [1] are important performance indicators used in the assessment and optimisation of mechanical systems intended as function generating linkages designed by means of approximate synthesis. The design error is the residual of the identified linkage in satisfying the synthesis equations [5], and is evaluated at each of $n > 3$ precision points, or poses, in a discrete set satisfying the prescribed function. Minimising the Euclidean norm of the design error leads to a linear least-squares problem. The structural error, on the other hand, is defined as the difference between the prescribed output angle, and

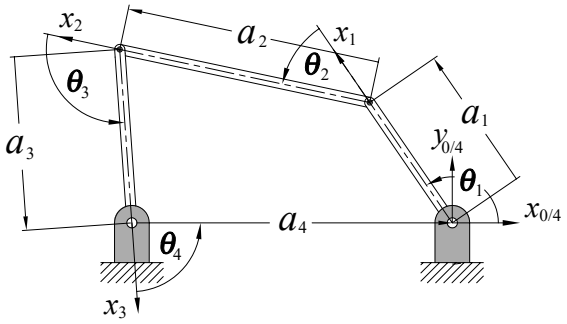

Figure 1: Planar 4R linkage with Denavit-Hartenberg coordinate systems and parameter assignments.

the output angle that is generated by the linkage at each precision point [8]. This problem is typically solved by minimising the norm of the array of the structural error evaluated at each precision point using some form of Gauss-Newton non-linear minimisation [14], requiring an iterative solution procedure that terminates when a desired minimum norm threshold is obtained. The structural error is arguably the metric that truly matters since it is directly related to the physical performance of the linkage.

It was observed in [15] that as the cardinality of the data set used to compute the design error minimising linkage becomes large, on the order of $n \geq 40$, the design error minimising linkage tends to converge to the structural error minimising linkage. Hence, one may avoid the non-linear structural error computation provided a sufficient number of precision points are specified. The natural question is then "how large must n be?" The obvious response is to extend the cardinality of the data set used to compute the design error minimising linkage to infinity by way of integration. Unfortunately, while it was demonstrated in [16] that this extension is possible through the integration of the trigonometric Freudenstein equation, the generalisation of the process is computationally prohibitive and any advantage obtained through the elimination of the need for an explicit solution to the non-linear structural error problem is lost to the numerical complexity of the integration. A less cumbersome continuous approximate synthesis method was needed, and was realised with the algebraic IO equations [17, 18, 19]. These algebraic IO equations were subsequently used for planar RRRP and PRRP function generator synthesis problems in [18], and used to extend the observations made in [15] to develop the algebraic *continuous approximate synthesis* technique reported in [20], which will be relied upon to develop a preliminary form of multi-modal continuous approximate synthesis reported in this paper.

2 The Denavit-Hartenberg Convention and the Planar 4R IO Equation

Before discussing the continuous approximate synthesis approach, it will be useful to recall the matrix method for kinematic analysis and synthesis of linkages, which we call the DH method, developed by Jacques Denavit and Richard Hartenberg and first published in 1955 [13], and subsequently in their textbook on kinematic synthesis [1] in 1964. The first step in the DH method applied to an arbitrary kinematic chain requires the identification and numbering of all joint axes.

In order to align with our previous publications we will be using the same, slightly modified DH parameter coordinate system naming convention in the interest of consistency. The slight modification is that we have as the relatively stationary coordinate system at the start of a kinematic chain the $x_0,\ y_0,\ z_0$ coordinate system. Hence, at any joint in the kinematic chain we measure, for example, the relative angle θ_i of link a_i about joint axis z_{i-1} from x_{i-1} to x_i, see Figure 2a. Whereas, in the original paper [13] the relatively stationary coordinate system at the start of a kinematic chain is the $x_1,\ y_1,\ z_1$ coordinate system, and the relative angle θ_i of link a_i is measured about z_i from x_i to x_{i+1}, see Figure 2b. Because the modification is so subtle, and because the mechanical engineering world has moved away from the original assignment rules found in [1, 13], we will henceforth refer to our version of the parametrisation simply as the DH method.

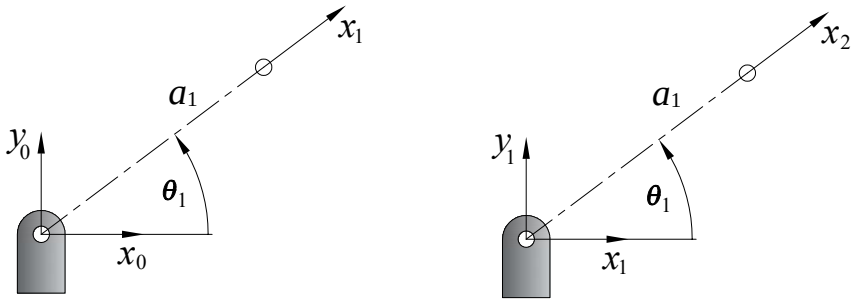

(a) Slightly modified definition of θ_1.

(b) Original definition of θ_1.

Figure 2: Enumeration of the DH coordinate systems and assignment rules.

The DH parametrisation involves the allocation of coordinate systems to each link in the chain that move with the link, using a set of rules to locate the origin of the coordinate system and the orientation of the basis vectors. The position and orientation of consecutive links is defined by a homogeneous transformation matrix which maps coordinates of points in the coordinate system attached to link i to those of the same points described in a coordinate system attached to link $i-1$.

To visualise the four DH parameters consider two sequential arbitrary neighbouring links, $i-1$ and i. Two such links are illustrated, together with their DH parameters, in Figure 3. The DH parameters [13] are defined in the following way with our subtle modification.

θ_i, joint angle: the angle from x_{i-1} to x_i measured about z_{i-1}.

d_i, link offset: the distance from x_{i-1} to x_i measured along z_{i-1}.

τ_i, link twist: the angle from z_{i-1} to z_i measured about x_i.

a_i, link length: the directed distance from z_{i-1} to z_i measured along x_i.

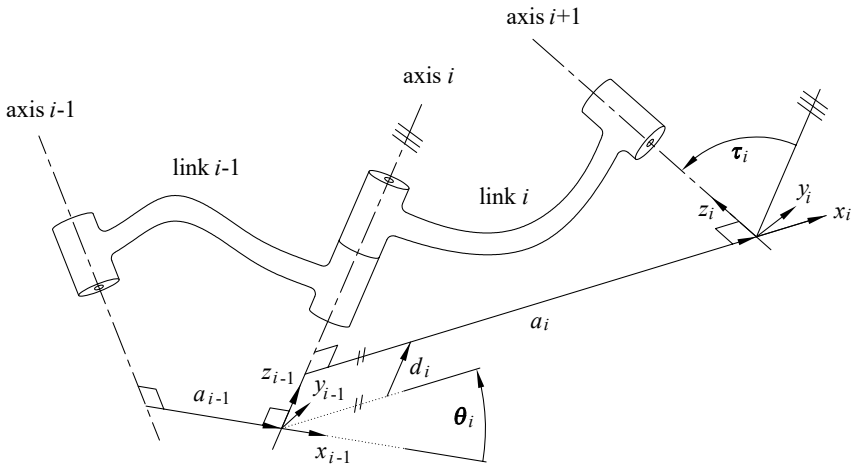

Figure 3: DH parameters in a general serial 3R kinematic chain.

The DH coordinate transformation matrix, using the European convention for homogeneous coordinate arrays $[w,\ x,\ y,\ z]^T$, where w is the homogenising coordinate, is

$$ {}^{i-1}\mathbf{T}_i = \begin{bmatrix} 1 & 0 & 0 & 0 \\ a_i \cos\theta_i & \cos\theta_i & -\sin\theta_i \cos\tau_i & \sin\theta_i \sin\tau_i \\ a_i \sin\theta_i & \sin\theta_i & \cos\theta_i \cos\tau_i & -\cos\theta_i \sin\tau_i \\ d_i & 0 & \sin\tau_i & \cos\tau_i \end{bmatrix}. \tag{1} $$

We then algebraise Equation (1) using the tangent half-angle substitutions for the joint and twist angles where

$$ v_i = \tan\left(\frac{\theta_i}{2}\right), \ \Rightarrow \cos\theta_i = \frac{1-v_i^2}{1+v_i^2}, \quad \sin\theta_i = \frac{2v_i}{1+v_i^2}, $$

$$ \alpha_i = \tan\left(\frac{\tau_i}{2}\right), \ \Rightarrow \cos\tau_i = \frac{1-\alpha_i^2}{1+\alpha_i^2}, \quad \sin\tau_i = \frac{2\alpha_i}{1+\alpha_i^2}. $$

The detailed computations leading to the results presented herein use the Maple library MyKinematics [21] which requires the European homogeneous coordinate convention. Regardless, those details remain unseen in this paper, but will be provided to the interested reader upon request.

The forward and inverse kinematics of serial chains are the concatenations of the individual transformation matrices in the appropriate order [22]. For example the forward kinematics problem of determining the position and orientation of the n^{th} link in a serial kinematic chain described in a relatively fixed non-moving base coordinate system 0, given the relevant DH parameters and values for the n joint variables becomes conceptually simple matrix multiplication.

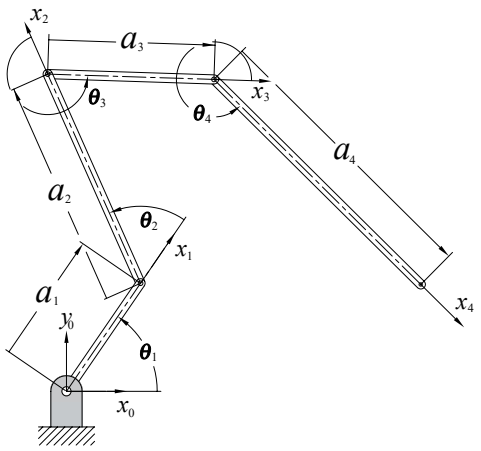

Figure 4: DH parameters assigned to a serial planar 4R linkage.

The DH method was largely intended for planar, spherical, and spatial four-bar simple closed kinematic chains, but has since become nearly universally applied and synonymous with the kinematics of mechanical systems in general, and robot mechanical systems in particular, see [23, 24, 25, 26] for instance, but there are many other modern examples. The serial nR chain is conceptually closed by equating the forward kinematics transformation matrix to the identity.

$$ {}^{0}\mathbf{T}_{n} = {}^{0}\mathbf{T}_{1}\,{}^{1}\mathbf{T}_{2}\,{}^{2}\mathbf{T}_{3}\cdots{}^{n-2}\mathbf{T}_{n-1}\,{}^{n-1}\mathbf{T}_{n} \;=\; \mathbf{I}. \tag{2} $$

The resulting matrix represents a set of implicit equations in terms of the link constants and all n joint angles. If we restrict ourselves to the planar 4R simple closed kinematic chain, and the IO equation that relates θ_4 to θ_1 then the intermediate angles θ_2 and θ_3 must be eliminated using the available equations. What remains is a single implicit equation in θ_4 and θ_1.

2.1 The Planar 4R Algebraic IO Equations

Consider the serial 4R kinematic chain illustrated in Figure 4. Equating the forward kinematics to the identity creates the kinematic closure equation. This closure means that the serial kinematic chain becomes a single loop parallel chain and the fourth link described by a_4 becomes stationary while links a_1, a_2, and a_3 move with a single degree of freedom relative motion. The serial chain can be closed such that the axis numbers circulate either clockwise (CW) or counter clockwise (CCW). The CCW circulation will be used herein.The CCW circulation found in [13], and illustrated in Figure 1, does not lead to the results 21^{st}-century mechanical engineers have come to expect. Rather, the convention has evolved away from the DH relative angles and reverts to Freudenstein's absolute angular measures, often combined with relative measures as seen in Figure 5a. However, the standard circulation found in nearly every text on the subject not penned by Denavit or Hartenberg is CW and absolute, see [27, 28, 29] for example. The absolute angle measures are not compatible with the original DH method.

The detailed derivation of the planar algebraic IO equations for function generators are to be found in [18, 19], but will be briefly summarised here. Using the coordinate

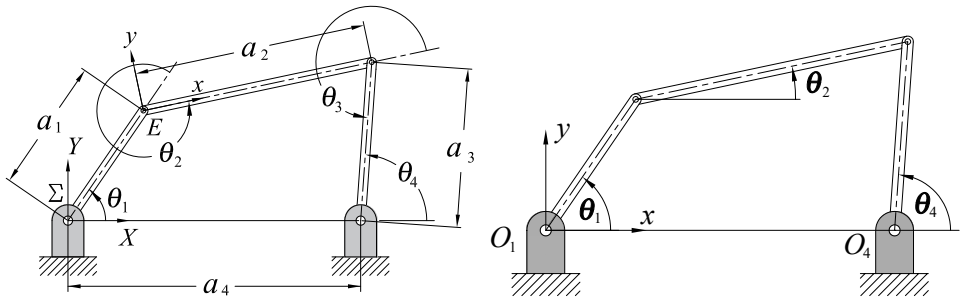

(a) Hybrid CW angle measures. (b) Absolute CW angle measures.

Figure 5: Planar 4R with hybrid absolute-relative and absolute angle measures.

system assignments and DH parameters in Figure 1, the DH transformation matrix ${}^0\mathbf{T}_4$ is computed. This homogeneous transformation matrix is then mapped to the eight Study soma coordinates [30, 31] and the corresponding 8×1 Study array is equated to the identity array $[1,\ 0,\ 0,\ 0,\ 0,\ 0,\ 0,\ 0]^T$. This results in eight equations in the DH parameter constants and the four $v_1,\ v_2,\ v_3,\ v_4$ variable angle parameters. The first equation is the trivial normalising condition, meaning that there are seven useful equations to work with. However, because we are concerned only with displacements all in the same plane, four of the soma coordinates identically vanish, leaving only three useful equations, see [17] for details. To obtain the v_1-v_4 algebraic IO equation the v_2 and v_3 intermediate joint angle parameters are eliminated using the three non-trivial equations and the Gröbner basis elimination monomial term ordering called "`lexdeg`" in Maple 2021, revealing:

$$Av_1^2v_4^2 + Bv_1^2 + Cv_4^2 - 8a_1a_3v_1v_4 + D = 0, \tag{3}$$

where,

$$\begin{aligned}
A &= A_1A_2 = (a_1 - a_2 + a_3 - a_4)(a_1 + a_2 + a_3 - a_4),\\
B &= B_1B_2 = (a_1 + a_2 - a_3 - a_4)(a_1 - a_2 - a_3 - a_4),\\
C &= C_1C_2 = (a_1 - a_2 - a_3 + a_4)(a_1 + a_2 - a_3 + a_4),\\
D &= D_1D_2 = (a_1 + a_2 + a_3 + a_4)(a_1 - a_2 + a_3 + a_4),\\
v_1 &= \tan\frac{\theta_1}{2}, \quad v_4 = \tan\frac{\theta_4}{2}.
\end{aligned}$$

The coefficients A, B, C, and D are products of bilinear factors of the a_i directed link lengths representing the constants to be identified in the synthesis. Following derivation steps listed in [19], the remaining five v_i-v_j IO equations are, respectively [32],

$$A_1B_2v_1^2v_2^2 + A_2B_1v_1^2 + C_1D_2v_2^2 - 8a_2a_4v_1v_2 + C_2D_1 = 0, \tag{4}$$

$$A_1B_1v_1^2v_3^2 + A_2B_2v_1^2 + C_2D_2v_3^2 + C_1D_1 = 0, \tag{5}$$

$$A_1D_2v_2^2v_3^2 + B_2C_1v_2^2 + B_1C_2v_3^2 - 8a_1a_3v_2v_3 + A_2D_1 = 0, \tag{6}$$

$$A_1C_1v_2^2v_4^2 + B_2D_2v_2^2 + A_2C_2v_4^2 + B_1D_1 = 0, \tag{7}$$

$$A_1C_2v_3^2v_4^2 + B_1D_2v_3^2 + A_2C_1v_4^2 + 8a_2a_4v_3v_4 + B_2D_1 = 0. \tag{8}$$

3 Continuous Approximate Synthesis

While multi-modal continuous approximate IO function generation is the subject of this paper, it is built upon the foundation of the continuous approximate synthesis algorithm [20]. This approach involves integrating the synthesis equations between the bounds of the minimum and maximum input angles. The inspiration for this is that it has been observed that as the cardinality of the prescribed discrete IO data set of precision pairs that satisfy the prescribed function and the corresponding overdetermined set of synthesis equations increases, the identified linkages that minimise the Euclidean norm, or L_2-norm as is also called, of the design and structural errors tend to converge to the same set of link lengths [15].

It is worth noting that the most common L_p-norms [33] for a continuous function f on a closed interval $[a, b]$, and in fact, the most commonly used vector norms [34] are the Chebyshev norm, the Euclidean norm, and the Manhattan norm, which are respectively defined to be [33]:

$$\begin{aligned}
\|f\|_\infty &= \max_{x\in[a,b]} |f(x)|; \\
\|f\|_2 &= \left(\int_a^b f(x)^2 dx \right)^{1/2}; \\
\|f\|_1 &= \int_a^b |f(x)| dx.
\end{aligned}$$

The term Manhattan norm arises because this vector norm corresponds to sums of distances along the basis vector directions, as one would travel along a rectangular street plan. The Manhattan and Chebyshev norms are the limiting cases $p = 1$ and $p = \infty$, respectively, of the family of L_p-norms. The L_p-norms obey the following relationship:

$$\|f\|_\infty \leq \cdots \leq \|f\|_2 \leq \|f\|_1.$$

Typically, the most appropriate norm must be selected to evaluate the magnitude of the objective function for the error minimisation, given a function that is to be approximated by the resulting linkage. However, it turns out that Lawson's algorithm [35, 36] can be used to sequentially minimise the Chebyshev norm via the minimisation of the Euclidean norm [37]. This means that the continuous approximate synthesis approach to structural or design error minimisation is independent of the L_p-norm because it applies to both the Chebyshev and Euclidean norms, and hence all intermediate ones.

The important implication of this observation is that the minimisation of any L_p-norm of the structural error can be accomplished indirectly via the minimisation of the corresponding norm of the design error, provided that a suitably large number of IO pairs is prescribed. Again, this is desirable because the design error, which indicates the error residual incurred by a specific linkage regarding the verification of the synthesis equations, results in a linear least-squares problem, while the structural error is the difference between the prescribed linkage output angle and the generated output angle for a prescribed input angle value, which leads to a nonlinear optimisation problem generally requiring an iterative solution [8].

If the question is: "how large must the data set cardinality be?"; the easy answer is: "it doesn't matter if the cardinality is infinite!". Hence, the following six-step algorithm [20]:

1. Square the algebraic IO equation for the desired planar four bar linkage architecture.

2. Separate this squared IO equation into an array containing the linkage coefficients, $\mathbf{c}$, and an array containing the corresponding variable angle parameters, $\mathbf{s}$.

3. Substitute the prescribed function between the input and output variable pairs $(v_i,\ v_j)$ into the output parameter $v_j = f(v_i)$ in the variable array, $\mathbf{s}$.

4. To establish the synthesis equation take the Euclidean inner product of $\mathbf{c}$ with the integral of $\mathbf{s}$ over the prescribed bounds thus: $\mathbf{c} \cdot \int_{v_{i_{\min}}}^{v_{i_{\max}}} \mathbf{s}\left(v_i,\ v_j = f(v_i)\right) dv_i$.

5. Generate an initial guess for the optimal linkage parameters from the exact precision point synthesis satisfying the algebraic IO equation.

6. Minimise the residual of this integrated synthesis equation for the a_i link lengths over the field of real numbers.

The output of this algorithm is the four link lengths, a_i, that minimise both the design and structural errors for the planar 4R linkage in generating the prescribed $v_j = f(v_i)$ function. This algorithm can be summarised by the equation

$$\min_{(a_1,a_2,a_3,a_4)\in\mathbb{R}} \left(\mathbf{c} \cdot \int_{v_{i_{\min}}}^{v_{i_{\max}}} \mathbf{s}(v_i, f(v_i)) dv_i \right) = 0. \tag{9}$$

The *Minimize* command used in Maple 2021 to solve the problem computes a local minimum of an objective function subject to constraints. If the problem is convex, as when the objective function and constraints are linear, for example, the solution will also be a global minimum. The algorithms that this command use assume the objective function and constraints are twice continuously differentiable.

In this context, the Euclidean norm of the structural error over every point in the generated function is nothing more than the area between the prescribed function and the generated function in the variable angle parameter plain, which is equivalent to the design error. Examples of the continuous approximate synthesis will be described in Section 4.

4 Multi-Modal Continuous Approximate Synthesis

The concept of continuous approximate synthesis for function generation from [20] will be extended in order to enable the simultaneous approximate generation of multiple different, though not arbitrary competing, prescribed functions between different pairs of joint variable parameters in a single planar, spherical, or spatial four-bar mechanism, which we call *multi-modal continuous approximate synthesis*. We propose that this can be accomplished with the following:

$$\min_{(a_1,a_2,a_3,a_4)\in\mathbb{R}} \left(\mathbf{c}_1 \cdot \int_{v_{i_{1_{\min}}}}^{v_{i_{1_{\max}}}} \mathbf{s}_1(v_{i_1}, f_1(v_{i_1})) dv_{i_1} + \mathbf{c}_2 \cdot \int_{v_{i_{2_{\min}}}}^{v_{i_{2_{\max}}}} \mathbf{s}_2(v_{i_2}, f_2(v_{i_2})) dv_{i_2} \right) = 0. \tag{10}$$

The typical function generation problem concerns $\theta_4 = f(\theta_1)$ and the corresponding v_1-v_4 IO equation; however, considering Figure 1, one may wish to also consider the θ_1-θ_3 pair of angles, or any other of the remaining four pairs. For this *proof-of-concept* of the proposed multi-modal continuous approximate synthesis method we shall begin with the synthesis of two arbitrarily different functions $v_4 = f_1(v_1)$ and $v_3 = f_2(v_1)$. The reason

for this choice is that the v_3 angle parameter is a measure of the transmission angle, which is useful as a metric to discriminate between four bar mechanisms which have practical use and those that do not.

This idea has a philosophical existential question associated with it. Namely, when a mechanism is identified to generate, for example, $v_4 = f_1(v_1)$, the five other $v_j = f_2(v_i)$ functions are explicitly defined. Suppose a $v_3 = f_2(v_1)$ function was needed that was different from the one imposed by the initially generated $v_4 = f_1(v_1)$ function. The question we ask now is "does a linkage exist that is the best compromise between the competing prescribed functions?". The answer is, in general, no. However, we will show that polynomial interpolants can be used to perturb one of the functions and we can succeed. We define the design parameter space of planar 4R function generator linkages [3, 38, 39] as the four-dimensional homogeneous space spanned by the mutually orthogonal basis vectors $\mathbf{a}_1,\ \mathbf{a}_2,\ \mathbf{a}_3$ normalised with respect to frame length $a_4 = 1$. Distinct points in this homogeneous space, $(a_1 :\ a_2 :\ a_3 :\ 1)$, where the delimiter : has been used to indicate the use of homogeneous coordinate ratios, represent distinct planar 4R linkages. Each point is a linkage that generates six distinct functions between the six distinct angle parings between different links. The linkages identified to generate the prescribed $v_4 = f_1(v_1)$ and $v_3 = f_2(v_1)$ functions represent two distinct points, and therefore two distinct linkages. We will illustrate in Section 4.1.1 that in general the synthesis of competing functions is not possible in any useful way. However, in Section 4.1.2 we will show that it is possible to subtly perturb one of the functions leading to useful results.

4.1 Planar 4R Multi-modal Function Generation

Let the prescribed $v_4 = f_1(v_1)$ function be

$$v_4 = f_1(v_1) = 2 + \tan\left(\frac{v_1}{{v_1}^2 + 1}\right), \quad -\frac{1}{2} \leq v_1 \leq 2. \tag{11}$$

We proceed to identify the linkage that will approximately generate this function using continuous approximate synthesis. The first step is to square Equation (3), then separate the link length coefficients into arrays $\mathbf{c}_1$ and $\mathbf{s}_1$, yielding

$$\mathbf{c}_1 = \begin{bmatrix} A^2 \\ 2AB \\ B^2 \\ -16Aa_1a_3 \\ -16Ba_1a_3 \\ 2AC \\ 64a_1^2a_3^2 + 2AD + 2BC \\ 2BD \\ -16Ca_1a_3 \\ -16Da_1a_3 \\ C^2 \\ 2CD \\ D^2 \end{bmatrix}, \quad \mathbf{s}_1 = \begin{bmatrix} v_1^4v_4^4 \\ v_1^4v_4^2 \\ v_1^4 \\ v_1^3v_4^3 \\ v_1^3v_4 \\ v_1^2v_4^4 \\ v_1^2v_4^2 \\ v_1^2 \\ v_1v_4^3 \\ v_1v_4 \\ v_4^4 \\ v_4^2 \\ 1 \end{bmatrix} = \begin{bmatrix} v_1^4f_1(v_1)^4 \\ v_1^4f_1(v_1)^2 \\ v_1^4 \\ v_1^3f_1(v_1)^3 \\ v_1^3f_1(v_1) \\ v_1^2f_1(v_1)^4 \\ v_1^2f_1(v_1)^2 \\ v_1^2 \\ v_1f_1(v_1)^3 \\ v_1f_1(v_1) \\ f_1(v_1)^4 \\ f_1(v_1)^2 \\ 1 \end{bmatrix}. \tag{12}$$

We solve the exact synthesis problem to obtain an initial guess for the optimisation, using the prescribed function pairs that satisfy Equation (11):

$$(v_1,\ v_4)\ =\ \left(-\frac{1}{2},\ \frac{32287}{20471}\right);\ \left(\frac{3}{4},\ \frac{49597}{20471}\right);\ \left(2,\ \frac{48857}{19383}\right).$$

Note that to obtain these three precision IO pairs we have selected the lower and upper bounding values for v_1 and an arbitrary value in between, while the corresponding value of v_4 satisfies the prescribed function, Equation (11).

In this classic 4R exact synthesis problem we obtain a unique solution that contains the link length a_4 as a free parameter:

$$a_1 = -\frac{21111}{109000}a_4,\ a_2 = \frac{21021}{18196}a_4,\ a_3 = \frac{21518}{15263}a_4,\ a_4. \tag{13}$$

We arbitrarily set $a_4 = 1$ and evaluate the integral, then minimise the residual using the normalised link lengths in Equation (13) as the initial guess:

$$\min_{(a_1,a_2,a_3,a_4)\in\mathbb{R}} \left(\mathbf{c}_1 \cdot \int_{v_1=-\frac{1}{2}}^{v_1=2} \mathbf{s}_1(v_1, f_1(v_1))\right) = 0. \tag{14}$$

The minimisation is accomplished using the `Optimization` solvers in Maple 2021 which converge to the link lengths listed in Table 1.

Table 1 Continuous approximate synthesis results generating Equation (11).

Link length	a_1	a_2	a_3	a_4
Rational	$-\frac{13077}{78259}$	$\frac{45079}{42170}$	$\frac{27203}{20556}$	$\frac{101727}{110482}$
Floating point	-0.167098992	1.068982689	1.323360576	0.920756322
Normalised	-0.1814801460	1.160983273	1.437253857	1

Table 2 Structural error generating Equation (11).

Structural error	Exact synthesis	Continuous approximate synthesis
	0.024159094	-0.002471306

Comparisons of the structural error, defined as the area between the prescribed and generated functions, in the v_1-v_4 plane are enumerated in Table 2. One can see that the structural error for the function generated by the continuous approximate synthesis linkage is an order of magnitude smaller than that of the function generated by the exact synthesis linkage, as can be observed by casual visual inspection of the graphs plotted in Figure 6.

This approximately generated $v_4 = f_1(v_1)$ function exactly generates five additional $v_j = f_2(v_i)$ functions given the link lengths identified to approximately generate the prescribed function; exact in the sense that these functions have not been explicitly prescribed. These five functions between the angle parameters v_1-v_2, v_1-v_3, v_2-v_3, v_2-v_4, and v_3-v_4 are generated by the identified link lengths, and are illustrated in Figure 7 along with the prescribed and continuous approximate $v_4 = f_1(v_1)$ functions.

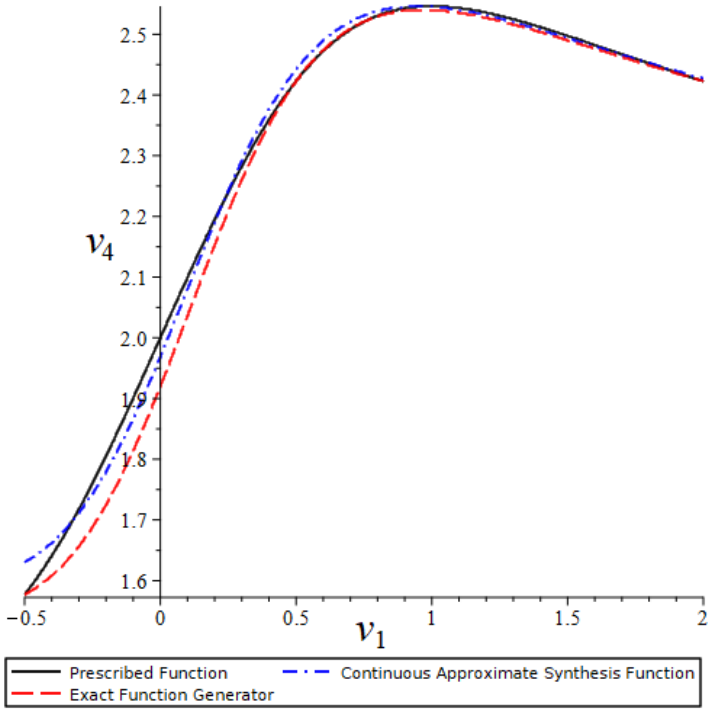

Figure 6: The prescribed, exact, and continuous synthesis approximation of Equation (11) in the v_1-v_4 plane.

4.1.1 First Multi-Modal Synthesis Attempt

Suppose we now wish to additionally identify a linkage that can approximately generate the v_1-v_4 function in Equation (11) and approximately generate a competing v_1-v_3 function that is very different from the v_1-v_3 function generated by the link lengths listed in Table 1. The pragmatic mechanical engineer response to such a wish is simply that it is not possible with a planar 4R. But, should it not be possible to identify a compromise linkage that will generate both desired functions with tolerable structural error? The naïve answer is surely "why not?!?".

Let us first look at this from the pragmatic mechanical engineer perspective and select the additional v_1-v_3 function to be

$$v_3 = f_2(v_1) = 2 + \tan\left(\frac{v_1^2}{{v_1}^2 + 1}\right), \quad -2 \leq v_1 \leq 2. \tag{15}$$

The v_1-v_3 function generated by the linkage that approximately generated the prescribed v_1-v_4 function can be seen in Figure 7, and is reproduced for comparison with the very different desired v_1-v_3 function in Figure 8. We select the range $-2 \leq v_1 \leq 2$ for the prescribed v_1-v_3 function, and $0 \leq v_1 \leq 2$ for the prescribed v_1-v_4 function, then select initial guesses for the four link lengths and compute Equation (10). We arbitrarily select $(a_1,\ a_2,\ a_3,\ a_4) = (1,\ 1,\ 1,\ 1)$ for link length initial guesses. This yields in the remarkably poor results illustrated in Figure 9.

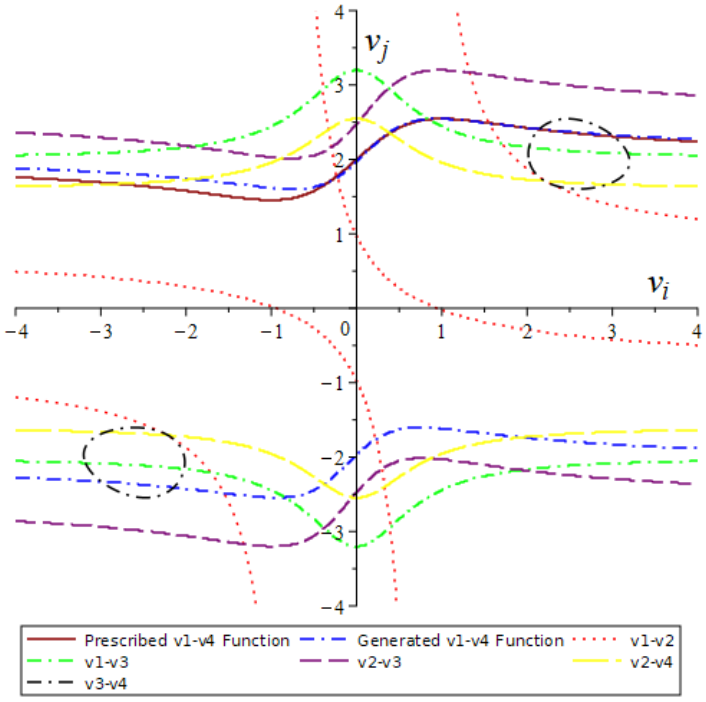

Figure 7: The prescribed, continuous synthesis approximate, and the five functions generated by the identified link lengths in the v_i-v_j planes.

4.1.2 Second Multi-Modal Synthesis Attempt

Clearly, the second, third, fourth, et c., prescribed functions need to be constrained with respect to the five functions generated by the link lengths that approximately generate the first prescribed function in the absence of a useful initial guess. Enter: polynomial interpolation. If we wish to generate a different, though heavily constrained, $v_3 = f_2(v_1)$ function we can specify a generatable function that is an interpolant of the one determined by the specified primary $v_4 = f_1(v_1)$ function. To do this we arbitrarily choose to use Lagrange polynomial interpolation [40].

The first step is to solve the v_1-v_3 IO equation imposed by the generated $v_4 = f_1(v_1)$ function. This yields the exact $v_3 = f_2(v_1)$ function generated by the identified a_i link lengths that approximately satisfy the specified $v_4 = f_1(v_1)$ function. Select n (v_1, v_3) IO pairs from the exact $v_3 = f_2(v_1)$ function generated by the identified a_i to use as inputs for the Lagrange polynomial interpolation formula. In general, this method takes the n points in an arbitrary x-y plane, with no two x_i the same and returns a polynomial of degree at most $d \leq n - 1$.

The Lagrange polynomial interpolant is a linear combination

$$L(x) = \sum_{i=1}^{n} y_i l_i(x)$$

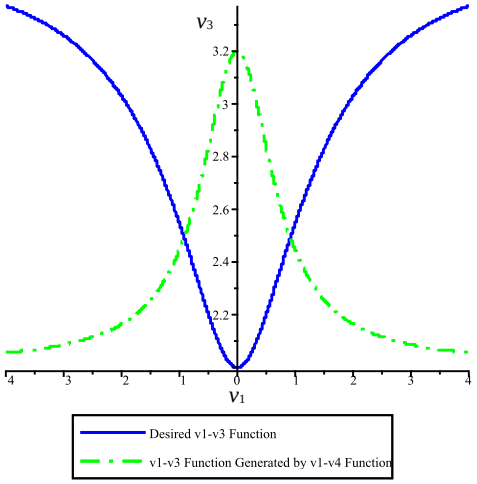

Figure 8: The desired competing v_1-v_3 function and the one generated by the linkage that approximates Equation 11.

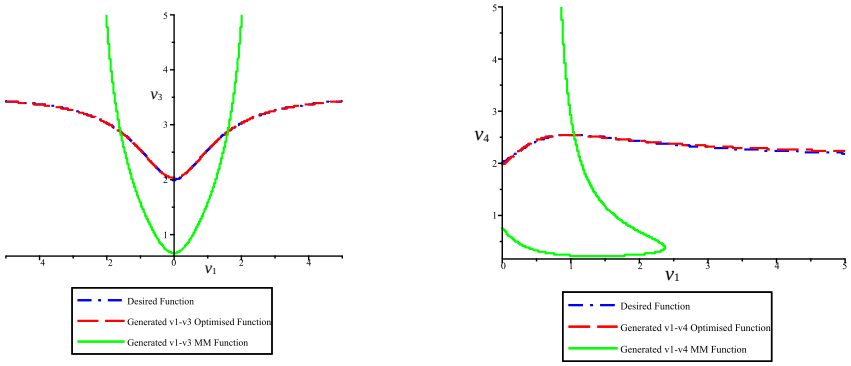

(a) The v_1-v_3 multi-modal results.

(b) The v_1-v_4 multi-modal results.

Figure 9: Multi-modal synthesis results for two competing functions.

of Lagrange basis polynomials

$$l_i(x) = \prod_{\substack{1 \leq m \leq n \\ m \neq i}} \frac{x - x_m}{x_i - x_m} = \left(\frac{x - x_1}{x_i - x_1}\right)\left(\frac{x - x_2}{x_i - x_2}\right)\cdots\left(\frac{x - x_n}{x_i - x_n}\right).$$

For our computational *proof-of-concept* example we will use a system of primary and secondary prescribed functions. The primary function is arbitrary. But the secondary is some Lagrange polynomial interpolant of the function imposed by the link lengths identified that approximately generate the primary function. The link lengths that approximately generate the primary function will be used as initial guesses for the multi-modal synthesis with the secondary polynomial interpolant function. The primary function we wish to generate with

a planar 4R closed kinematic chain is Equation (11). The corresponding v_1-v_3 function exactly generated by the identified link lengths is obtained from the v_1-v_3 IO equation, Equation (5), using the a_i from the $v_4 = f_1(v_1)$ continuous approximate synthesis step listed in Table 1 is

$$v_3 = \pm \frac{11268158900\sqrt{\left(v_1^2 + \frac{28145}{62561}\right)\left(v_1^2 + \frac{43467}{38278}\right)}}{5593605380v_1^2 + 2516456313}. \tag{16}$$

Suppose that this crank-rocker four-bar linkage was required to precisely time two punch presses. Four holes created by the presses are required to be precisely located on a single automotive quarter panel which is advanced in a jig under the action of the input link of the mechanism. One quarter panel completely advances per 360° rotation of the input crank link. The first punch press is actuated by a trigger that is activated under the action of θ_4, while the second is actuated by θ_3. The $v_4 = f_1(v_1)$ trigger function is that of Equation (11). However, after the linkage is synthesised, the resulting $v_3 = f_2(v_1)$ function, Equation (16), does not satisfy the angle requirement. The trigger for this punch press must be actuated when the input angle locating the quarter panel has the precise values $\theta_1 = 0.00° \pm 0.05°$ and $\theta_1 = 90.00° \pm 0.05°$. At these input angles the corresponding values of θ_3 must be precisely $\theta_3 = 145.25° \pm 0.05°$ and $\theta_3 = 135.25° \pm 0.05°$. Unfortunately, while the values of θ_4 generated by the linkage obtained by continuous approximate synthesis as listed in Table 1 are within tolerance for the required input angles those for θ_3 are not. The required angle generated by this linkage at $\theta_1 = 0.00° \pm 0.05°$ is $\theta_3 = 145.50° \pm 0.05°$ and at $\theta_1 = 90.00° \pm 0.05°$ is $\theta_3 = 135.10° \pm 0.05°$, both out of tolerance, though only marginally, see Table 3. Relaxing the tolerances is deemed to not be an acceptable design course of action. In this case, subtly perturbing the $v_3 = f_2(v_1)$ function generated by the required $v_4 = f_1(v_1)$ function, Equation (11), may yield the required θ_4 and θ_3 output angles.

Table 3 Required and $v_4 = f_1(v_1)$ generated values of θ_3 at required θ_1.

Required θ_1	$0.00° \pm 0.05°$	$90.00° \pm 0.05°$
Required θ_3	$145.25° \pm 0.05°$	$135.25° \pm 0.05°$
Generated θ_3	$145.50°$	$135.10°$

To achieve this, we will attempt to use Lagrange polynomial interpolation to obtain a different, but constrained function using $n = 4$ points on the (upper signed) $v_3 = f_2(v_1)$ curve, Equation (16):

$$(v_1, v_3) \;=\; \left(-\frac{1}{2}, \frac{62167}{21933}\right), \left(\frac{1}{4}, \frac{80364}{26089}\right), \left(\frac{3}{5}, \frac{64227}{23462}\right), \left(\frac{11}{10}, \frac{39821}{16629}\right).$$

The resulting degree 3 Lagrange polynomial function $v_3 = f_2(v_1)$ is

$$v_3 = \frac{140152452564627675650}{146115499161206849967}v_1^3 - \frac{148500638129317309265}{97410332774137899978}v_1^2$$
$$-\frac{136182081139230857387}{584461996644827399868}v_1 + \frac{57010242995943671417}{17710969595297799996}, \tag{17}$$
$$\text{for} \quad -\frac{1}{10} \le v_1 \le \frac{5}{4}.$$

Let this be the specified secondary function. Both the interpolant, Equation (18), and the precise v_1-v_3 function, Equation (16), generated by the link lengths that were identified to approximately generate Equation (11) are illustrated in Figure 10.

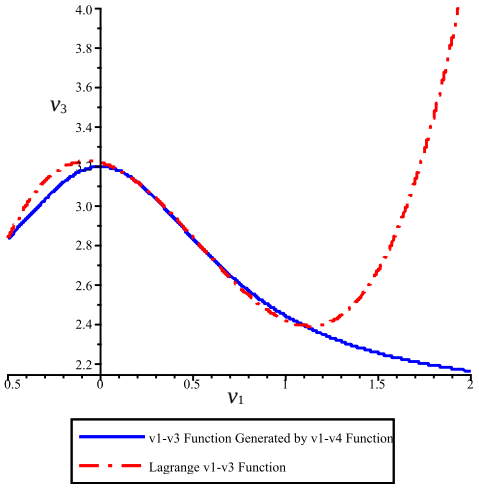

Figure 10: The polynomial interpolant, Equation (18), and the v_1-v_3 function, Equation (16), generated by the linkage that approximates Equation (11).

Careful examination of Figure 10 reveals that both Equation (16) and (18) are very close to each other in the range $-\frac{1}{10} \leq v_1 \leq \frac{5}{4}$. To demonstrate that our kinematic model of the geometry of multi-modal synthesis will lead to a computationally useful result, we will use these as the integration limits for the v_1-v_3 secondary function. Hence, the primary $v_4 = f_1(v_1)$, Equation (11), and secondary $v_3 = f_2(v_1)$, Equation (18), are used to generate the respective synthesis equations with variable angle parameters expressed as v_1 and $f_1(v_1)$ in the primary, and v_1 and $f_2(v_1)$ in the secondary. The two synthesis equations are squared, then the coefficients and variables are separated into the arrays $\mathbf{c}_1$, $\mathbf{s}_1(v_1, f_1(v_1))$, $\mathbf{c}_2$, and $\mathbf{s}_2(v_1, f_2(v_1))$. We then evaluate

$$\min_{(a_1,a_2,a_3,a_4)\in\mathbb{R}} \left(\mathbf{c}_1 \cdot \int_{v_1=-\frac{1}{2}}^{v_1=2} \mathbf{s}_1(v_1, f_1(v_1)) dv_1 + \mathbf{c}_2 \cdot \int_{v_1=-\frac{1}{10}}^{v_1=\frac{5}{4}} \mathbf{s}_2(v_1, f_2(v_1)) dv_1 \right). \quad (18)$$

The multi-modal computations for Equation (18) converge to the link lengths listed in Table 5. The results are graphically illustrated in Figure 11 and the structural errors, defined as the areas between the prescribed and generated functions are listed in Table 6. It is to be seen that the structural error for the $v_4 = f_1(v_1)$ results increases by a factor of nearly four, but is still tolerably small. While the structural error for the $v_3 = f_2(v_1)$ multi-modal results decreases modestly. However, the important outcome in this case is that at the required input angles the corresponding required values of θ_4 are still within tolerance, and those of θ_3 are as well. When $\theta_1 = 0.00^\circ \pm 0.05^\circ$ the multi-modal linkage generates $\theta_3 = 145.25^\circ \pm 0.05^\circ$ and at $\theta_1 = 90.00^\circ \pm 0.05^\circ$ we obtain $\theta_3 = 135.28^\circ \pm 0.05^\circ$, both within tolerance. The relevant values of this outcome are listed in Table 4.

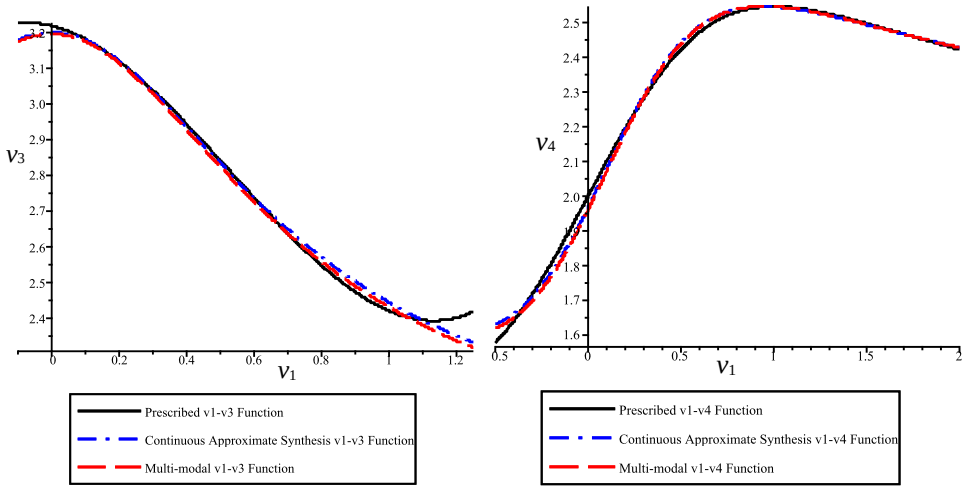

(a) The v_1-v_3 multi-modal results. (b) The v_1-v_4 multi-modal results.

Figure 11: Multi-modal 4R results.

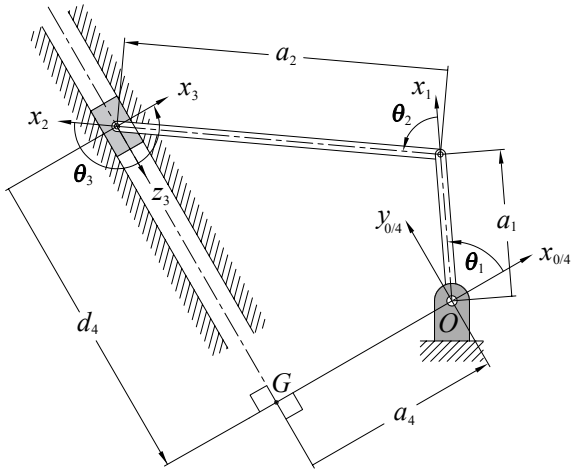

Figure 12: Planar RRRP linkages with Denavit-Hartenberg coordinate systems and parameter assignments.

Table 4 Required and multi-modal generated values of θ_3 at required θ_1.

Required θ_1	$0.00^\circ \pm 0.05^\circ$	$90.00^\circ \pm 0.05^\circ$
Required θ_3	$145.25^\circ \pm 0.05^\circ$	$135.25^\circ \pm 0.05^\circ$
Generated θ_3	145.25°	135.28°

Table 5 The $v_4 = f_1(v_1)$ and $v_3 = f_2(v_1)$ planar 4R multi-modal synthesis results.

Link length	a_1	a_2	a_3	a_4
Floating point	-0.1478064777	0.9299394483	1.148016662	0.8023065449
Normalised	-0.1842269375	1.159082466	1.430895297	1

Table 6 The $v_4 = f_1(v_1)$ and $v_3 = f_2(v_1)$ planar 4R multi-modal synthesis structural errors.

	Structural error
$v_4 = f_1(v_1)$ only	-0.002471306
$v_4 = f_1(v_1)$ multi-modal	0.009542948
$v_3 = f_2(v_1)$ only	0.005358289
$v_3 = f_2(v_1)$ multi-modal	0.004161159

4.2 Planar RRRP Multi-modal Function Generation

Next we shall list the six algebraic IO equations for planar RRRP mechanisms and perform multi-modal synthesis. An arbitrary RRRP linkage is illustrated in Figure 12. The P-pair z_3-axis induces the two link twist angles listed in Table 7.

Table 7 DH parameters for the RRRP.

i	θ_i	d_i	a_i	τ_i	α_i
1	θ_1	0	a_1	0	0
2	θ_2	0	a_2	0	0
3	θ_3	0	0	$\pi/2$	1
4	0	d_4	a_4	-$\pi/2$	-1

By applying the methods in [19] to the DH parameters by algebraising the angle parameters with tangent half-angle equivalents, projecting the DH closure equation into Study's kinematic mapping image space as soma coordinates, then eliminating the intermediate joint variable parameters leads to the RRRP algebraic IO equation:

$$v_1^2 d_4^2 + R v_1^2 + d_4^2 - 4 a_1 v_1 d_4 + S = 0, \tag{19}$$

where

$$R = R_1 R_2 = (a_1 + a_2 - a_4)(a_1 - a_2 - a_4),$$
$$S = S_1 S_2 = (a_1 + a_2 + a_4)(a_1 - a_2 + a_4),$$
$$v_1 = \tan\frac{\theta_1}{2}.$$

Using the same approach [19], the five remaining joint variable parameter pairings lead to the following five RRRP algebraic IO equations:

$$R_2 v_1^2 v_2^2 + R_1 v_1^2 - S_2 v_2^2 + 4a_2 v_1 v_2 - S_1 = 0; \tag{20}$$
$$R_1 v_1^2 v_3^2 + R_2 v_1^2 - S_2 v_3^2 - S_1 = 0; \tag{21}$$
$$S_2 v_2^2 v_3^2 - R_2 v_2^2 - R_1 v_3^2 - 4a_1 v_2 v_3 + S_1 = 0; \tag{22}$$
$$v_2^2 d_4^2 - R_2 S_2 v_2^2 + d_4^2 - R_1 S_1 = 0; \tag{23}$$
$$v_3^2 d_4^2 + R_1 S_2 v_3^2 + d_4^2 + 4a_2 v_3 d_4 - R_2 S_1 = 0. \tag{24}$$

Our primary $d_4 = f_1(v_1)$ function is arbitrarily chosen to be

$$d_4 = 2 - \ln\left(\frac{v_1^2}{v_1^2 + 1}\right), \quad \frac{1}{10} \leq v_1 \leq 6. \tag{25}$$

To generate an initial guess for the multi-modal synthesis, we first perform exact followed by continuous approximate synthesis and identify the following link lengths:

$$a_1 = -\frac{21527}{19453},\ a_2 = \frac{62456}{9833},\ a_4 = \frac{66527}{13759}. \tag{26}$$

After following similar computation steps as for the planar 4R multi-modal synthesis example in Section 4.1.2, we determine the secondary $v_3 = f_2(v_1)$ function again as a degree 3 Lagrange interpolant:

$$v_3 = \frac{8575459781525718313}{2128203922635547524924}v_1^3 - \frac{926446934929263804951}{7094013075451825083080}v_1^2$$
$$+\frac{145850030457909132287}{123732786199741135170}v_1 + \frac{3255237430904027623667}{1773503268862956270770}. \tag{27}$$

We arbitrarily, but without loss of generality, assign the integration limits for this perturbed secondary function to be the same as those of the primary function. The multi-modal synthesis is then performed by evaluating

$$\min_{(a_1,a_2,a_4)\in\mathbb{R}} \left(\mathbf{c}_1 \cdot \int_{v_1=\frac{1}{10}}^{v_1=6} \mathbf{s}_1(v_1, f_1(v_1)) dv_1 + \mathbf{c}_2 \cdot \int_{v_1=\frac{1}{10}}^{v_1=6} \mathbf{s}_2(v_1, f_2(v_1)) dv_1 \right). \tag{28}$$

The numerical optimiser in Maple 2021 converges to the link lengths listed in Table 8, while the structural errors for each of the two generated functions are listed in Table 9. To help visualise the areas between the prescribed and generated functions the results are illustrated in Figure 13. It can be seen that the structural error decreases for the multi-modal synthesis results.

Table 8 The $d_4 = f_1(v_1)$ and $v_3 = f_2(v_1)$ planar RRRP multi-modal synthesis results.

Link length	a_1	a_2	a_4
Rational	$-\frac{26513}{23888}$	$\frac{85324}{13461}$	$\frac{127711}{26510}$
Floating point	-1.10988780904891	6.33860782950366	4.81746510770270

Table 9 The $d_4 = f_1(v_1)$ and $v_3 = f_2(v_1)$ planar RRRP multi-modal synthesis structural errors.

	Structural error
$d_4 = f_1(v_1)$ only	-0.24046271
$d_4 = f_1(v_1)$ multi-modal	-0.23104280
$v_3 = f_2(v_1)$ only	0.23488469
$v_3 = f_2(v_1)$ multi-modal	0.15360825

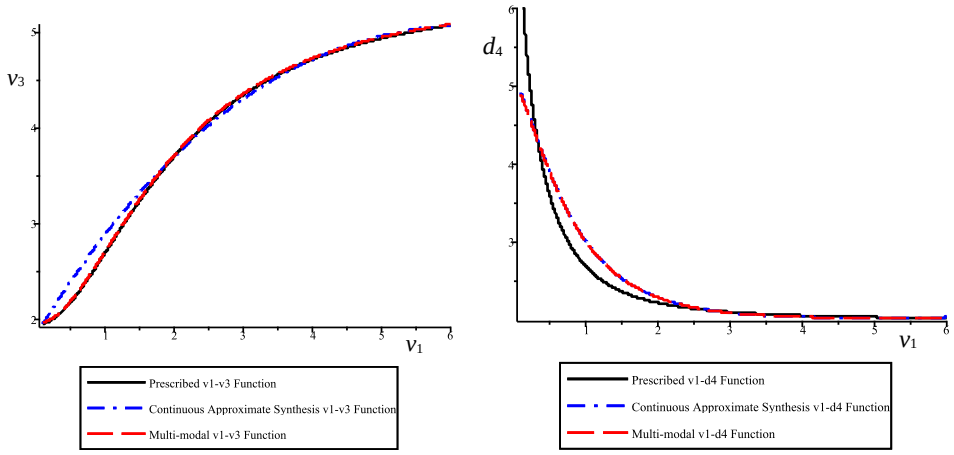

(a) The v_1-v_3 RRRP multi-modal results. (b) The v_1-d_4 RRRP multi-modal results.

Figure 13: Multi-modal RRRP results.

5 Conclusion

The main goal of this paper was to describe a novel four-bar planar mechanism algorithm that implicitly drives the cardinality of the IO data set used to generate the over constrained set of synthesis equations to infinity, and to use it to identify link parameters to simultaneously satisfy two desired functions between different IO pairs. This is accomplished by integrating the square of the algebraic IO equation for the desired kinematic architecture over the specified range of input parameter, v_i or d_i, where the output parameter, v_j or d_j, depending on the kinematic architecture, is expressed in terms of the prescribed function, $v_j = f(v_i)$, et c., for each desired function. The synthesis equation, which we have termed multi-modal,

is the sum of the squared IO equations integrated over the desired input parameter ranges. Because of this, we denote the entire procedure as multi-modal continuous approximate synthesis.

The algorithm was demonstrated with two multi-modal synthesis examples, in a proof-of-concept fashion, to simultaneously generate primary and perturbed secondary functions in each of a 4R and an RRRP planar linkage, and to demonstrate that generation of competing functions with a planar four-bar linkage is, in general, not possible. Comparing the prescribed and generated continuous functions over their specified ranges we have observed that both the design and structural errors are simply the difference in the areas under the prescribed and generated IO curves in the joint variable parameter planes. The multi-modal synthesis results lead to reductions in the structural errors, or at worst a reasonably modest increase. Certainly, any planar four-bar mechanism generates an output joint parameter that is a distinct function of the input joint variable parameter. The linkage that generates this distinct function also exactly determines five additional functions between the remaining pairs of variable joint parameters. The synthesis examples in this paper have demonstrated that it is possible to approximately generate two distinct, though heavily constrained, IO functions between different variable joint pairs that have not been already determined by the linkage geometry. This simple result illustrates the tremendous value represented by the algebraic IO equations as design and analysis tools.

The algebraic IO equations described herein, together with the multi-modal continuous approximate synthesis algorithm, stand to enable designers of industrial automated production and assembly systems to approach optimisation in a new way: different linkages in the mechanical system that are capable of generating multiple different prescribed functions so that each link in the chain can simultaneously perform different tasks. While the practicality of this is, of course, conjecture, it does suggest the continued generalisation and development of multi-modal continuous approximate synthesis is justified and worth the investigative effort. The next step involves research on how to determine suitable initial guesses for the multi-modal synthesis that will yield useful results without heavily constrained secondary functions, and to what degree this is possible. The authors believe this knowledge is to be uncovered in the geometry of the associated design parameter spaces.

References

[1] R.S. Hartenberg and J. Denavit. *Kinematic Synthesis of Linkages*. McGraw-Hill Book Co., New York, N.Y., U.S.A., 1964.

[2] J. Angeles, A. Alivizatoss, and R. Akhras. An Unconstrained Nonlinear Least-squares Method of Optimization of RRRR Planar Path Generators. *Mechanism and Machine Theory*, 23(5):343–353, 1988.

[3] C.M. Gosselin and J. Angeles. Optimization of Planar and Spherical Function Generators as Minimum-defect Linkages. *Mechanism and Machine Theory*, 24(4):293–307, 1989.

[4] C.M. Gosselin, B. Moore, and J. Schicho. Dynamic Balancing of Planar Mechanisms Using Toric Geometry. *Journal of Symbolic Computation*, 44(9):1346–1358, 2009.

[5] F. Freudenstein. *Design of Four-link Mechanisms.* PhD thesis, Columbia University, New York, N.Y., USA, 1954.

[6] F. Freudenstein. Approximate Synthesis of Four-bar Linkages. *Trans. ASME*, 77:853–861, 1955.

[7] D.J. Wilde. Error Linearization in the Least-Squares Design of Function Generating Mechanisms. *ASME, J. of Mech. Des.*, 104(4):881–884, 1982.

[8] S.O. Tinubu and K.C. Gupta. Optimal Synthesis of Function Generators Without the Branch Defect. *ASME, J. of Mech., Trans., and Autom. in Design*, 106(3):348–354, 1984.

[9] Z. Liu and J. Angeles. Data Conditioning in the Optimization of Function-generating Linkages. In *Advances in Design Automation: Proc. 19th Annual ASME Design Automation Conference*, pages 419–426, 1993.

[10] M. Shariati and M. Norouzi. Optimal Synthesis of Function Generator of Four-bar Linkages Based on Distribution of Precision Points. *Mechanica*, 45(3):1007–1021, 2011.

[11] J. Zhang, J. Wang, and X. Du. Time-dependent Probabilistic Synthesis for Function Generator Mechanisms. *Mechanism and Machine Theory*, 46(9):1236–1250, 2011.

[12] P.A. Simionescu. A Restatement of the Optimum Synthesis of Function Generators with Planar Four-bar and Slider-crank Mechanisms Examples. *International Journal of Mechanisms and Robotic Systems*, 3(31):60–79, 2016.

[13] J. Denavit and R.S. Hartenberg. A Kinematic Notation for Lower-pair Mechanisms Based on Matrices. *J. of Applied Mechanics*, pages 215–221, 1955.

[14] W.H. Press, S.A. Teukolsky, W.T. Vetterling, and B.P. Flannery. *Numerical Recipes in C,* 2^{nd} Edition. Cambridge University Press, Cambridge, England, 1992.

[15] M.J.D Hayes, K. Parsa, and J Angeles. The Effect of Data-set Cardinality on the Design and Structural Errors of Four-bar Function-generators. In *Proceedings of the Tenth World Congress on the Theory of Machines and Mechanisms,* Oulu, Finland, pages 437–442, 1999.

[16] A. Guigue and M.J.D. Hayes. Continuous Approximate Synthesis of Planar Function-generators Minimising the Design Error. *Mechanism and Machine Theory*, 101:158–167, 2016.

[17] M.J.D. Hayes, M.L. Husty, and M. Pfurner. Input-output Equation for Planar Four-bar Linkages. In *Advances in Robot Kinematics, 2018*, pages 12–19. Springer, 2018.

[18] M. Rotzoll, M.J.D. Hayes, and M.L. Husty. An Algebraic Input-output Equation for Planar RRRP and PRRP linkages. *Transactions of the Canadian Society for Mechanical Engineering*, 44(4):520–529, 2019.

[19] M. Rotzoll, M.J.D. Hayes, M.L. Husty, and M. Pfurner. A General Method for Determining Algebraic Input-output Equations for Planar and Spherical 4R inkages. In *International Symposium on Advances in Robot Kinematics*, pages 90–97, 2020.

[20] Z. Copeland, M. Rotzoll, and M.J.D. Hayes. Concurrent Type and Dimensional Continuous Approximate Function Generator Synthesis for All Planar Four-bar Mechanisms. In S. Nokleby and P. Cardou, editors, *11th CCToMM Symposium on Mechanisms, Machines, and Mechatronics,* Ontario Tech University, Oshawa, ON, Canada, 2021.

[21] M. Pfurner and M.L. Husty. MyKinematics: Maple Library for Kinematics Using Study's Soma Coordinates. Private communication, *IFToMM 2019 World Congress*, Kraków, Poland, July 2, 2019.

[22] M.L. Husty, M. Pfurner, and H.-P. Schröcker. A New and Efficient Algorithm for the Inverse Kinematics of a General Serial 6R Manipulator. *Mechanism and Machine Theory*, 47:66–81, 2007.

[23] J.J. Craig. *Introduction to Robotics, Mechanics and Control,* 2^{nd} Edition. Addison-Wesley Publishing Co., Reading, Mass., U.S.A., 1989.

[24] M.L. Husty, A. Karger, H. Sachs, and W. Steinhilper. *Kinematik und Robotik*. Springer-Verlag, Berlin, Germany, 1997.

[25] L.W. Tsai. *Robot Analysis: the Mechanics of Serial and Parallel Manipulators*. Wiley-Interscience, New York, N.Y., U.S.A., 1999.

[26] L. Sciavicco and B. Sciliano. *Modeling and Control of Robot Manipulators*. Springer-Verlag, New York, N.Y., U.S.A., 2000.

[27] J.M. McCarthy and G.S. Soh. *Geometric Design of Linkages,* 2^{nd} Edition, Interdiciplinaty Applied Mathematics. Springer, New York, N.Y., 2011.

[28] R.L. Norton. *Kinematics and Dynamics of Machinery,* 5^{th} Edition. McGraw-Hill, New York, N.Y., U.S.A., 2012.

[29] J.J. Uicker, Jr., G.R. Pennock, and J.E. Shigley. *Theory of Machines and Mechanisms,* 5^{th} Edition. Oxford University Press, New York, N.Y., U.S.A., 2017.

[30] M.L. Husty and H.-P. Schröcker. Kinematics and algebraic geometry. In J.M. McCarthy, editor, *21st Century Kinematics*, pages 85–123. Springer-Verlag, London, U.K., 2013.

[31] E. Study. *Geometrie der Dynamen*. Teubner Verlag, Leipzig, Germany, 1903.

[32] M. Rotzoll, Q. Bucciol, and M.J.D. Hayes. Algebraic Input-output Angle Equation Derivation Algorithm for the Six Distinct Angle Pairings in Arbitrary Planar 4R Linkages. In *20th International Conference on Advanced Robotics, ICAR 2021,* Ljubljana, Slovenia, 2021.

[33] G. Dahlquist and Å Björck. *Numerical Methods, translated by Anderson*. Prentice-Hall, Inc., U.S.A., 1969.

[34] J. E. Gentle. *Numerical Linear Algebra for Applications in Statistics*. Springer, New York, U.S.A., 1998.

[35] C. L. Lawson. *Contributions to the Theory of Linear Least Maximum Approximations*. PhD thesis, UCLA, Los Angeles, CA, U.S.A., 1961.

[36] J. R. Rice and K. H. Usow. The Lawson Algorithm and Extensions. *Mathematics of Computation*, 22(101):118–126, 1967.

[37] F. Angeles and J. Angeles. Synthesis of Function-Generating Linkages with Minimax Structural Error: the Linear Case. In *Proceedings of the 13th IFToMM World Congress,* Guanajuato, Mexico, 2011.

[38] C.M. Gosselin and J. Angeles. Mobility Analysis of Planar and Spherical Linkages. *Computers in Mechanical Engineering*, July/August 1988.

[39] M. Rotzoll and M.J.D. Hayes. Mobility Classification in the Design Parameter Space of Spherical 4R Linkages. In S. Nokleby and P. Cardou, editors, *11th CCToMM Symposium on Mechanisms, Machines, and Mechatronics,* Ontario Tech University, Oshawa, ON, Canada, 2021.

[40] E. Waring. Problems Concerning Interpolations. *Philosophical Transactions of the Royal Society*, 69:59–67, 1779.

Proceedings of DETC/CIE'02
2002 ASME Design Engineering Technical Conferences
September 29 - October 02, 2002, Montréal , Québec, Canada

DETC2002/MECH-34378

SOLVING THE BURMESTER PROBLEM USING KINEMATIC MAPPING

M.J.D. Hayes*
Carleton University
Deptartment of Mechanical &
Aerospace Engineering
1125 Colonel By Drive
Ottawa, Ontario,
Canada, K1S 5B6
Email: jhayes@mae.carleton.ca

P.J. Zsombor-Murray
McGill University
Dept. of Mechanical Engineering
Centre for Intelligent Machines
817 Sherbrooke St. W.
Montréal, Québec,
Canada, H3A 2K6
Email: paul@cim.mcgill.ca

ABSTRACT

Planar kinematic mapping is applied to the five-position Burmester problem for planar four-bar mechanism synthesis. The problem formulation takes the five distinct rigid body poses directly as inputs to generate five quadratic constraint equations. The five poses are on the fourth order curve of intersection of up to four hyperboloids of one sheet in the image space. Moreover, the five poses uniquely specify these two hyperboloids. So, given five positions of any reference point on the coupler and five corresponding orientations, we get the fixed revolute centres, the link lengths, crank angles, and the locations of the coupler attachment points by solving a system of five quadratics in five variables that always factor in such a way as to give two pairs of solutions for the five variables (when they exist).

1 Introduction

The determination of a planar four-bar mechanism that can guide a rigid-body through five finitely separated *poses* (position and orientation) is known as the *five-position Burmester problem*, see Burmester (1888). It may be stated as follows. Given five positions of a point on a moving rigid body and the corresponding five orientations of some line on that body, design a four-bar mechanism whose coupler crank pins are located on the moving body and is assemblable upon these five poses. The coupler must assume the five required poses, however sometimes not all five may lie in the same assembly branch.

The problem formulation engenders as many variables as equations so the synthesis is exact. However, most approaches to synthesizing a mechanism that can guide the rigid body exactly through the five positions are rooted in the Euclidean geometry of the plane in which the rigid body must move. From time to time this problem has been revisited (Chang, *et al*, 1991). Readers are refered to this document which contains a recent solution method and a quite adequate and relevant bibliography. More recently, classical finite position synthesis has been reviewed by McCarthy (2000).

We propose a solution obtained in a three-dimensional projective image space of the rigid body motion. An algebraic approach to this exact problem based on quaternions is to be found in Murray and McCarthy (1996). Instead, we use planar kinematic mapping. The planar kinematic mapping was introduced independently by Blaschke and Grünwald in 1911 (Blaschke, 1911; Grünwald, 1911). But, their writings are difficult. In North America Roth, De Sa, Ravani (De Sa and Roth, 1981; Ravani and Roth, 1983), as well as others, have made contributions. However, we choose to build upon interpretations by Husty (1995, 1996), who used the accessible language of Bottema and Roth (1990).

Kinematic synthesis of four-bar mechanisms using kinematic mapping was discussed in Bottema and Roth (1990), originally published in 1979, and expanded upon in great detail by Ravani (1982), and Ravani and Roth (1983). In this early work, Ra-

*Address all correspondence to this author.

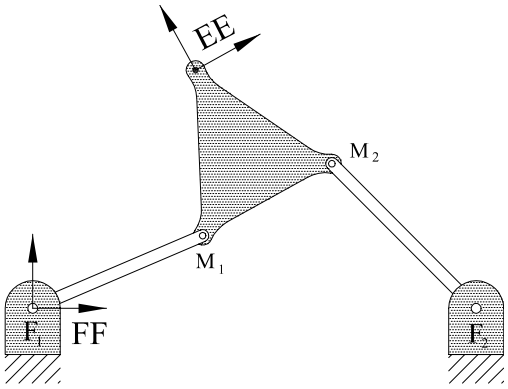

Figure 1. A FOUR-BAR LINKAGE.

vani and Roth developed the framework for performing *approximate* dimensional synthesis. While *exact* dimensional synthesis for the Burmester problem may have been implied, it has never, to our knowledge, been implemented. Results are so elegantly obtained in the kinematic mapping image space that we are compelled to expose the methodology and procedure by which these are produced.

In this image space, the kinematic constraint implied by the motion of a point bound to move upon a circle of fixed centre and radius maps to a hyperboloid of one sheet. Thus, the motion of the coupler of a planar four-bar mechanism connected with four revolute (R) pairs can be characterized by the fourth order curve of intersection of two distinct hyperboloids of one sheet in the image space.

When the kinematic constraint dictates a point moving on a line with fixed line coordinates, as with a prismatic (P) pair, the constraint surface is a hyperbolic paraboloid. Hyperboloids of one sheet and hyperbolic paraboloids are the only types of constraint surfaces associated with planar mechanisms containing only lower pair joints (Hayes and Husty, 2001). Here, we assume solutions of the five-position Burmester problem confined to four-bar mechanisms jointed with four R-pairs, not slider-cranks. Thus only image space hyperboloids of one sheet will apply.

2 Planar Kinematic Mapping

One can consider the relative displacement of two rigid-bodies in the plane as the displacement of a Cartesian reference coordinate frame EE attached to one of the bodies with respect to a Cartesian reference coordinate frame FF attached to the other. Without loss of generality, FF may be considered as fixed while EE is free to move, as is the case with the four-bar mechanism illustrated by Figure 1. Then the position of a point in EE in terms of the basis of FF can be expressed compactly as

$$\mathbf{p}' = \mathbf{R}\mathbf{p} + \mathbf{d}, \tag{1}$$

where, $\mathbf{p}$ is the 2×1 position vector of a point in EE, $\mathbf{p}'$ is the position vector of the same point in FF, $\mathbf{d}$ is the position vector of the origin of frame EE in FF, and $\mathbf{R}$ is a 2×2 proper orthogonal rotation matrix (*i.e.*, its determinant is $+1$) defined by the orientation of EE in FF indicated by ϕ.

Equation (1) can always be represented as a linear transformation by making it *homogeneous* (see McCarthy (1990), for example). Let the homogeneous coordinates of points in the fixed frame FF be the ratios $[X : Y : Z]$, and those of points in the moving frame EE be the ratios $[x : y : z]$. Then Equation (1) can be rewritten as

$$\begin{bmatrix} X \\ Y \\ Z \end{bmatrix} = \begin{bmatrix} \cos\phi & -\sin\phi & a \\ \sin\phi & \cos\phi & b \\ 0 & 0 & 1 \end{bmatrix} \begin{bmatrix} x \\ y \\ z \end{bmatrix}. \tag{2}$$

Equation (2) clearly reflects the fact that a general displacement in the plane is fully characterized by three parameters, in this case a, b, and ϕ.

2.1 Image Space Coordinates and Pole Position

The essential idea of the kinematic mapping introduced by Blashke (1911) and Grünwald (1911)is to map the three homogeneous coordinates of the pole of a planar displacement, in terms of (a, b, ϕ), to the points of a three dimensional projective image space.

The pole, P, of a planar displacement may be described in the following way. Any planar displacement that is a combination of translation and rotation may be represented by a single rotation through a finite angle about a unique fixed axis normal to the plane. Even a pure translation can be considered a rotation through an infinitesimal angle about a point at infinity on a line perpendicular to the direction of the translation. The coordinates of the piercing point of this axis with the plane of the displacement describe the pole, P. If EE and FF are initially coincident, then the coordinates of P are invariant under the its related displacement. That is, P has the same coordinates in both EE and FF. This is illustrated in Figure 2.

By using the dehomogenized form of Equation (2) one may immediately write, after setting $X_P = x_P$ and $Y_P = y_P$ and solving the resulting two simultaneous equations

$$x_P = \frac{a}{2} - \frac{b\sin\phi}{2(1-\cos\phi)}; \quad y_P = \frac{a\sin\phi}{2(1-\cos\phi)} + \frac{b}{2}.$$

The value of the homogenizing coordinate is arbitrary and may, without loss of generality, be set to $z = 2\sin\phi/2$. This means that

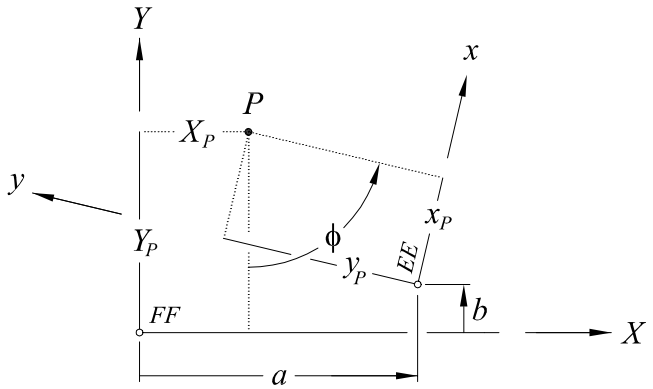

Figure 2. POLE POSITION.

both x_P and y_P must also be multiplied by this value. Then the double angle relationships

$$\sin 2\phi = 2\sin\phi\cos\phi; \quad \cos 2\phi = \cos^2\phi - \sin^2\phi$$

can be used to obtain the following homogeneous coordinates of the pole:

$$\begin{aligned} X_P = x_P &= a\sin(\phi/2) - b\cos(\phi/2) \\ Y_P = y_P &= a\cos(\phi/2) + b\sin(\phi/2) \\ Z_P = z_P &= 2\sin(\phi/2) \end{aligned} \tag{3}$$

The kinematic mapping image coordinates are defined, with respect to the pole P as follows.

$$\begin{aligned} X_1 &= a\sin(\phi/2) - b\cos(\phi/2) \\ X_2 &= a\cos(\phi/2) + b\sin(\phi/2) \\ X_3 &= 2\sin(\phi/2) \\ X_4 &= 2\cos(\phi/2). \end{aligned} \tag{4}$$

Since each distinct displacement described by (a,b,ϕ) has a corresponding unique image point, the inverse mapping can be obtained from Equation (4): for a given point of the image space, the displacement parameters are

$$\begin{aligned} \tan(\phi/2) &= X_3/X_4, \\ a &= 2(X_1X_3 + X_2X_4)/(X_3^2 + X_4^2), \\ b &= 2(X_2X_3 - X_1X_4)/(X_3^2 + X_4^2). \end{aligned} \tag{5}$$

Equations (5) give correct results when either X_3 or X_4 is zero. Caution is in order, however, because the mapping is injective, not bijective: *there is at most one pre-image for each image point*. Thus, not every point in the image space represents a displacement. It is easy to see that any image point on the real line $X_3 = X_4 = 0$ has no pre-image and therefore does not correspond to a real displacement of EE. From Equation (5), this condition renders ϕ indeterminate and places a and b on the line at infinity.

Armed with Equations (4) and (5) any displacement in terms of X_1, X_2, X_3, X_4 can be conveniently converted to the displacement of EE in terms of FF.

2.2 Representing Planar Displacements in Terms of Image Space Coordinates

By virtue of the relationships expressed in Equation (4), the transformation matrix from Equation (2) may be expressed in terms of the homogeneous coordinates of the image space. This yields a linear transformation to express a displacement of EE with respect to FF in terms of the image point:

$$\lambda \begin{bmatrix} X \\ Y \\ Z \end{bmatrix} = \begin{bmatrix} X_4^2 - X_3^2 & -2X_3X_4 & 2(X_1X_3 + X_2X_4) \\ 2X_3X_4 & X_4^2 - X_3^2 & 2(X_2X_3 - X_1X_4) \\ 0 & 0 & X_3^2 + X_4^2 \end{bmatrix} \begin{bmatrix} x \\ y \\ z \end{bmatrix}, \tag{6}$$

where λ is a proportionality constant arising from the use of homogeneous coordinates. The inverse transformation can be obtained with the inverse of the 3×3 matrix in Equation (6) as follows.

$$\mu \begin{bmatrix} x \\ y \\ z \end{bmatrix} = \begin{bmatrix} X_4^2 - X_3^2 & 2X_3X_4 & 2(X_1X_3 - X_2X_4) \\ -2X_3X_4 & X_4^2 - X_3^2 & 2(X_2X_3 + X_1X_4) \\ 0 & 0 & X_3^2 + X_4^2 \end{bmatrix} \begin{bmatrix} X \\ Y \\ Z \end{bmatrix}, \tag{7}$$

with μ being another proportionality constant. The product of these matrices is homogeneously proportional to a unit matrix:

$$\begin{bmatrix} (X_3^2 + X_4^2)^2 & 0 & 0 \\ 0 & (X_3^2 + X_4^2)^2 & 0 \\ 0 & 0 & (X_3^2 + X_4^2)^2 \end{bmatrix}.$$

Clearly, by construction in Equation (4), $X_3^2 + X_4^2 \equiv 2$.

2.3 Planar Constraint Equations

Consider the case of an R-R joint dyad. A point on EE moves on a circle on FF, whose homogeneous equation may be expressed by:

$$C_0(X^2 + Y^2) + 2C_1XZ + 2C_2YZ + C_3Z^2 = 0. \tag{8}$$

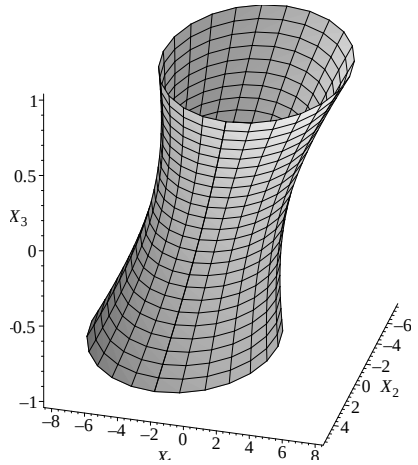

Figure 3. A HYPERBOLOID OF ONE SHEET.

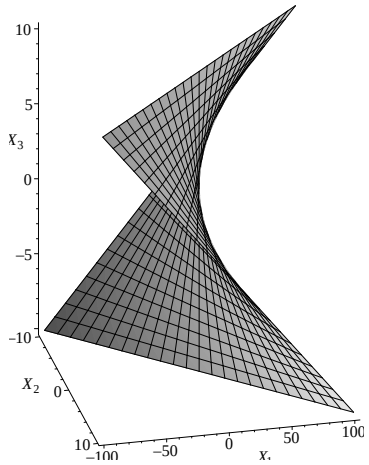

Figure 4. A HYPERBOLIC PARABOLOID.

In Equation (8) $C_0 = k$, an arbitrary constant, while $C_1 = -X_m$, $C_2 = -Y_m$, the circle centre coordinates, and $C_3 = X_m^2 + Y_m^2 - r^2$ with r being the circle radius.

Expanding Equation (6) and substituting the expressions for X, Y, and Z into Equation (8) produces a hyperboloid of one sheet in the image space, see Figure 3. The hyperboloid takes the form:

$$\begin{aligned} &C_0 z^2(X_1^2+X_2^2)+(-C_0x+C_1z)zX_1X_3 \\ &+(-C_0y+C_2z)zX_2X_3+(-C_0y-C_2z)zX_1X_4 \\ &+(C_0x+C_1z)zX_2X_4+(-C_1y+C_2x)zX_3X_4 \\ &+\frac{1}{4}[C_0(x^2+y^2)-2C_1xz-2C_2yz+C_3z^2]X_3^2 \\ &+\frac{1}{4}[C_0(x^2+y^2)+2C_1xz+2C_2yz+C_3z^2]X_4^2=0. \end{aligned} \tag{9}$$

Recall that the coordinates of a point in the moving frame EE are $(x:y:z)$. The hyperboloid is specified when a reference point $(x:y:z)$ is given together with the circle coordinates $(C_0 : C_1 : C_2 : C_3)$. The points $(X_1 : X_2 : X_3 : X_4)$ represent all possible displacements of EE relative to FF under the constraint that one point in FF moves on a circle in EE.

We can generalize the constraint hyperboloid by considering the kinematic inversion: a point on FF bound to move on a circle in EE. We thus expand Equation (5) and substitute the expressions for x, y, and z into Equation (8) and make the following simplifications. For the given circular constraint it is clear that $C_0 = 1$. We may also set $z = X_4 = 1$. The general constraint hyperboloid then becomes

$$\begin{aligned} &(X_1^2+X_2^2)+(C_1-x)X_1X_3+(C_2-y)X_2X_3 \\ &\mp(C_2+y)X_1\pm(C_1+x)X_2\pm(C_2x-C_1y)X_3 \\ &+\frac{1}{4}[(x^2+y^2)-2C_1x-2C_2y+C_3]X_3^2 \\ &+\frac{1}{4}[(x^2+y^2)+2C_1x+2C_2y+C_3]=0. \end{aligned} \tag{10}$$

When (x,y) are the coordinates of the moving point expressed in EE with $z=1$ the *upper* signs apply. If the constraint is intended to express the inverse, a point on FF bound to a circle in EE, then the *lower* signs apply *and* x, y or z is substituted wherever X, Y or Z appears. The situation of a circle moving on a point is never required in problem formulation.

However if a point is bound to a line, *i.e.*, in the case of a prismatic joint, and if one desires to treat inversions, the line may be either on FF *or* EE. Equation (10) reduces to Equation (11) if a point is bound to a line and $C_0 = 0$. This produces a hyperbolic paraboloid in the image space, see Figure 4:

$$\begin{aligned} &C_1X_1X_3+C_2X_2X_3\mp C_2X_1\pm C_1X_2\pm(C_2x-C_1y)X_3 \\ &-\frac{1}{4}[2C_1x+2C_2y-C_3]X_3^2+\frac{1}{4}[2C_1x+2C_2y+C_3]=0. \end{aligned} \tag{11}$$

The above constraint surfaces completely describe the displacements of all possible planar dyads constructed with lower pairs.

3 The Five-Position Burmester Problem

The goal of the dimensional synthesis problem for rigid body guidance of a 4R planar mechanism is to find the *moving*

circle points, M_1 and M_2 of the coupler, i.e., the revolute centres that move on fixed centred, fixed radii circles as a reference coordinate system, EE, attached to the coupler, passes through the desired poses. The *fixed centre points* for each circle are the fixed, or grounded revolute centres, F_1 and F_2, respectively. The circle and centre points are illustrated with the four-bar mechanism shown in Figure 1. For these constraints, the synthesis equations are determined using Equation (10).

What we set out to do here is to use the methods of planar kinematic mapping outlined in (Zsombor-Murray, *et al*, 2002) and set up five simultaneous constraint equations, each of which represents the image space constraint surface for a rigid body moving freely in the plane except that one point is bound to the circumference of a fixed circle. These equations are expressed in terms of the following eight variables.

i. X_1, X_2, X_3, $X_4 = 1$, the dehomogenized coordinates of the coupler pose in the image space.
ii. C_1, C_2, C_3, the coefficients of a circle equation ($C_0 = 1$).
iii. x, y, $z = 1$,the coordinates of the moving crank-pin revolute centre, on the coupler, which moves on a circle.

Since X_1, X_2, X_3 are given for five desired coupler poses, one may in principle solve for the remaining five variables (C_1, C_2, C_3, x, y) . The geometric interpretation is, five given points in space are common to, at most, four hyperboloids on one sheet. Each hyperboloid represents a 2R dyad. If two real solutions occur then all 4R mechanism design information is available (there are two circles in a feasible mechanism design result):

i. Circle centre is at $X_m = -C_1$, $Y_m = -C_2$.
ii. Circle radius is given by $r^2 = C_3 - (X_m^2 + Y_m^2)$.
iii. Coupler length is given by $L^2 = (x_2 - x_1)^2 + (y_2 - y_1)^2$.

4 Analysis

4.1 Converting Pose to Image Space Coordinates

Examine Equations (4) and divide by X_4.

$$X_1 = \frac{\left(a\tan\frac{\phi}{2} - b)\right)}{2},\ X_2 = \frac{\left(a + b\tan\frac{\phi}{2}\right)}{2},\ X_3 = \tan\frac{\phi}{2},\ X_4 = 1.$$

The five given poses being specified as (a_i, b_i, ϕ_i), $i \in \{1, ..., 5\}$, the planar coordinates of the moving point and the orientation of a line on the moving rigid body, all with respect to $(0, 0, 0^\circ)$ expressed in FF. Note that the location of the origin of FF is arbitrary, it is only shown on the fixed revolute centre in Figure 1 for convenience.

4.2 Crank Angles

If the desired five poses can be realized with a planar 4R four-bar mechanism, then at least two real solutions in

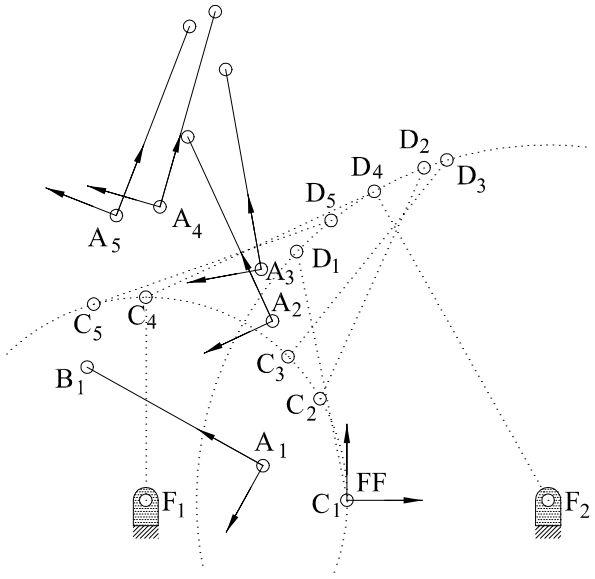

Figure 5. GENERATING THE FIVE DESIRED POSES.

(C_1, C_2, C_3, x, y) will be obtained, defining two 2R dyads sharing the coupler. To construct the mechanism in its five configurations the crank angles must be determined. To obtain the crank angles one just takes (x_1, y_1) and (x_2, y_2) and performs the linear transformation, expressed in image space coordinates, five times.

$$\begin{bmatrix} X \\ Y \\ 1 \end{bmatrix} = \begin{bmatrix} 1 - X_3^2 & -2X3 & 2(X_1X_3 + X2) \\ 2X_3 & 1 - X_3^2 & 2(X_2X_3 - X_1) \\ 0 & 0 & 1 + X_3^2 \end{bmatrix} \begin{bmatrix} x \\ y \\ 1 \end{bmatrix}.$$

(X, Y) come in five pairs because five poses are specified. These are the Cartesian coordinates of the moving revolute centres expressed in FF, and implicitly define the crank angles. For a practical design one must check that the solution did not separate crank pin coordinates in unconnected mechanism branches.

4.3 Pose Constraint Equation

Given the constraints imposed by four revolute joints, the pose constraint equation (synthesis equation) is given by Equation (10) with the upper signs used. For each of the five poses we obtain:

$$\begin{aligned} &(X_1^2 + X_2^2) + (C_1 - x)X_1X_3 + (C_2 - y)X_2X_3 \\ &-(C_2 + y)X_1 + (C_1 + x)X_2 + (C_2x - C_1y)X_3 \\ &+\tfrac{1}{4}[(x^2 + y^2) - 2C_1x - 2C_2y + C_3]X_3^2 \\ &+\tfrac{1}{4}[(x^2 + y^2) + 2C_1x + 2C_2y + C_3] = 0. \end{aligned} \tag{12}$$

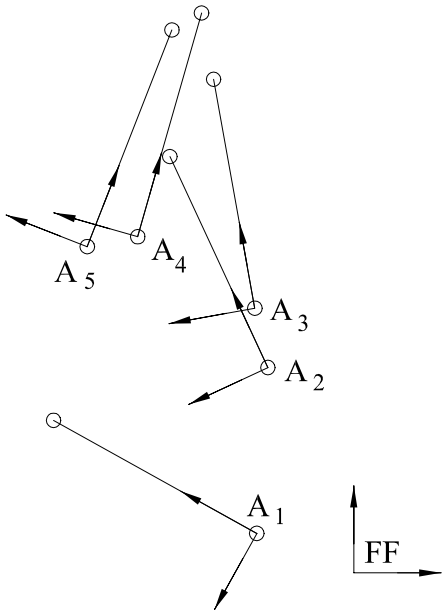

Figure 6. THE FIVE DESIRED POSES.

Parameter	Value
F_1	(-8,0)
F_2	(8,0)
F_1F_2	16
F_1C	8
CD	10
DF_2	14

Table 1. THE GENERATING MECHANISM

i^{th} Pose, A_i	a	b	φ (deg)
1	-3.339	1.360	150.94
2	-2.975	7.063	114.94
3	-3.405	9.102	100.22
4	-7.435	11.561	74.07
5	-9.171	11.219	68.65

Table 2. FIVE RIGID BODY POSES IN FF.

5 Example and Verification

The kinematic mapping solution to the five-position Burmester problem is illustrated with the following example problem. In order to verify our synthesis results, we started with Figure 5, wherein one sees a four-bar mechanism design represented by dotted crank pin circles and a coupler CD which has been placed in five feasible poses. Then an arbitrary point A and orientation line AB were specified. These were used to specify the given five poses, listed in Table 2. The fixed revolute centres and link lengths of the four-bar mechanism used to generate the poses, which we can check for verification, are listed in Table 1, all coordinates given relative to FF. The coordinate information obtained from these were inserted into the five synthesis equations. The results at the end constitute obvious confirmation concerning the effectiveness of the kinematic mapping approach to solving the Burmester problem.

Given the Cartesian coordinates of five positions of a reference point on a rigid body, together with five orientations of the rigid body which correspond to the positions, all relative to an arbitrary fixed reference frame, FF. The reference point is the origin of a coordinate system, A, attached to the rigid body. In Figure 6 the five poses are indicated by the position of A and the orientation of a line in the direction x_A axis. The coordinates and orientations are listed in Table 2.

The given five poses are mapped to five sets of coordinates in the image space. Using a computer algebra software package, we substitute the corresponding values for X_1, X_2, X_3, together with $X_4 = 1$ into Equation (12) yields the following five quadratics in C_1, C_2, C_3, x, and y:

$$\begin{aligned} &51.62713350 - 26.52347891C_1 + 28.43187273x \\ &+3.439909575y + 10.80321393C_2 + 3.971769828y^2 \\ &+3.971769828x^2 - 6.943539655C_1x + 3.971769828C_3 - \\ &6.943539655C_2y - 3.858377808C_1y + 3.858377808C_2x = 0 \end{aligned} \quad (13)$$

$$\begin{aligned} &50.78111719 - 5.144112496C_1 + 13.24300208x \\ &-.485305000y + 12.21272826C_2 + .8645567222y^2 \\ &+.8645567222x^2 - .7291134440C_1x + .8645567222C_3 \\ &-.7291134440C_2y - 1.567873365C_1y + 1.567873365C_2x = 0 \end{aligned} \quad (14)$$

$$\begin{aligned} &57.40558942 - 4.139456673C_1 + 11.62418825x \\ &+2.110482435y + 11.06529652C_2 + .6078497318y^2 \\ &+.6078497318x^2 - .2156994635C_1x + .6078497318C_3 \\ &-.2156994635C_2y - 1.196410852C_1y + 1.196410852C_2x = 0 \end{aligned} \quad (15)$$

$$\begin{aligned} &74.12376162 - 5.833830775C_1 + 7.121746695x \\ &+8.099525062y + 9.071273378C_2 + .3923221773y^2 \\ &+.3923221773x^2 + .2153556452C_1x + .3923221773C_3 \\ &+.2153556452C_2y - .7545122328C_1y + .7545122328C_2x = \end{aligned} \quad (16)$$

$$\begin{aligned} &76.96602922 - 6.723290851C_1 + 5.212549019x \\ &+9.256210937y + 8.224686519C_2 + .3665516768y^2 \\ &+.3665516768x^2 + .2668966465C_1x + .3665516768C_3 \\ &+.2668966465C_2y - .6827933120C_1y + .6827933120C_2x = 0 \end{aligned} \quad (17)$$

Solving the system of Equations (13)-(17) yields four sets of values for C_1, C_2, C_3, x, and y, two being real, and the remaining two being complex conjugates. The two real sets of hyperboloid coefficients are listed in Table 3. The corresponding synthesized four-bar fixed revolute centres and link lengths are listed in Table 4, rounded to same three decimal places as the graphically determined generating mechanism listed in Table 1.

Coefficient	Solution 1	Solution 2
C_1	-7.983138944	7.997107716
C_2	-.027859304	-.000953257
C_3	-131.4773813	-.022545268
x	2.932070052	-3.579426217
y	-8.023883728	-.435620093

Table 3. THE HYPEBOLOID COEFFICIENTS

Parameter	Value
F_1	(-7.997,0.001)
F_2	(7.983,-0.023)
F_1F_2	15.980
F_1C	7.999
CD	10.003
DF_2	13.972

Table 4. THE SYNTHESIZED MECHANISM

While the synthesized mechanism link lengths and centre coordinates are affected by the numerical resolution of the graphical construction of the generating mechanism, we believe this example demonstrates the utility of kinematic mapping to solving the five-position Burmester problem.

6 Computational Pathology

Notice that feasible slider-crank solutions were implicitly excluded by choosing to set $C_0 = z = 1$ rather than, say, $C_2 = y = 1$. This is similar to excluding half-turn EE orientations by setting $X_4 = 1$ rather than, say, $X_3 = 1$. It is recommended that algorithmic implementation should retain $X_4 = 2\cos(\phi/2)$ and contain features to replace $C_0 = 1$ with C_1, C_2 or $C_3 = 1$ and $z = 1$ with x or $y = 1$ should results where $x \to y \to \infty$ with $C_0 = z = 1$ occur.

7 Conclusions

We have used kinematic mapping to solve the five position planar Burmester problem. Five rigid body poses are mapped to points in a three dimensional projective image space and are used directly as inputs to generate five quadratic constraint surface equations in that space. The solutions, when they exist, give the coefficients of the hyperboloids having the five points in common. Each hyperboloid yields a fixed revolute centre, link lengths, crank angles, and coupler attachment points. This method is elegant in that the design task for any composition of R and P joints (open RR, PR, and RP chains) can be treated with a single formulation with no special cases.

REFERENCES

1. Blaschke, W., 1911, "Euklidische Kinematik und nichteuklidische Geometrie", *Zeitschr. Math. Phys.*, Vol. 60, pp. 61-91 and 203-204.
2. Bottema, O. & Roth, B., 1990, *Theoretical Kinematics*, Dover, ch.XI, pp.393-445.
3. Burmester, L., 1888, *Lehrbuch der Kinematik*, A. Felix, Leipzig.
4. Ching Yu Chang, Angeles, J., González-Palacios, M., 1991, "A Semi-graphical Method for the Solution of the Burmester Problem", *ASME Adv. in Des. Auto.*, DE-Vol. 32-2, pp 321-326.
5. Grünwald, J., 1911, "Ein Abbildungsprinzip, welches die ebene Geometrie und Kinematik mit der räumlichen Geometrie verknüpft", *Sitzber. Ak. Wiss. Wien*, Vol. 120, pp. 677-741.
6. De Sa, S., Roth, B., 1981, "Kinematic Mappings. Part 1: Classification of Algebraic Motions in the Plane", *ASME, J. of Mech. Design*, Vol. 103, pp. 585-591.
7. Hayes, M.J.D., Husty, M.L., 2001, "On the Kinematic Constraint Surfaces of General Three-Legged Planar Robot Platforms", submitted to *Mechanism and Machine Theory*.
8. Husty, M.L., 1995, "Kinematic Mapping of Planar Tree(*sic.*)-Legged Platforms, *Proc. of 15th Cdn. Conf. of Appl. Mech.*, Victoria, v.2, ISBN 0920049-06, pp. 876-877.
9. Husty, M.L., 1996, "An Algorithm for Solving the Direct Kinematics of General Stewart-Gough Platforms", *Mechanism and Machine Theory*, Vol. 31, No. 4, pp. 365-379.
10. McCarthy, J.M., 1990, *An Introduction to Theoretical Kinematics*, The M.I.T. Press, Cambridge, Mass., U.S.A..
11. McCarthy, J.M., 2000, *Geometric Design of Linkages*, Springer, New York, NY., U.S.A..

12. Murray, A.P., McCarthy, J.M., August 1996, *Constraint Manifold Synthesis of Planar Linkages*, Proceedings of ASME DETC: Mechanisms Conference, Irvine CA.
13. Ravani, B., 1982, *Kinematic Mappings as Applied to Motion Approximation and Mechanism Synthesis*, Ph.D. Dissertation, Stanford University, Stanford, Ca., U.S.A..
14. Ravani, B., Roth, B., 1983, "Motion Synthesis Using Kinematic Mappings", ASME, *J. of Mechanisms, Transmissions, & Automation in Design*, Vol. 105, pp. 460-467.
15. Zsombor-Murray, P.J., Chen, C. & Hayes M.J.D., 2002, "Direct Kinematic Mapping for General Planar Parallel Manipulators", to appear in *Proc. CSME Forum*, Kingston, ON, Canada.

Towards Integrated Type and Dimensional Synthesis of Mechanisms for Rigid Body Guidance

M.J.D. Hayes[1], P.J. Zsombor-Murray[2]

[1]*Department of Mechanical & Aerospace Engineering, Carleton University, 1125 Colonel By Drive, Ottawa, ON, K1S 5B6, Canada,*
jhayes@mae.carleton.ca

[2]*Centre for Intelligent Machines, McGill University, 817 Sherbrooke Street West, Montreal, QC, H3A 2K6, Canada*
paul@cim.mcgill.ca

In this paper kinematic mapping is used to take the first steps towards development of a general algorithm combining both type and dimensional synthesis of planar mechanisms for rigid body guidance. In the present work we develop an algorithm that can size link lengths, locate joint axes, and using heuristics decide between RR- and PR-dyads that, when combined, can guide a rigid body exactly through five specified positions and orientations, i.e., the five-position Burmester problem. An example is given providing proof-of-concept.

1 Introduction

The determination of a planar four-bar mechanism that can guide a rigid body through five finitely separated *poses* (position and orientation) is known as the *five-position Burmester problem*. It may be stated as follows: given five positions of a point on a moving rigid body and the corresponding five orientations of some line on that body, design a four-bar mechanism whose coupler is the moving body and is assemblable upon these five poses. The coupler must assume the five required poses, even though it may be that not all five lie in the same assembly branch. Burmester showed that the problem leads to, at most, four dyads that can be taken two at a time: there can be as many as six different four-bar mechanisms that can guide a rigid body exactly through five specified poses [1].

From time to time dimensional synthesis for the Burmester problem has been revisited, see for example [2]. More recently, classical finite position synthesis has been reviewed in [3]. An algebraic approach to this exact problem based on quaternions is to be found in [4]. Instead, we use planar kinematic mapping whose geometry is analogous to quaternions. The planar kinematic mapping was introduced independently by Blaschke and Grünwald in 1911 [5, 6], and is summarized in [7].

In general, dimensional synthesis for rigid body guidance assumes a mechanism *type*: i.e., planar $4R$; slider-crank; crank-slider; trammel, etc.. Our aim is to develop a completely general planar mechanism synthesis algorithm that integrates both *type* and *dimensional* synthesis for five-position exact synthesis. It was shown in [8] how kinematic mapping can be used for exact dimensional synthesis.

We employ the Blashke-Grünwald mapping of planar kinematics [5, 6] to regard the problem from a projective geometric perspective, thereby obtaining a system of five non-linear equations in five unknowns expressed in terms of a sixth *homogenizing*, or *influence coefficient*. The value of the sixth unknown determines *type*. The six unknowns represent one dyad. The solutions of the system of equations leads to, at most, four dyads, thereby agreeing with Burmester theory.

It is convenient to characterize rigid body displacements by a coordinate system E that moves relative to a fixed coordinate system Σ, see Figure 1. General planar displacements are then the transformation of points described in E to the coordinates of the same points described in Σ. The constraints on linkages imposed by different joint types can then be described geometrically.

Planar linkages contain either revolute (R-pairs), or prismatic (P-pairs). These kinematic pairs permit rotations about one axis, or translations parallel to one direction, respectively. In the kinematic mapping image space an RR-dyad (three binary links jointed end to end by two R-pairs) constraint involving a point with fixed coordinates in E forced to move on a circle with fixed radius and centre in

Σ is a hyperboloid of one sheet. A PR-dyad (three binary links jointed in series by a P-pair and an R-pair) imposes the constraint where a point with fixed coordinates in E is restricted to move on a line with fixed line coordinates in Σ. This constraint maps to a hyperbolic paraboloid in the image space. The RP-dyad is the kinematic inversion of the PR-dyad. It's constraints also map to hyperbolic paraboloids. The PP-dyad constraints map to a plane in the image space. These are the four possible lower pair dyads for planar mechanisms.

The algorithm that performs both type and dimensional synthesis for rigid body guidance must identify the constraint surfaces that intersect in the curve specified by the image space points of the five given poses. The way the constraints are formulated, the influence coefficient, mentioned earlier, can have either the value 1 or 0, indicating either an RR- or PR-dyad, respectively.

The planar $RRRP$ four-bar linkage shown in Figure 1 can be decomposed into an RR- and a PR-dyad. The RR-dyad is composed of the grounded R-pair centred at the base-fixed point F_1 and the moving R-pair centred at the point M_1. The PR-dyad is composed of the sliding P-pair and the R-pair connected to it with centre at M_2. In the PR-dyad, the P-pair slides on a line with fixed position and direction relative to the base-fixed R-pair centred at F_1. This $RRRP$ linkage is used to generate the five specified poses. Clearly, the algorithm must identify the constraint surfaces corresponding to the given RR- and PR-dyads. Using heuristics, we succeed in identifying these dyads, together with two additional RR-dyads, thereby agreeing with Burmester theory. These are the first steps towards the general algorithm.

2 Kinematic Mapping

The motion of the coupler in a four-bar mechanism can be described by the motion of a reference frame E that moves with the coupler, relative to a ground-fixed non moving reference frame Σ. The $RRRP$ linkage shown in Figure 1 illustrates these two coordinate reference frames. The homogeneous coordinates of points represented in E are given by the ratios $(x : y : z)$. Those of points represented in Σ are given by the ratios $(X : Y : Z)$.

The homogeneous transformation that maps the coordinates of points in E to Σ, which also describes the displacement of E relative to Σ, can be written:

$$\begin{bmatrix} X \\ Y \\ Z \end{bmatrix} = \begin{bmatrix} \cos\varphi & -\sin\varphi & a \\ \sin\varphi & \cos\varphi & b \\ 0 & 0 & 1 \end{bmatrix} \begin{bmatrix} x \\ y \\ z \end{bmatrix}. \qquad (1)$$

Equation (1) indicates that general planar displacements are characterized by the three parameters a, b, and φ, where the pair (a, b) are the $(X/Z, Y/Z)$ Cartesian coordinates of the origin of E expressed in Σ, and φ is the orientation of E relative to Σ, respectively.

All general planar displacements (*i.e.*, any combination of translations and rotations) may be represented by a single rotation through a finite angle about a fixed axis normal to the plane of the displacement. Even a pure translation may be considered a rotation through an infinitesimal angle about the point at infinity in the direction normal to the translation. The coordinates of the piercing point of the rotation axis with the plane of the displacement describe the *pole* of the displacement. The coordinates of the pole are invariant under the associated transformation described by Equation (1).

The pole coordinates for a particular displacement come from the eigenvector corresponding to the one real eigenvalue of Equation (1). Denoting them by the subscript p, the homogeneous pole coordinates, which are the same in both E and Σ, are:

$$\begin{aligned} X_p = \quad x_p = \quad & a\sin(\varphi/2) - b\cos(\varphi/2), \\ Y_p = \quad y_p = \quad & a\cos(\phi/2) + b\sin(\varphi/2), \\ Z_p = \quad z_p = \quad & 2\sin\varphi/2. \end{aligned}$$

Note that the value of the homogenizing coordinate is arbitrary. Without loss in generality it is set $Z_p = z_p = 2\sin\varphi/2$.

The essential idea of kinematic mapping is to map the three homogeneous coordinates of the pole of a planar displacement, in terms of three parameters that characterize it, (a, b, φ), to the points of a three dimensional projective image space. The kinematic mapping image coordinates are defined as:

$$\begin{aligned} X_1 &= a\sin(\varphi/2) - b\cos(\varphi/2) \\ X_2 &= a\cos(\varphi/2) + b\sin(\varphi/2) \\ X_3 &= 2\sin(\varphi/2) \\ X_4 &= 2\cos(\varphi/2). \end{aligned} \qquad (2)$$

Since each distinct displacement described by (a, b, φ) has a corresponding unique image point, the inverse mapping can be obtained from Equation (2): for a given point of the image space, the displacement parameters are

$$\begin{aligned} \tan(\varphi/2) &= X_3/X_4, \\ a &= 2(X_1X_3 + X_2X_4)/(X_3^2 + X_4^2), \\ b &= 2(X_2X_3 - X_1X_4)/(X_3^2 + X_4^2). \end{aligned} \qquad (3)$$

By virtue of the relationships expressed by Equations (2), the transformation matrix from Equation (1) may be expressed in terms of the homogeneous coordinates of the image space. This yields a

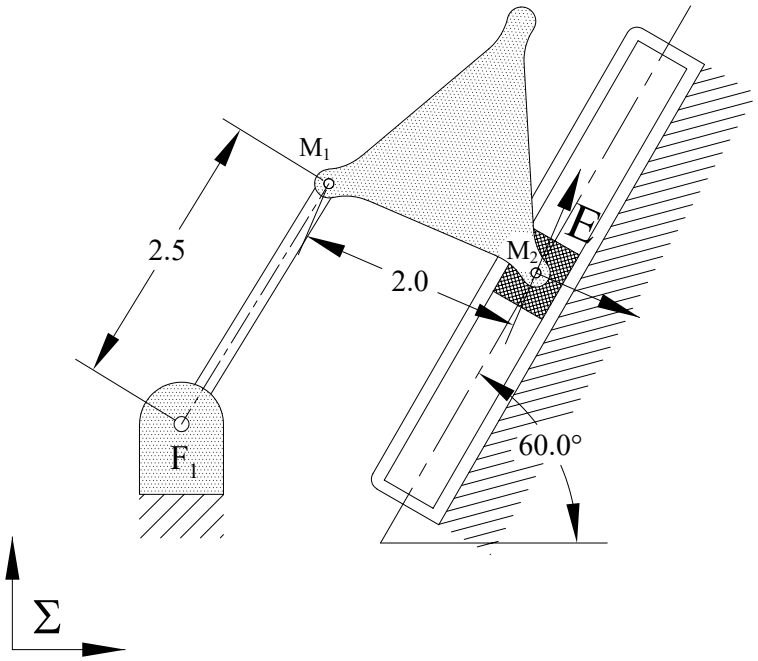

Figure 1: $RRRP$ linkage used to generate the five poses for the example.

linear transformation to express a displacement of E with respect to Σ in terms of the image point [7]:

$$\lambda \begin{bmatrix} X \\ Y \\ Z \end{bmatrix} = \boldsymbol{T} \begin{bmatrix} x \\ y \\ z \end{bmatrix}, \tag{4}$$

where λ is some non-zero constant arising from the use of homogeneous coordinates and

$$\boldsymbol{T} = \begin{bmatrix} X_4^2 - X_3^2 & -2X_3X_4 & 2(X_1X_3 + X_2X_4) \\ 2X_3X_4 & X_4^2 - X_3^2 & 2(X_2X_3 - X_1X_4) \\ 0 & 0 & X_3^2 + X_4^2 \end{bmatrix}.$$

The inverse transformation can be obtained with the inverse of the matrix in Equation (4) as follows.

$$\gamma \begin{bmatrix} x \\ y \\ z \end{bmatrix} = \boldsymbol{T}^{-1} \begin{bmatrix} X \\ Y \\ Z \end{bmatrix}, \tag{5}$$

with γ being another non-zero constant arising from the use of homogeneous coordinates and

$$\boldsymbol{T}^{-1} = \begin{bmatrix} X_4^2 - X_3^2 & 2X_3X_4 & 2(X_1X_3 - X_2X_4) \\ -2X_3X_4 & X_4^2 - X_3^2 & 2(X_2X_3 + X_1X_4) \\ 0 & 0 & X_3^2 + X_4^2 \end{bmatrix}.$$

2.1 Kinematic Constraints

There is a specific type of constrained motion corresponding to each type of planar lower-pair dyad: RR-type; PR-type; RP-type; and PP-type. Because a motion is a continuous set of displacements, and because a displacement maps to a point, a constrained motion will map to a continuous set of points in the image space. As shown in [9], the constraints imposed by the four different dyad types are quadric surfaces with special properties in the image space.

A clearer picture of the image space constraint surface that corresponds to the possible kinematic constraints emerges when $(X : Y : Z)$, or $(x : y : z)$ from Equations (4), or (5) are substituted into the general equation of a circle, the form of the most general constraint [10]:

$$K_0(X^2+Y^2)+2K_1XZ+2K_2YZ+K_3Z^2 = 0. \tag{6}$$

The K_i in Equation (6) depend on the constraint imposed by the dyad. The result is that the constraint surfaces corresponding to RR, PR, and RP-dyads can be represented by *one* equation [10]. It is obtained by substituting the results from Equations (4), or (5) into Equation (6). However, the expression is greatly simplified under the following assumptions:

1. No mechanism of practical significance will have a point at infinity, so it is safe to set $z = 1$.

2. Coupler rotations of $\varphi = \pi$ (half-turns) have images in the plane $X_4 = 0$. Because the X_i are implicitly defined by Equation (2), setting $\varphi = \pi$ gives

$$(X_1 : X_2 : X_3 : X_4) = (a : b : 2 : 0). \tag{7}$$

When we remove the one parameter family of image points for coupler orientations of $\varphi = \pi$ we can, for convenience, normalise the image space coordinates by setting $X_4 = 1$. Conceptually, this implies dividing the X_i by $X_4 = 2\cos\varphi/2$ giving

$$\begin{aligned} X_1 &= \frac{1}{2}\left(a\tan\left(\varphi/2\right) - b\right) \\ X_2 &= \frac{1}{2}\left(a + b\tan\left(\varphi/2\right)\right) \\ X_3 &= \tan\left(\varphi/2\right) \\ X_4 &= 1. \end{aligned} \tag{8}$$

Applying these assumptions to Equations (4), or (5) gives the simplified constraint surface equation upon substitution in Equation (6):

$$\begin{gathered} K_0(X_1^2 + X_2^2) + (-K_0x + K_1)X_1X_3 \\ +(-K_0y + K_2)X_2X_3 \mp (K_0y + K_2)X_1 \\ \pm(K_0x + K_1)X_2 \mp (K_1y - K_2x)X_3 \\ +\tfrac{1}{4}[K_0(x^2 + y^2) - 2(K_1x + K_2y) + K_3]X_3^2 \\ +\tfrac{1}{4}[K_0(x^2 + y^2) + 2(K_1x + K_2y) + K_3] = 0. \end{gathered} \tag{9}$$

The X_i are the image space coordinates that represent a displacement of E relative to Σ. The x and y, after setting $z = 1$, are the Cartesian coordinates of the coupler attachment point in E. For both the RR- and PR-dyads the coupler and base-fixed link are joined by an R-pair, hence these coordinates are conveniently selected to be the rotation centre of the R-pair. The constraint surfaces for these dyads are obtained by using the *upper* signs in Equation (9). Note that for RP-dyads the kinematic constraint is inverted: instead of an R-pair centre constrained to move along a fixed line yielding a fixed range of points, we have a movable line constrained to move on a fixed point yielding a planar pencil of lines on the fixed point. For this case we use the alternate form of Equation (9) where the coordinates $(X : Y : 1)$ of the fixed R-pair centre are used in place of $(x : y : 1)$, and the *lower* signs are used. See [10] for a detailed explanation.

PP-dyads represent a special case. The image space constraint surface corresponding to possible displacements of a PP-dyad is a degenerate quadric that splits into a real and an imaginary plane. This is because only curvilinear motion of the coupler can result. Because φ is constant, the image space coordinates $X_3 = f(\varphi)$ and $X_4 = g(\varphi)$ must also be constant. Hence, the finite part of the two dimensional constraint manifold is linear and must be a hyper-plane. The plane is completely determined by the coupler orientation. When the image space is normalised by setting $X_4 = 1$, the surface equation is simply $X_3 = \tan\left(\varphi/2\right)$.

In what follows only RR- and PR-dyads will be considered to provide some degree of *proof-of-concept*. Development, refinement, and generalization of this approach will come in subsequent publications.

2.2 RR-type Circular Constraints

The ungrounded R-pair in an RR-dyad is constrained to move on a circle with a fixed centre. Meanwhile, the coupler can rotate about the moving R-pair when the coupler connection to the other dyad has been removed. This two parameter family of displacements corresponds to a two parameter hyperboloid of one sheet in the image space. An important property of the hyperboloid is that sections in planes parallel to $X_3 = 0$ are circles [9]. Each one of these image space circles represents possible coupler displacements with a fixed orientation. Thus the constraints imposed by RR-dyads are called *circular constraints*. The exact coefficients of the hyperboloid are determined by substituting in Equation (9) the appropriate values for the kinematic parameters:

$$\begin{aligned} K_0 &= 1, \\ K_1 &= -X_c, \\ K_2 &= -Y_c, \\ K_3 &= K_1^2 + K_2^2 - r^2, \end{aligned} \tag{10}$$

where (X_c, Y_c) are the Cartesian coordinates of the fixed circle centre in the reference frame that is considered to be non-moving, and r is the circle radius. If the kinematic constraint is a fixed point in E bound to fixed circle in Σ, then (x, y) are the Cartesian coordinates of the coupler reference point in E, and the upper signs apply. If the kinematic constraint is a fixed point in Σ bound to fixed circle in E, then (X, Y) are substituted for (x, y) as the coordinates of the coupler reference point in Σ, and the lower signs apply.

2.3 PR-type Linear Constraints

Linear constraints result when PR- and RP-dyads are employed. The linear coefficients are defined as

$$[K_0 : K_1 : K_2 : K_3] = [0 : \tfrac{1}{2}L_1 : \tfrac{1}{2}L_2 : L_3], \tag{11}$$

where the L_i are line coordinates obtained by Grassmann expansion of the determinant of any two distinct points on the line [11].

Of these in the present work we consider only PR-dyads. The direction of the line is a design constant, described by the angle it makes with respect to the fixed base frame Σ, indicated by ϑ_Σ. The point at infinity contained on the line is determined by the

direction of the line, and hence can be specified as $(\cos\vartheta_\Sigma : \sin\vartheta_\Sigma : 0)$. Additionally, the location of a fixed point on the line, also expressed in Σ, is given by the coordinates F_Σ. The line equation in Σ for a given PR-dyad is obtained from the Grassmann expansion:

$$\begin{vmatrix} X & Y & Z \\ F_{X/\Sigma} & F_{Y/\Sigma} & F_{Z/\Sigma} \\ \cos\vartheta_\Sigma & \sin\vartheta_\Sigma & 0 \end{vmatrix} = 0, \qquad (12)$$

where the notation $F_{X/\Sigma}$, $F_{Y/\Sigma}$, $F_{Z/\Sigma}$, represent the homogeneous coordinates $(X : Y : Z)$, expressed in reference frame Σ, of a fixed point on the line that is fixed relative to Σ. Applying Equations (11) and (12) we obtain

$$\begin{aligned} K_0 &= 0, \\ K_1 &= -\frac{F_{Z/\Sigma}}{2}\sin\vartheta_\Sigma, \\ K_2 &= \frac{F_{Z/\Sigma}}{2}\cos\vartheta_\Sigma, \\ K_3 &= F_{X/\Sigma}\sin\vartheta_\Sigma - F_{Y/\Sigma}\cos\vartheta_\Sigma. \end{aligned} \qquad (13)$$

The direction of the translation permitted by the P-pair is specified by the angle the line makes expressed in Σ, ϑ_Σ. When the coordinates of a fixed point on the line are known, we obtain the line coefficients $[K_0 : K_1 : K_2 : K_3]$. These, along with the design values of the coordinates of the coupler attachment point (x, y), expressed in reference frame E, substituted into Equation (9) reveals the image space constraint surface for the given PR-dyad. This surface is an hyperbolic paraboloid [9] with one regulus ruled by skew lines that are all parallel to the plane $X_3 = 0$.

2.4 The Burmester Problem in the Image Space

Each specified pose of E determines a point, $(X_1 : X_2 : X_3 : X_4)$, in the image space. If the displacements are feasible, the five points lie on the curve of intersection of the dyad constraint surfaces. The five points are enough to determine the intersecting quadrics. Recall that, in general, nine points are required to specify a quadric. The special nature of the constraint surfaces represent four constraints on these quadrics.

The hyperboloids, corresponding to RR-dyads, intersect planes parallel to $X_3 = 0$ in circles. Thus, all constraint hyperboloids contain the image space equivalent of the *imaginary circular points*, J_1 and J_2: $(1 : \pm i : 0 : 0)$. The points J_1 and J_2 are imaginary points on the real line, l, of intersection of the planes $X_3 = 0$ and $X_4 = 0$. This real line is the axis of a pencil of planes that includes the complex conjugate planes V_1 and V_2, defined by: $X_3 = \pm iX_4$. The hyperboloids all have V_1 and V_2 as tangent planes, though not necessarily at J_1 and J_2.

The hyperbolic paraboloids, corresponding to PR- and RP-dyads, contain l as a generator. Therefore all constraint hyperbolic paraboloids contain J_1 and J_2, moreover V_1 and V_2 are the tangent planes at these two points. Thus every constraint surface for RR-, PR-, and RP-dyads have these four conditions in common, reducing the number of independent parameters to five.

Our approach is to leave K_0 as an unspecified variable homogenizing coordinate and solve the synthesis equations in terms of K_0. In general, the constants K_1, K_2, and K_3 will depend on K_0. If these multipliers become very large (on the order of 10^6) indicating a very large crank radius then we set $K_0 = 0$ and use line coordinate definitions for K_1, K_2, and K_3 in Equation 13 giving a PR-dyad. Otherwise, $K_0 = 1$, and the circle coordinate definitions for K_1, K_2, and K_3 in Equation 10 are used yielding an RR-dyad.

3 Example

The mechanism illustrated in Figure 1 was used to generate the five poses listed in Table 1 and displayed in Figure 2. For this generating mechanism, the origin of reference frame E, O_E, is on the centre of the R-pair on the coupler point M_2. Homogeneous coordinates in E are described by the triples of ratios $(x : y : z)$. The coupler reference points M_1 and M_2 define the direction of the x-axis. The positive y-axis is as shown in Figures 1 and 2. Frame Σ is as shown in the same two figures. Reference frame E moves with the coupler. The fixed R-pair center is located on point F_1. The geometry of the generating mechanism is listed in the right hand side of Table 1.

The given five poses are mapped to the coordinates of five points in the image space. Using a computer algebra software package, we substitute the corresponding values for X_1, X_2, X_3, together with $X_4 = 1$ and $z = 1$ into Equation (9), effectively projecting the points onto the embedded Euclidean Space. This produces the following five nonlinear equations in terms of K_0, K_1, K_2, K_3, x, and y, which are quadratic when K_0 is considered constant:

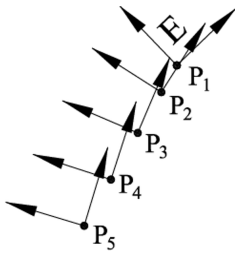

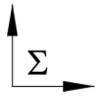

Figure 2: The five poses.

pose	a	b	φ (deg)	parameter	value
1	5.24080746	4.36781272	43.88348278	F_1	$(X:Y:Z)=(1.5:2:1)$
2	5.05087057	4.03883237	57.45578356	M_1	$(x:y:z)=(-2:0:1)$
3	4.76358093	3.54123213	66.99534998	M_2	$(x:y:z)=(0:0:1)$
4	4.43453496	2.97130779	72.10014317	M_1M_2	$l=2$
5	4.10748142	2.40483444	72.30529428	F_1M_1	$r=2.5$
				P-pair angle	$\vartheta_\Sigma=60$ (deg)

Table 1: Five poses of the $RRRP$ mechanism; Geometry of the $RRRP$ generating mechanism.

$$(13.52428430+3.954702976x-0.281732470y+0.2905708072x^2+0.2905708072y^2)K_0+$$
$$(3.045651308+0.4188583855x-0.4028439264y)K_1+$$
$$(2.538317736+0.4028439264x+0.4188583855y)K_2+0.2905708072K_3; \quad (14)$$

$$(13.59714292+3.980465638x-1.355748810y+0.3251080324x^2+0.3251080324y^2)K_0+$$
$$(3.284157186+0.3497839351x-0.5481168944y)K_1+$$
$$(2.626113690+0.3497839351y+0.5481168944x)K_2+0.3251080324K_3; \quad (15)$$

$$(12.66604850+3.682213684x-2.157608235y+0.3595038128x^2+0.3595038128y^2)K_0+$$
$$(3.425051014+0.2809923744x-0.6618272064y)K_1+$$
$$(2.546172905+0.6618272064x+0.2809923744y)K_2+0.3595038128K_3; \quad (16)$$

$$(10.89749412+3.205294435x-2.529259406y+0.3824518134x^2+0.3824518134y^2)K_0+$$
$$(3.391991875+0.2350963732x-0.7278785984y)K_1+$$
$$(2.272764106+0.7278785984x+0.2350963732y)K_2+0.3824518134K_3; \quad (17)$$

$$(8.686958330+2.714462017x-2.440453512y+0.3834517468x^2+0.3834517468y^2)K_0+$$
$$(3.150041851+0.2330965065x-0.7306209600y)K_1+$$
$$(+1.844275934+0.7306209600x+0.2330965065y)K_2+0.3834517468K_3; \quad (18)$$

Parameter	Surface 1	Surface 2	Surface 3	Surface 4
K_1	$-1.500K_0$	$-4.2909 \times 10^6 K_0$	$-15.6041K_0$	$-8.3011K_0$
K_2	$-2.0000K_0$	$2.4773 \times 10^6 K_0$	$3.4362K_0$	$-5.0837K_0$
K_3	$-2.5801 \times 10^{-6} K_0$	$2.3334 \times 10^7 K_0$	$107.3652K_0$	$93.4290K_0$
x	-2.0000	8.1749×10^{-7}	0.2281	3.7705
y	3.4329×10^{-7}	-1.3214×10^{-6}	-0.7845	-2.0319

Table 2: The identified constraint surface coefficients.

Parameter	Relation	Value
F_1	$(-K_{1_1}, -K_{2_1})$	$(1.500, 2.000)$
M_1	(x_1, y_1)	$(-2.000, 3.4329 \times 10^{-7})$
M_2	(x_2, y_2)	$(8.1749 \times 10^{-7}, -1.3214 \times 10^{-6})$
ϑ_Σ	$\arctan\left(\frac{-K_{1_2}}{K_{2_2}}\right)$	60.0°

Table 3: Geometry of one of six synthesized mechanisms that is a good approximation of the generating $RRRP$ linkage in Figure 1.

Solving the system of Equarions (14-18) for the unknowns K_1, K_2, K_3, x, and y in terms of K_0 yields the set of four solutions listed in Table 2. Substituting these values into Equation (9) gives four distinct constraint surfaces in the image space, in terms of the homogenizing circle, or line coordinate, K_0.

At the present time, heuristics must be used to select an appropriate value for K_0 by comparing the relative magnitudes of K_1 and K_2. Recall that the circle coordinates are defined to be $K_1 = -X_c$, and $K_2 = -Y_c$, the Cartesian coordinates of the fixed revolute centres, multiplied by -1, expressed in Σ. The crank radius is given by $r = +\sqrt{K_3^2 - (K_1^2 + K_2^2)}$. The coefficients for Surfaces 1, 3, and 4 represent RR-dyads with finite rotation centres when $K_0 = 1$. However, the coefficients for Surface 2, relative to the other three, have a rotation centre whose location approaches infinity, $(4.2909 \times 10^6, -2.4773 \times 10^6)$ with a crank radius of 4.9547×10^6, also approaching infinity, while the relative values of x and y indicate this attachment point is on O_E. This surface should clearly be recomputed as an hyperbolic paraboloid revealing the corresponding PR-dyad. Recall the line coordinate definition, with K_0 left unspecified:

$$\begin{aligned} K_0 &= K_0, \\ K_1 &= -\frac{F_{Z/\Sigma}}{2} \sin\vartheta_\Sigma, \\ K_2 &= \frac{F_{Z/\Sigma}}{2} \cos\vartheta_\Sigma, \\ K_3 &= F_{X/\Sigma} \sin\vartheta_\Sigma - F_{Y/\Sigma} \cos\vartheta_\Sigma. \end{aligned} \quad (19)$$

The angle of the direction of translation of the P-

Solution	Dyad surface pairing
1	Dyad 1 - Dyad 2
2	Dyad 2 - Dyad 3
3	Dyad 2 - Dyad 4
4	Dyad 1 - Dyad 3
5	Dyad 1 - Dyad 4
6	Dyad 3 - Dyad 4

Table 4: Dyad pairings yielding the six synthesized mechanisms.

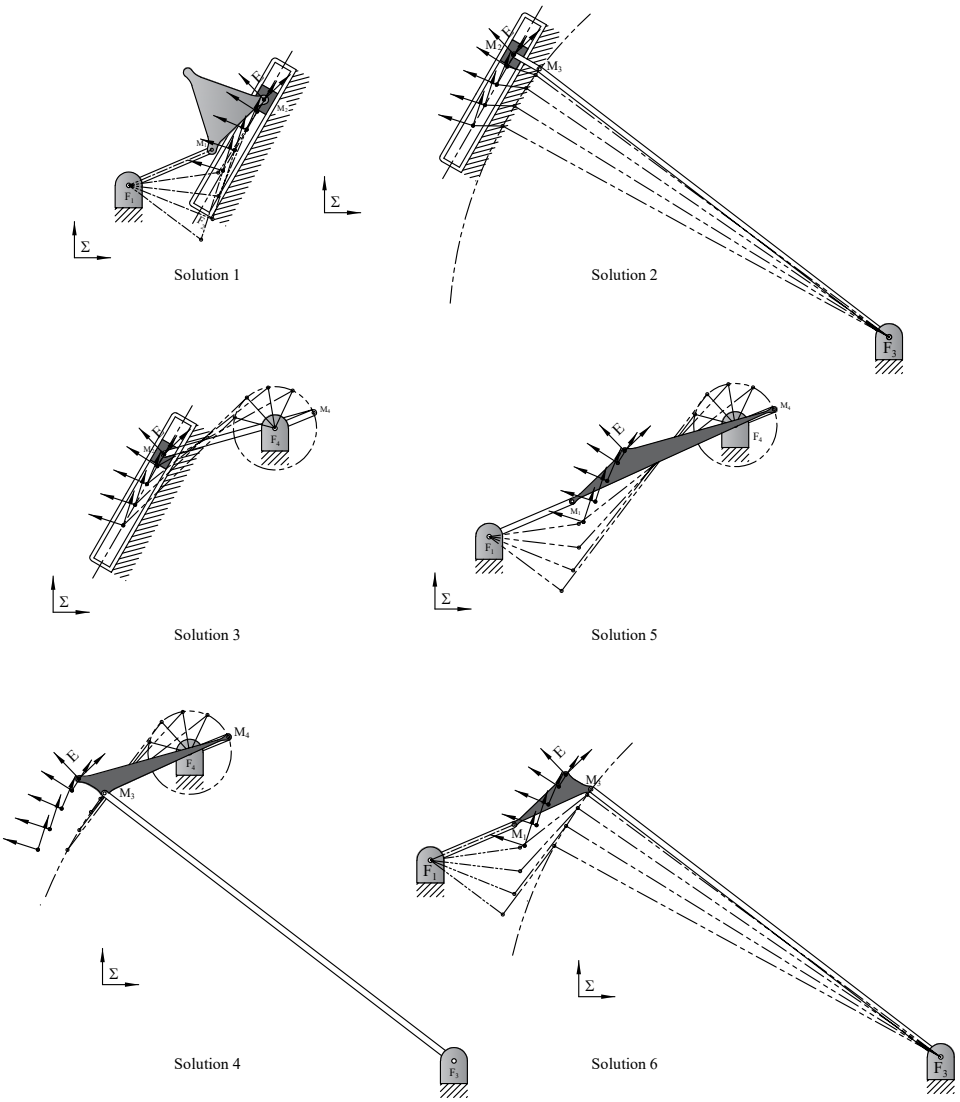

Figure 3: The six synthesized mechanisms.

pair relative to the X-axis of Σ is ϑ_Σ. The translation direction of a PR-dyad that could be combined with any of the three RR-dyads is thus

$$\begin{aligned} \vartheta_\Sigma &= \arctan\left(\frac{-K_1}{K_2}\right) \\ &= \arctan\left(\frac{4.2909\times10^6 K_0}{2.4773\times10^6 K_0}\right) \\ &= 60.0^\circ. \end{aligned} \tag{20}$$

Employing plane trigonometry, it is simple to extract the link lengths and joint locations of the dyad associated with each of the four constraint surfaces. The generating mechanism is reproduced when the dyads corresponding to Surfaces 1 and 2 are paired. We obtain the geometry listed in Table 3 (note, the second subscript refers to the particular surface). The six possible mechanisms are the combinations of the four dyads taken two at a time. These are listed in Table 4 and are illustrated in Figure 3.

4 Conclusions

The example presented herein illustrates that the general image space constraint surface equation, leaving K_0 unspecified, can be used for general type and dimensional synthesis for planar mechanisms. For a set of five poses generated by a particular slider-crank, we synthesized six mechanisms, including the one that generated the poses, that can

guide the coupler through the five poses. Three of the six synthesized linkages are slider-cranks while the remaining three are $4R$ mechanisms. The coupler point is the centre of the R-pair connecting the coupler to the P-pair. This coupler point is clearly bound to a line in the $RRRP$ linkages, but not in the case of the $4R$'s. This approach to planar four-bar mechanisms stands to offer the designer *all* possible linkages that can attain the desired poses, not just $4R$'s and not just slider-cranks, but *all* feasible four-bar linkage architectures along with their dimensions.

Outstanding issues involve the following. The heuristics must be rethought so that an algorithm for type selection can be developed. Moreover, the problem formulation must be reconsidered in such a way that both PR- and RP-dyads can be typed, and extracted from the solutions. The geometric reasoning explaining why five image space points are sufficient to define four unique quadrics must be formalized. Additionally, the geometric interpretation of K_0 must be investigated. How, for example, are the constraint hyperbolic paraboloids parameterized in the image space without setting $K_0 = 0$?

Finally, methods to apply this technique to approximate synthesis should be investigated. The resulting problem would involve fitting a suitable number of points to surfaces in the image space. More specifically, fitting points to the curve of intersection of constraint surfaces. To do this some form of least-squares error minimization would have to be employed. The outcome would be a single dyad pair: the one corresponding to the two constraint surfaces whose intersection best approximates the given set of desired poses

References

[1] L. Burmester. *Lehrbuch der Kinematik*. Arthur Felix Verlag, Leipzig, Germany, 1888.

[2] Y.C. Ching, J. Angeles, and M. González-Palacios. "A Semi-graphical Method for the Solution of the BurmesterProblem". *ASME Adv. in Des. Auto.*, DE-Vol. 32-2: pages 321–326, 1991.

[3] J.M. McCarthy. *Geometric Design of Linkages*. Springer-Verlag, New York, N.Y., U.S.A., 2000.

[4] A.P. Murray and J.M. McCarthy. "Constraint Manifold Synthesis of Planar Linkages". *Proceedings of ASME DETC: Mechanisms Conference, Irvine CA.*, 1996.

[5] W. Blaschke. "Euklidische Kinematik und Nichteuklidische Geometrie". *Zeitschr. Math. Phys.*, vol. 60: pages 61–91 and 203–204, 1911.

[6] J. Grünwald. "Ein Abbildungsprinzip, welches die ebene Geometrie und Kinematik mit der räumlichen Geometrie verknüpft". *Sitzber. Ak. Wiss. Wien*, vol. 120: pages 677–741, 1911.

[7] O. Bottema and B. Roth. *Theoretical Kinematics*. Dover Publications, Inc., New York, N.Y., U.S.A., 1990.

[8] M.J.D. Hayes and P.J. Zsombor-Murray. "Solving the Burmester Problem Using Kinematic Mapping". *Proc. of the ASME Design Engineering Technical Conferences: Mechanisms Conference,* Montréal, QC, Canada, on CD, Sept. 2002.

[9] M.J.D. Hayes and M.L. Husty. "On the Kinematic Constraint Surfaces of General Three-Legged Planar Robot Platforms". *Mechanism and Machine Theory*, vol. 38, no. 5: pages 379–394, 2003.

[10] M.J.D. Hayes, P.J. Zsombor-Murray, and C. Chen. "Kinematic Analyais of General Planar Parallel Manipulators". *ASME, Journal of Mechanical Design*, in-press, 2004.

[11] F. Klein. *Elementary Mathematics from an Advanced Standpoint: Geometry*. Dover Publications, Inc., New York, N.Y., U.S.A., 1939.

Quadric Surface Fitting Applications to Approximate Dimensional Synthesis

M. John D. Hayes* S. Radacina Rusu†
Mechanical and Aerospace Engineering,
Carleton University,
Ottawa, ON., Canada

Abstract— *An approximate synthesis method is presented that takes a given set of n desired poses of the coupler of a four-bar planar mechanism and finds the "best" mechanism that can achieve them. This is accomplished by solving an equivalent unconstrained non-linear minimization problem. The hyperboloids of one sheet or hyperbolic paraboloids that minimize the distance between the given n poses in the kinematic mapping image space and n corresponding points that belong to the quadric surfaces, represent the "best" mechanism that can achieve the desired poses. The procedure is tested successfully on an RRRR mechanism.*

Keywords: kinematic mapping; quadric surface fitting; approximate dimensional synthesis.

I. Introduction

Kinematic synthesis of planar four-bar mechanisms for rigid body guidance was first proposed by Burmester [1]. Burmester theory states that five finitely separated poses (positions and orientations) of a rigid body define a planar four-bar mechanism that can guide a rigid body exactly through those five poses. Burmester showed that the problem leads to at most four dyads that, when paired, determine at most six different four-bar mechanisms that can guide the rigid body exactly through the poses.

Although the solution to the five-pose Burmester problem yields mechanisms that have no deviation from the prescribed poses, a major disadvantage is that only five positions and associated orientations may be prescribed. The designer has no control over how the mechanism behaves for any intermediate pose. This can be a difficult challenge in confined and crowded operating spaces. To gain a measure of control over the intermediate poses it is necessary to have a means by which to synthesize a mechanism that guides a rigid body through n prescribed poses, with $n > 5$. In general, an exact solution does not exist to this problem. The problem is known as *approximate synthesis*, where the mechanism determined to be the solution will guide a rigid-body through the prescribed poses with the smallest error, typically in a least-squares sense. The approximate solution will be unique up to the error minimization criteria. The literature is rich with a large variety of numerical approaches to pure approximate kinematic synthesis of this type, see [2], [3], [4], [5] for example.

A possibly much more intuitive approach is to build the approximation algorithm in the kinematic mapping image space introduced simultaneously, but independently in 1911 in [6] and [7]. In this paper, a novel approach to approximate kinematic synthesis for rigid body guidance is presented that uses the geometry of the image space to fit a set of points, representing desired positions and orientations, to quadric surfaces representing mechanism dyads. It is important to note that the optimization considers only kinematics. Dynamics and static force issues such as transmission angle and mechanical advantage are not considered. Such a restriction still applies to a vast array of planar four bar mechanism applications [8]. A very detailed summary of the geometry on the kinematic mapping image space can be found in [9], but a brief description of properties germane to algorithm presented in this paper is presented below.

II. Kinematic Mapping

One can consider the relative displacement of two rigid-bodies in the plane as the displacement of a Cartesian reference coordinate frame E attached to one of the bodies with respect to a Cartesian reference coordinate frame Σ attached to the other. Without loss of generality, Σ may be considered fixed with E free to move.

The homogeneous coordinates of points represented in E are given by the ratios $(x : y : z)$. Those of the same points represented in Σ are given by the ratios $(X : Y : Z)$. The position of a point $(X : Y : Z)$ in E in terms of the basis of Σ can be expressed compactly as

$$\begin{bmatrix} X \\ Y \\ Z \end{bmatrix} = \begin{bmatrix} \cos\varphi & -\sin\varphi & a \\ \sin\varphi & \cos\varphi & b \\ 0 & 0 & 1 \end{bmatrix} \begin{bmatrix} x \\ y \\ z \end{bmatrix}, \qquad (1)$$

where the pair (a, b) are the $(X/Z, Y/Z)$ Cartesian coordinates of the origin of E expressed in Σ, and φ is the orientation of E relative to Σ, respectively.

The essential idea of kinematic mapping is to map the three homogeneous coordinates of the pole of a planar displacement, in terms of (a, b, φ), to the points of a three dimensional projective image space. The image space coordinates are defined as:

*jhayes@mae.carleton.ca
†srrusu@connect.carleton.ca

$$X_1 = a\sin(\varphi/2) - b\cos(\varphi/2); \qquad X_3 = 2\sin(\varphi/2)$$
$$X_2 = a\cos(\varphi/2) + b\sin(\varphi/2); \qquad X_4 = 2\cos(\varphi/2). \quad (2)$$

The mapping is injective, not bijective: *there is at most one pre-image for each image point*. Any image point on the real line l, defined by the intersection of the coordinate planes $X_3 = X_4 = 0$, has no pre-image and therefore does not correspond to a real displacement of E. See [9], for a detailed analysis of the geometry of the image space.

To be practical, we can remove the one parameter family of image points for coupler orientations of $\varphi = \pi$, and normalize the image space coordinates by setting $X_4 = 1$. Conceptually, this implies dividing the X_i by $X_4 = 2\cos(\varphi/2)$ giving

$$X_1 = \frac{1}{2}\left(a\tan(\varphi/2) - b\right); \qquad X_3 = \tan(\varphi/2)$$
$$X_2 = \frac{1}{2}\left(a + b\tan(\varphi/2)\right); \qquad X_4 = 1. \quad (3)$$

Since each distinct displacement described by (a, b, φ) has a corresponding unique image point, the inverse mapping can be obtained from Eqs. (3): for a given point of the image space, the displacement parameters are

$$\begin{aligned} \tan(\varphi/2) &= X_3, \\ a &= 2(X_1X_3 + X_2)/(X_3^2 + 1), \\ b &= 2(X_2X_3 - X_1)/(X_3^2 + 1). \end{aligned} \quad (4)$$

By virtue of the relationships expressed in Eqs. (3), the transformation matrix from Eq. (1) may be expressed in terms of the homogeneous coordinates of the image space. After setting $z = 1$, which is done because no practical coupler will have a point at infinity, one obtains a linear transformation to express a displacement of E with respect to Σ in terms of the coordinates of the image point:

$$\begin{bmatrix} X \\ Y \\ Z \end{bmatrix} = \begin{bmatrix} 1 - X_3^2 & -2X_3 & 2(X_1X_3 + X_2) \\ 2X_3 & 1 - X_3^2 & 2(X_2X_3 - X_1) \\ 0 & 0 & X_3^2 + 1 \end{bmatrix} \begin{bmatrix} x \\ y \\ 1 \end{bmatrix}. \quad (5)$$

A. Planar Constraint Equations

Corresponding to the kinematic constraints imposed by RR- and PR-dyads are quadric constraint surfaces in the image space. A general equation is obtained when $(X : Y : Z)$ from Eqs. (5) are substituted into the general equation of a circle, the form of the most general constraint, [10]:

$$K_0(X^2 + Y^2) + 2K_1XZ + 2K_2YZ + K_3Z^2 \quad = \quad 0. \quad (6)$$

The result is that the constraint surfaces corresponding to RR, and PR-dyads can be represented by *one* equation (see [10], for how to include RP- and PP-dyads as well). After re-arranging in terms of the constraint surface *shape* parameters K_0, K_1, K_2, K_3, x, and y, treating the image space coordinates X_1, X_2, and X_3 as constants yields Eq. (7).

$$\begin{gathered} \left[\tfrac{1}{4}(X_3^2 + 1)x^2 + (X_2 - X_1X_3)x + \tfrac{1}{4}(X_3^2 + 1)y^2 - \right. \\ \left. (X_1 + X_2X_3)y + X_2^2 + X_1^2\right] K_0 + \\ \left[\tfrac{1}{2}(1 - X_3^2)x - X_3y + X_1X_3 + X_2\right] K_1 + \\ \left[X_3x + \tfrac{1}{2}(1 - X_3^2)y - X_1 + X_2X_3\right] K_2 + \\ \tfrac{1}{4}(X_3^2 + 1)K_3 = 0. \end{gathered} \quad (7)$$

For a particular dyad the associated $[K_0 : K_1 : K_2 : K_3]$, along with the design values of the coordinates of the coupler attachment point (x, y), expressed in reference frame E, are substituted into Eq. (7) revealing the image space constraint surface for the given dyad. The K_i in Eqs. (6) and (7) depend on the constraints imposed by the dyad.

For RR-dyads $K_0 = 1$ and the surface is a hyperboloid of one sheet, when projected into the hyperplane $X_4 = 1$, that intersects planes parallel to $X_3 = 0$ in circles, [11]. The K_i are termed *circular coefficients* and are defined as:

$$[K_0 : K_1 : K_2 : K_3] = [1 : -X_c : -Y_c : (K_1^2 + K_2^2 - r^2)], \quad (8)$$

where the ungrounded R-pair in an RR-dyad is constrained to move on a circle of constant radius, r, and fixed centre coordinates in Σ, (X_c, Y_c).

Linear constraints result when PR-dyads are employed. In this case $K_0 = 0$ and the constraint surface is an hyperbolic paraboloid, when projected into the hyperplane $X_4 = 1$, with one regulus ruled by skew lines that are all parallel to the plane $X_3 = 0$, [11]. The *linear coefficients* are defined as

$$[K_0 : K_1 : K_2 : K_3] = [0 : \tfrac{1}{2}L_1 : \tfrac{1}{2}L_2 : L_3], \quad (9)$$

where the L_i are line coordinates obtained by Grassmann expansion of the determinant of any two distinct points on the line, [12]. We obtain

$$\begin{gathered} [K_0 : K_1 : K_2 : K_3] = \\ [0 : -\tfrac{1}{2}\sin\vartheta_\Sigma : \tfrac{1}{2}\cos\vartheta_\Sigma : F_{X/\Sigma}\sin\vartheta_\Sigma - F_{Y/\Sigma}\cos\vartheta_\Sigma] \end{gathered} \quad (10)$$

where ϑ_Σ is the angle the direction of translation makes with respect to the X-axis, expressed in Σ, $F_{X/\Sigma}$, $F_{Y/\Sigma}$, represent the homogeneous coordinates $(X : Y : 1)$, expressed in reference frame Σ, of a point on the line that is fixed relative to Σ.

III. Fitting Displacements (Image Space Points) to Constraint Surfaces

To use kinematic mapping for approximate synthesis requires the best approximation, in a least squares sense, of the constraint surface coefficients K_0, K_1, K_2, K_3, x, and y given a suitably over constrained set of image space coordinates X_1, X_2, X_3, and X_4 which represent the desired set of positions and orientations of the coupler. The given image space points are on some space curve. The points on this curve must be projected onto the *best* fourth order curve of intersection of two constraint surfaces corresponding to two possible dyads from which a mechanism can be constructed which possesses motion characteristics *closest* to those specified. The solution to this problem *is* the solution to the approximate synthesis problem using kinematic mapping for rigid body guidance.

We may begin the search for a solution by generating a set of image space points that satisfy a known image space constraint hyperboloid. If the cardinality of the set of points is much larger than the number of constants required to define the hyperboloid then we should be able to fit the points to the surface. In other words, identify the equation, in a least squares sense, that the points satisfy.

One possibility is to identify the implicit quadric surface equations in the nullspace of the set of equations. That is, an arbitrary quadric surface has the following implicit second order equation:

$$c_0X_4^2 + c_1X_1^2 + c_2X_2^2 + c_3X_3^2 + c_4X_1X_2 + c_5X_2X_3 + c_6X_3X_1 + c_7X_1X_4 + c_8X_2X_4 + c_9X_3X_4 = 0. \quad (11)$$

Given a sufficiently large set of points, one may be able to identify the 10 coefficients $c_0 \ldots c_9$ that define the quadric surface that is closest, in some sense, to the given points. But, two surfaces are required, one for each of the two dyads comprising the mechanism.

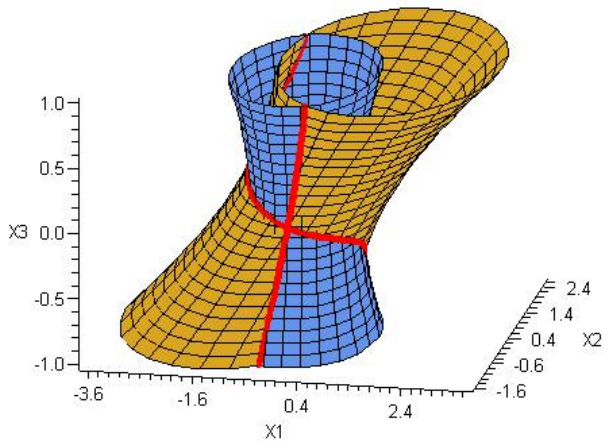

Fig. 1. Intersection curve of two RR hyperboloids of one sheet.

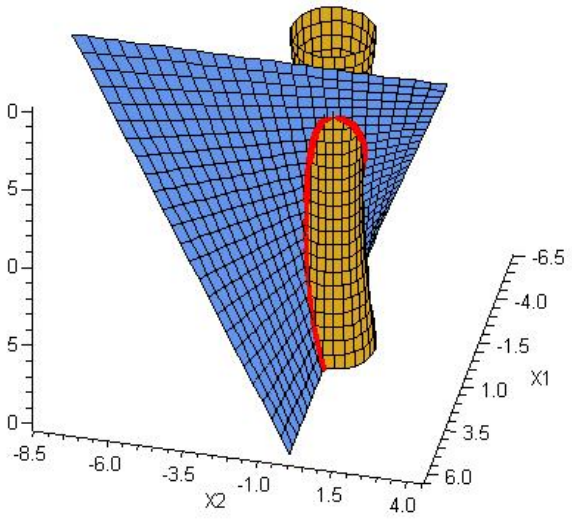

Fig. 2. Intersection curve of one RR hyperboloid of one sheet and one RP hyperbolic paraboloid.

The *best* four bar mechanism will be composed of RR, PR or RP-dyads. Due to their motion constraints, RR-dyads map to hyperboloids of one sheet, while PR and RP-dyads map to hyperbolic paraboloids in the image space [9], [11]. The two constraint surfaces that intersect in the curve closest to the reference curve will yield the best mechanism for the given set of desired poses in some sense. The curve of intersection of the quadric surfaces of the dyad pairs for $RRRR$, $RRRP$ and $PRRP$ mechanisms are illustrated in Figures 1, 2, and 3. Considering that the curve closest, in the least squares sense, to the reference curve must be the intersection of two quadric surfaces as shown above, it is obvious that the curve belongs to each of those

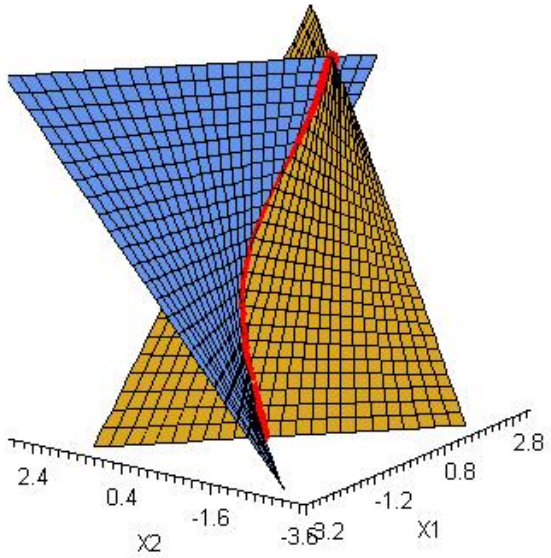

Fig. 3. Intersection curve of two PR hyperbolic paraboloids.

two quadric surfaces. Thus the solution to the approximate synthesis problem is finding the best two quadric surfaces (hyperboloid of one sheet or hyperbolic paraboloid) that contain a curve that is closest to the reference curve, in a least squares sense.

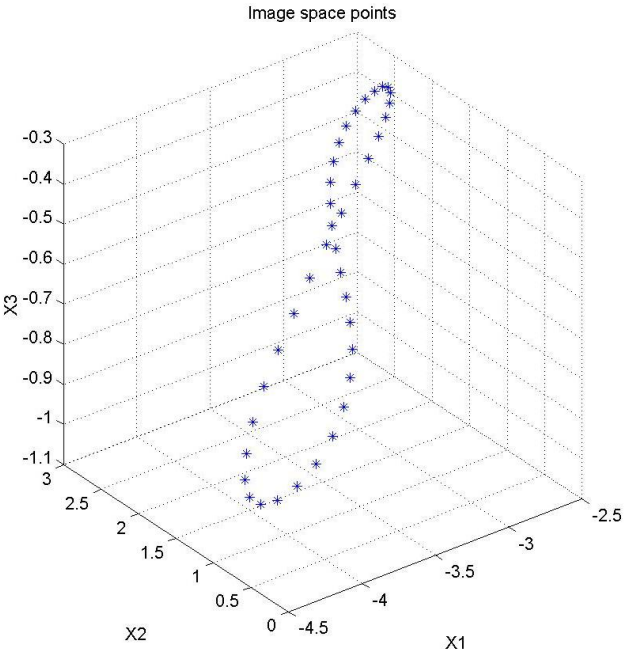

Fig. 4. Points on 4^{th}-order curve of intersection of two image space quadric constraint hyperboloids.

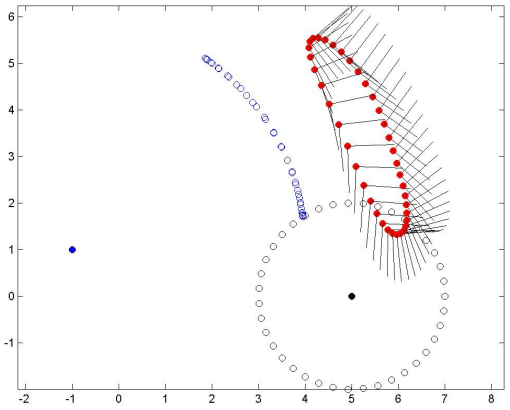

Fig. 5. The mechanism used to generate the poses.

IV. Example

The way the algorithm will be described is through an example. To generate a set of points that lie exactly on one of these constraint surfaces a parametric equation of the surface is required. It is a simple matter to parametrize Eq. (7), see [11]. Note the typo in this paper in Eq. (7): the $-$ signs should be replaced by $+$ signs so that it reads $K_0(X^2+Y^2)+2K_1XZ+2K_2YZ+K_3Z^2$. The parametrization is

$$\begin{bmatrix} X_1 \\ X_2 \\ X_3 \end{bmatrix} = \frac{1}{2}\begin{bmatrix} ([x-K_1]t+K_2+y)+(r\sqrt{t^2+1})\cos\zeta \\ ([y-K_2]t-K_1-x)+(r\sqrt{t^2+1})\sin\zeta \\ 2t \end{bmatrix}, \quad \begin{array}{c}\zeta\in\{0,\ldots,2\pi\},\\ t\in\{-\infty,\ldots,\infty\},\end{array} \tag{12}$$

where x and y are the coordinates of the moving revolute centre expressed in the moving frame E, K_1 and K_2 are the coordinates of the fixed revolute centre expressed in Σ multiplied by -1 (i.e., $K_1=-X_c$ and $K_2=-Y_c$), r is the length between the moving and fixed revolute centres, while t and ζ are free parameters. To simplify the coefficients begin with the surface having the following shape parameters: $K_0=X_4=z=1$, $K_1=K_2=x=y=0$, $r=2$, $K_3=-4$ (recall that $K_3=K_1^2+K_2^2-r^2$). A set of 40 image space points, shown in Figure 4 was generated by the linkage geometry, illustrated in Figure 5

Using the general quadric surface equation, Eq. (11), the image space coordinates of the 40 poses generate a set of 40 synthesis equations in terms of the 10 surface shape parameters $\{c_0,c_1,\cdots,c_9\}$. The two quadric surfaces that best fit the given points lie in the null space of the synthesis matrix $\mathbf{A}$, whose same numbered elements in each row are the terms of the $X_i, i\in\{1,2,3,4\}$ scaled by the surface shape parameters, $c_i, i\in\{0,1,\cdots,9\}$. The two surfaces closest, in a least squares sense, to the null space of $\mathbf{A}$ can be identified using singular value decomposition (SVD). Applying SVD to the overconstrained set of synthesis equations $\mathbf{Ac}=\mathbf{0}$ reveals that the matrix $\mathbf{A}$ is rank deficient by two. That is, two of its singular values are zero, or computationally close to zero. In this case the two smallest singular values are 1.0×10^{-15}, and 3.0×10^{-15}. Hence, the two smallest singular values may be considered to be effectively zero, and near the numerical resolution of the computer. The next smallest singular value is 6.5×10^{-3}, which is five orders of magnitude smaller than the largest singular value of 88.8. It is a simple matter to identify the array of surface shape parameters, $\mathbf{c}$, that correspond to the two smallest singular values of the synthesis matrix $\mathbf{A}$ [13]. The coefficients are listed as Surfaces M, N and O in Table I, with M corresponding to the smallest, N the second smallest, and O the third smallest singular value.

The quadric surface type information is embedded in its coefficients. The implicit equation of the quadric surface can be classified according certain invariants of its discriminant and quadratic form [14]. Written in discriminant form,

Surface	c_0	c_1	c_2	c_3	c_4	c_5	c_6	c_7	c_8	c_9
M	1.0000	0.1380	0.0738	-0.3967	-0.0962	0.1201	0.0473	0.8249	-0.3372	-0.2950
N	1.0000	0.2603	0.5297	2.1392	0.0424	-0.0456	0.0145	0.7035	-1.0782	3.9373
O	1.0000	-0.3583	-0.3583	-0.0271	0.0000	-0.4448	0.1494	-0.9881	0.1732	0.0509

TABLE I. The surface shape parameters identified with SVD.

Surface	rank($\mathbf{D}$)	rank($\mathbf{Q}$)	sign of det($\mathbf{Q}$)	sign of T_1	sign of T_2	Quadric surface
M	4	3	+	+	-	Hyperboloid of one sheet
N	4	3	-	+	+	Hyperboloid of two sheets
O	3	3	+	-	+	Hyperboloid of one sheet

TABLE II. Quadric constraint surface type.

Eq. (11) becomes:

$$\begin{bmatrix} X_1 \\ X_2 \\ X_3 \\ X_4 \end{bmatrix}^T \begin{bmatrix} c_1 & \frac{1}{2}c_4 & \frac{1}{2}c_6 & \frac{1}{2}c_7 \\ \frac{1}{2}c_4 & c_2 & \frac{1}{2}c_5 & \frac{1}{2}c_8 \\ \frac{1}{2}c_6 & \frac{1}{2}c_5 & c_3 & \frac{1}{2}c_9 \\ \frac{1}{2}c_7 & \frac{1}{2}c_8 & \frac{1}{2}c_9 & c_0 \end{bmatrix} \begin{bmatrix} X_1 \\ X_2 \\ X_3 \\ X_4 \end{bmatrix} = \mathbf{X^T D X}. \quad (13)$$

The associated quadratic form is:

$$\mathbf{Q} = \begin{bmatrix} c_1 & \frac{1}{2}c_4 & \frac{1}{2}c_6 \\ \frac{1}{2}c_4 & c_2 & \frac{1}{2}c_5 \\ \frac{1}{2}c_6 & \frac{1}{2}c_5 & c_3 \end{bmatrix}. \quad (14)$$

Both the discriminant, $\mathbf{D}$, and the quadratic form, $\mathbf{Q}$, are square symmetric matrices. It can be shown [14] that quadric surfaces can be classified by conditions on the rank of the discriminant, rank($\mathbf{D}$), the rank of the quadriatic form, rank($\mathbf{Q}$), the sign of the determinant of the discriminant, det($\mathbf{D}$), the sign of the product of det($\mathbf{Q}$) with the trace of $\mathbf{Q}$ (indicated by T_1), and the sign of the sum of the two-rowed principal minors of $\mathbf{Q}$ (indicated by T_2). This last invariant is more precisely defined as

$$T_2 = \sum_{i=1,j=2,i<j}^{3} \begin{vmatrix} q_{ii} & q_{ij} \\ q_{ij} & q_{jj} \end{vmatrix}, \quad (15)$$

where the q_{ij} are the elements of $\mathbf{Q}$.

A quadric surface is an hyperboloid of one sheet if rank($\mathbf{D}$) $= \mathbf{4}$, rank($\mathbf{Q}$) $= \mathbf{3}$, det($\mathbf{D}$) $> \mathbf{0}$, and either $T_2 \leq 0$, or both $T_1 \leq 0$ and $T_2 > 0$. A quadric surface is an hyperboloid of two sheets if all the above conditions on the invariants are met, with the exception that det($\mathbf{D}$) $< \mathbf{0}$. A quadric surface is an hyperbolic paraboloid if rank($\mathbf{D}$) $= \mathbf{4}$ and rank($\mathbf{Q}$) $= \mathbf{2}$. The values of these parameters for each of Surfaces M, N, and O are listed in Table II.

Surfaces M and O are two hyperboloids of one sheet, while Surface N is a hyperboloid of two sheets. Since a hyperboloid of two sheets does not represent a planar dyad constraint surface, the conclusion is that the quadric surfaces that best fit the reference curve, in the least squares sense, are two hyperboloids of one sheet. Despite the fact that the second RR-dyad constraint surface is far removed from the null space of the synthesis matrix, it nevertheless indicates that an $RRRR$ mechanism will best approximate the desired coupler poses.

A. *Minimization*

Points on a hyperboloid of one sheet can be obtained using Eq. (12), where K_1, K_2, K_3, x, and y are the constraint surface shape parameters described in Section II-A. The approximate synthesis problem can be solved using an equivalent unconstrained non-linear minimization problem. This problem can be stated in the following way: find the set of surface shape parameters (K_1, K_2, K_3, x, y) that minimize the total spacing between all 40 points on the reference curve and 40 points that lie on the surface of a hyperboloid of one sheet where $t = X_3 = X_{3_{ref}}$:

$$d = \sum_{i=1}^{40} \sqrt{(X_{1ref_i} - X_{1_i})^2 + (X_{2ref_i} - X_{2_i})^2}. \quad (16)$$

The two sets of parameters that minimize d represent the two *best* constraint surfaces that intersect *closest* to the reference curve. Therefore, they represent the *best* dyad pair that approximate the desired 40 poses. This formulation results from the fact that $t = X_3$ is a free parameter in the parametric equation for the hyperboloid of one sheet, Eq. (12). Thus, for any hyperboloid of one sheet there exist 40 points with the same $t = X_3$ coordinates as the 40 points on the reference curve. Furthermore X_1 and X_2 have the same form in Eq. (12), so the distance between each point on the reference curve and each corresponding point on the quadric surface in the hyperplane $t = X_3$ can be simply measured on the X_1X_2 hyperplane. Hence, d can be defined.

The second free parameter, ζ, in Eq. (12) is found by a minimization sub routine, which runs for each corresponding point generated on the quadric surface with the same $t = X_3$ coordinate as a point on the reference curve. This simply implies that for a constraint hyperboloid of one sheet

cut by a plane corresponding to $t = X_3$ there is only one point on the circular trace of the hyperboloid of one sheet in that hyperplane that is closest to the corresponding point on the reference curve and that the (X_1, X_2) coordinates of the closest point are only a function of ζ. Another implication is that the distance between the point generated with coordinates (X_1, X_2) and the corresponding point on the reference curve is only dependent on the surface shape parameters K_1, K_2, K_3, x, and y.

B. Initial Guesses

In order for the algorithm to converge to the solution that minimizes d, decent initial guess for the shape parameters are required. While initial guesses may be good or bad, the minimization algorithm above allows for each of them to converge to the best solution and to quantify the deviation of the poses generated by the identified mechanism. Out of the 40 points on the reference curve five points spaced relatively widely apart are arbitrarily chosen giving five equations in the five unknown surface shape parameters, after setting $K_0 = 1$ in Eq. (7), knowing that the surface should be a hyperboloid of one sheet. Seven initial guesses are tabulated in Table III.

The idea behind this technique is that the curve that is closest to the reference curve is by definition also closest to the points on the reference curve and thus a curve that exactly passes through five of the points may also be relatively close to the best curve being sought. The minimization algorithm will iteratively jump to the closest curve from curves that may be close to the reference curve by minimizing d. Furthermore, the initial guess procedure could be repeated for a different set of points on the reference curve and more initial guesses can be found. Statistics and heuristics could be used to actually narrow down the initial guesses. For the sake of testing this approximate synthesis method, this is not done, and all initial guesses are considered equal and all resulting solutions are evaluated.

C. Minimization Results

Non-linear unconstrained programming methods such as the Nelder-Mead simplex method [15] and the Hookes-Jeeves method [16] have been used with similar outcomes. The results of the minimization corresponding to each initial guess can be observed in Figures 6-12.

In each figure, the solid dots represent the desired 40 poses in the projection of the kinematic mapping image space into the hyperplane $X_4 = 1$. These 40 reference points lie on the solid reference curve. The small circles are the corresponding 40 points generated by the mechanism identified from the minimization algorithm. These points lie on the surface of a constraint hyperboloid of one sheet that the algorithm converged to starting from the particular initial guess. The results can now be visually compared. In each figure, the images on the left are the results and reference curve projected onto the plane $X_3 = 0$.

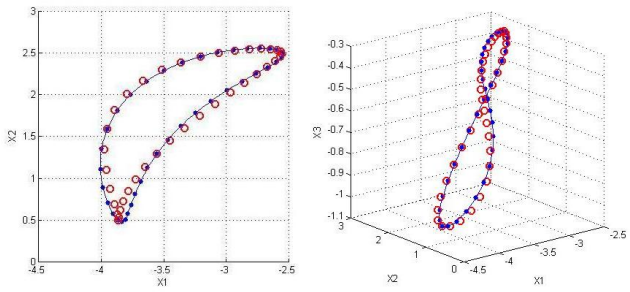

Fig. 6. Graphical results for Initial Guess 1.

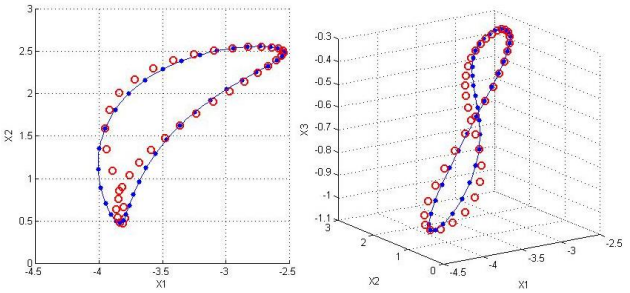

Fig. 7. Graphical results for Initial Guess 2.

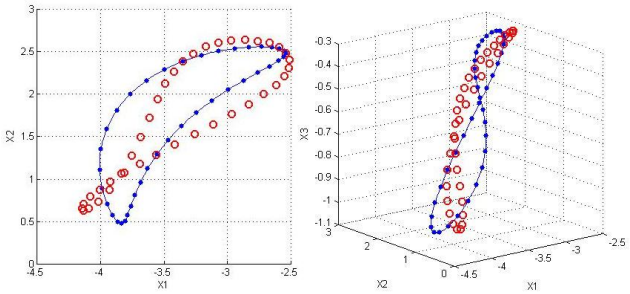

Fig. 8. Graphical results for Initial Guess 3.

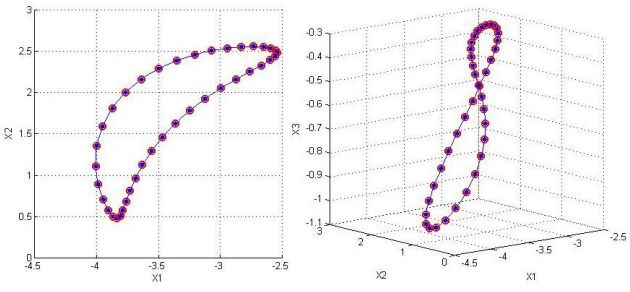

Fig. 9. Graphical results for Initial Guess 4.

Guess	K_1	K_2	K_3	x	y
1	-73.59218	-21.00890	5467.99420	23.99357	56.20798
2	-7.08742	-5.53320	46.84468	-1.58544	-3.19723
3	9.75170	5.29780	27.84599	-2.29188	-7.86290
4	-5.00000	0.00000	21.00000	3.00000	-2.00000
5	1.00000	-1.00000	-23.00000	-1.00000	-2.00000
6	-20.98570	-14.15501	297.79812	-1.28879	0.56361
7	-3.05304	-6.54866	48.44514	-3.82887	-1.05131

TABLE III. Initial Guesses.

Parameter	Guess 1	Guess 2	Guess 3	Guess 4	Guess 5	Guess 6	Guess 7
K_1	-97.720	-18.202	888.914	-5.000	1.000	-25.445	-1.398
K_2	-57.463	-12.363	432.395	0.000	-1.000	-17.073	-6.191
K_3	1491.757	261.650	-2374.375	21.000	-23.000	390.531	36.554
x	-1.133	-1.287	-0.894	3.000	-1.000	-1.309	-4.388
y	0.534	0.889	-5.375	-2.000	-2.000	1.030	-2.361
Iterations	450	623	718	101	176	745	436
d	1.1132	1.9333	6.726	0.0004	0.0010	1.5746	4.8138

TABLE IV. Results.

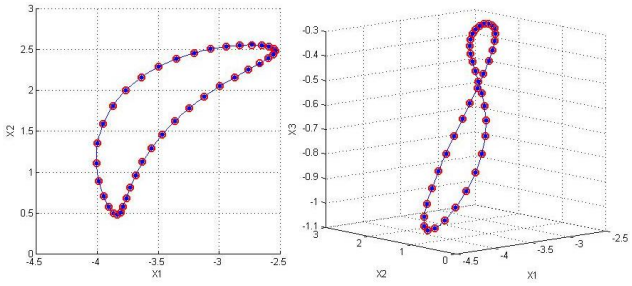

Fig. 10. Graphical results for Initial Guess 5.

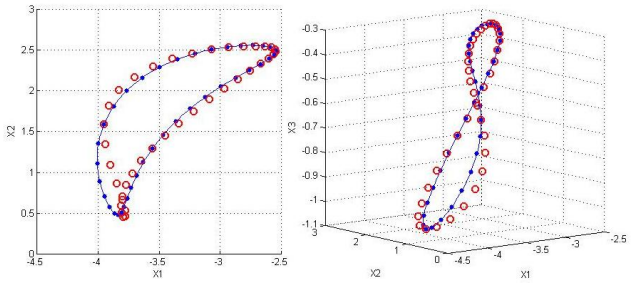

Fig. 11. Graphical results for Initial Guess 6.

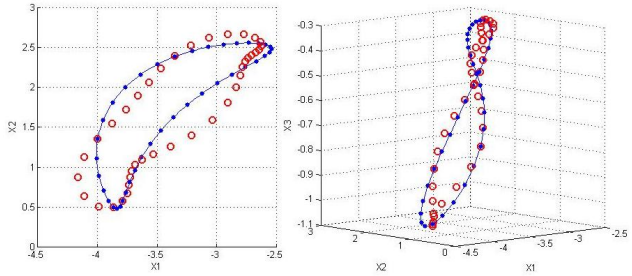

Fig. 12. Graphical results for Initial Guess 7.

The numerical results are tabulated in Table IV. The values of d that resulted from the minimization algorithm can now be compared. These values indicate how close the particular hyperboloid of one sheet obtained is to the reference curve. It is evident that Initial Guesses 4 and 5 generate the best hyperboloids of one sheet that intersect closest to the 40 points on the reference curve. The geometry of the best generating $RRRR$ mechanism can now be extracted using this pair of RR-dyads and their surface shape parameters.

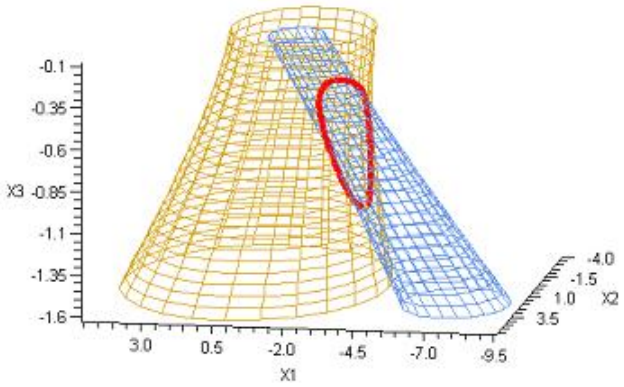

Fig. 13. Curve of intersection of *best* hyperboloids of one sheet.

It is to be noted that these are exactly the RR-dyads that were originally used to construct the initial given 40 poses, and hence the approximate synthesis was indeed successful. It should also be noted that the initial guess values for the shape parameters listed in Table III are completely different from the shape parameters that resulted from the minimization algorithm with the corresponding initial guess with the exception of Initial Guesses 4 and 5. This is not the case

for the other initial guesses because, even though the corresponding hyperboloid of one sheet fit the five arbitrarily chosen points on the reference curve well, the quadric surfaces very poorly fit the 40 points on the reference curve and the algorithm converged to a different, better solution. The curve of intersection of the best hyperboloids of one sheet corresponding to Initial Guesses 4 and 5 can be seen in Figure 13.

D. What Happens When Specified Poses are Not Perfect?

Arguably the example was contrived to be successful, but is also very illustrative of the importance of good initial guesses. The specified 40 poses lie exactly on the curve of intersection of two constraint hyperboloids of one sheet. To introduce poses that do not lie perfectly on such a 4^{th} order curve which lies exactly on two constraint hyperboloids of one sheet, the initial specified 40 poses were truncated to 2 decimal places to introduce error, and the approximate synthesis algorithm was rerun. The results obtained are listed in Table V.

Parameter	Truncated Guess 4	Truncated Guess 4
K_1	-5.01374158	1.00543179
K_2	0.00000497	-0.99534789
K_3	21.12526403	22.98658405
x	3.00653176	-1.00047287
y	-1.98696494	-2.01010896
Iterations	134	329
d	0.1194434	0.0740493

TABLE V. Truncated Results.

It is to be seen that the fit is worse than that for the mechanism identified from the results in Table IV, still the minimization converged to similar results in terms of the best RR-dyad pair.

V. Conclusions

Kinematic mapping of distinct displacement poles to distinct points in a 3D projective image space was successfully used for approximate kinematic synthesis for rigid body guidance. A new approximate synthesis method was developed and successfully tested, and could have a wide range of applications as it has been presented in a general way which can be further expanded or simplified.

For the case of a mechanism containing a PR-dyad, the same method can be used with the exception that the conditions on the identified quadratic form of the quadric that best satisfied the specified poses will indicate that the specified image space points best fit a constraint hyperbolic paraboloid. No heuristics are necessary and given the initial desired poses, the entire approximate synthesis can be carried out using software to return a list of the best generating mechanisms ranked according to d, their *closeness* to the given poses. The unconstrained non-linear programming problem developed has only five variables and is easily solved by several methods. A minimization algorithm could actually be further customized to "jump" from local minima to other local minima depending on the desired closeness to the given poses. Furthermore some relationships between the variables could be built in to the algorithm so it recognizes undesirable solutions from the perspective of surface shape parameters and avoids iterations in those directions.

The method developed drives the solution mechanism to achieve exactly the desired poses but not necessarily a line of best fit through the poses. This may be desirable for a mechanism designer who wants a point on the coupler to go through exactly some specified poses but does not care about the path in between them. If this is not satisfactory then the designer can simply specify more points where the path is not well defined and the approximate synthesis method will yield a more desirable solution.

References

[1] L. Burmester. *Lehrbuch der Kinematik*. Arthur Felix Verlag, Leipzig, Germany, 1888.

[2] J.E. Holte, T.R. Cahse, and A.G. Erdman. Mixed Exact-Approximate Position Synthesis of Planar Mechanisms. *ASME, J. of Mech. Des.*, 122: 278286, 2000.

[3] J. Yao and J. Angeles. Computation of All Optimum Dyads in the Approximate Synthesis of Planar Linkages for Rigid-Body Guidance. *Mechanism and Machine Theory*, 35(8): 10651078, 2000.

[4] A. Liu and T. Yang. Finding All Solutions to Unconstrained Nonlinear Optimization for Approximate Synthesis of Planar Linkages Using Continuation Method. *ASME, J. of Mech. Des.*, 121(3): 368374, 1999.

[5] X. Kong. Approximate Kinematic Synthesis of Linkages Using Generalized Inverse Matrix and Continuation. *Mechanical Science and Technology*, 18(1): 3840, 1999.

[6] W. Blaschke. Euklidische Kinematik und nichteuklidische Geometrie. *Zeit. Math. Phys.*, 60: 61-91 and 203-204, 1911.

[7] J. Grünwald. Ein Abbildungsprinzip, welches die ebene Geometrie und Kinematik mit der räumlichen Geometrie verknüpft. *Sitzber. Ak. Wiss. Wien*, 120: 677-741, 1911.

[8] A.G. Erdman, G.N. Sandor and S. Kota *Mechanism Design: Analysis and Synthesis, 4^{th} Ed.* Prentice Hall, 2001

[9] O. Bottema and B. Roth. *Theoretical Kinematics*. Dover Publications, Inc. New York, NY, U.S.A., 1990.

[10] M.J.D. Hayes, P.J. Zsombor-Murray, and C. Chen. "Kinematic Analysis of General Planar Parallel Manipulators". *ASME, Journal of Mechanical Design*, 126(5): 866-874, 2004.

[11] M.J.D. Hayes, M.L. Husty. "On the Kinematic Constraint Surfaces of General Three-Legged Planar Robot Platforms". *Mechanism and Machine Theory*, 38(5): 379-394, 2003.

[12] M.J.D. Hayes, T. Luu, X.-W. Chang. "Kinematic Mapping Application to Approximate Type and Dimension Synthesis of Planar Mechanisms". *9th Advances in Robotic Kinematics*, eds. Lenarčič, J. and Galletti, C., Kluwer Academic Publishers, Dordrecht, the Netherlands, pp. 41-48, 2004.

[13] W.H. Press, S.A. Teukolsky, W.T. Vetterling, and B.P. Flannery. *Numerical Recipes in C, 2nd Edition*. Cambridge University Press, Cambridge, England, 1992.

[14] A. Dresden. *Solid Analytical Geometry and Determinants*. Dover Publications, Inc. New York, NY, U.S.A., 1964.

[15] J.A. Nelder and R. Mead. "A Simplex Method for Function Minimization". *Computer Journal*, 7: 308-313, 1965.

[16] R. Hooke and T.A. Jeeves. "Direct Search Solution of Numerical and Statistical Problems". *Journal of the ACM (JACM)*, 8(2): 212-229, 1961.